

Orientational behavior of the antimicrobial peptide PGLa in a lipid membrane environment studied by solid-state ^2H -NMR spectroscopy

Zur Erlangung des akademischen Grades eines

DOKTORS DER NATURWISSENSCHAFTEN

(Dr. rer. nat.)

der Fakultät für Chemie und Biowissenschaften der
Universität Karlsruhe (TH)
vorgelegte

DISSERTATION

von

Dipl. d'Ing. ENSCL Pierre Tremouilhac

aus Verneuil-sur-Avre (F)

Dekan: Prof. Dr. Holger Puchta

Referent: Prof. Dr. Anne S. Ulrich

Korreferent: Prof. Dr. Joachim Podlech

Tag der mündlichen Prüfung: Dienstag, den 10. Juli 2007

"We have two ears and one mouth, so we should listen more than we say." (Zeno of Citium)

Aim of the study

The work presented in this study deals with the application of a solid-state ^2H -NMR method to study the action of a natural antimicrobial peptide (AMP), PGLa, on biological membranes. Such AMPs are promising compounds for developing new drugs and are interesting parts of the immune system. Though they are known to interact strongly with membranes, their mechanism of action against bacteria is not yet fully understood and more investigations are needed. To this aim, one can use solid-state NMR spectroscopy. Having a suitable model for the structure and the motion of the peptide, its orientation in biological membranes can be calculated from several local orientational constraints of the peptide backbone measured by NMR spectroscopy. Hence, its biophysical mechanism of action can be understood. A ^2H -labeling method has been developed for model transmembrane peptides and is used here on AMPs for the first time. A similar method using ^{19}F -labels in the potentially structure disturbing residue CF_3 -phenylglycine (CF_3 -Phg) has been previously used to study the orientation of the PGLa peptide in DMPC lipid membranes.

For this study, PGLa peptides carrying ^2H -labels at selected sites first need to be synthesized and characterized. Through several replacements (Ala, Ile or Gly replaced by Ala- d_3) and using different motional models, a rigorous analysis of the ^2H -NMR method is carried out, and its reliability for such amphipathic peptide is assessed. Using an appropriate motional model and the minimal number of data points to calculate an accurate orientation of the peptide, a reliable and simple method for further detailed experiments is validated. This ^2H -labeling strategy is compared to the CF_3 -Phg strategy, and their respective advantages are discussed.

From a biological point of view, AMPs like PGLa are assumed to permeabilize cytoplasmic bacterial membranes by forming pores. In such pores, the peptides are supposed to be inserted in a transmembrane state, and the lipid head groups are tilted to participate in the pore structure. This study has to confirm this mechanism of action for PGLa, and it investigates the influence of parameters like the peptide concentration, the presence of anionic lipids, and the sample hydration.

Another relevant parameter for the membrane permeabilization can be the presence of other peptides. PGLa and magainin 2 (Mag2) peptides have indeed been shown to act synergistically in this process. Hence, the orientational and dynamic behavior of PGLa in the presence of Mag2 is monitored using the same NMR methodology to shed light on how this synergism can be explained and to assess its critical structural features.

Zusammenfassung

Gen-codierte antimikrobielle Peptide (AMP) kommen üblicherweise im Pflanzen- oder Tierreich vor. Als Beispiel dient das aus der Haut eines Frosches sekretierte PGLa-Peptid. Es gehört mit Magainin2 (Mag2) zur Magainin-Peptid-Familie. Diese Peptide sind kationisch und haben im α -helikalen gespaltenen Zustand amphipathische Eigenschaften. Ihre Hauptwirkung im Abwehrsystem ist die Permeabilisierung von Bakterienmembranen. Um die Wirkung dieser Peptide auf biologische Membranen aufzuklären, wurde Festkörper-NMR-Spektroskopie benutzt, da sie dynamische und Orientierungs-Eigenschaften von NMR-markierten Peptiden relativ zur orientierten Lipidschichten zu untersuchen erlaubt. Dazu wurden die Aminosäuren an den Positionen 6, 8, 10, 14 (Ala Reste), 7, 11 (Gly Reste), 9, 13 (Ile Reste) entlang des PGLa-Peptides durch L-3,3,3-d₃-Alanine (Ala-d₃) mittels Peptidfestphasensynthese ersetzt. Die acht hergestellten PGLa Analoga wurden durch RP-HPLC gereinigt und mittels LC-MS identifiziert. Zirkulardichroismus- (CD-)Spektroskopie und antimikrobielle Wachstumsversuche zeigten den geringen strukturellen Einfluss der Substitutionen. Somit wurden die membrangebundenen PGLa-Analoga als gerades reguläres α -helikales Peptid modelliert.

Quadrupolaufspaltungen von ²H-markierten PGLa-Analoga wurden in verschiedenen Membransystemen (DMPC oder DMPC/DMPG (3:1), mit Überschuss- oder teilweiser Hydratisierung) im Flüssigkristallzustand (308K) und zu verschiedenen Peptid-Lipid-Verhältnissen, (P/L) von 1:200 bis 1:20, mit Hilfe von Solid Echo-Einpuls-Sequenzen bestimmt. Bewegungen wurden bei einem skalaren Ordnungsparameter S_{mol} oder mit dem ganzen Ordnungstensor, die beide die Quadrupolaufspaltung reduziert haben, modelliert. Die Quadratische-Mittelwert-Abweichungs-Analyse der gesammelten Winkeleinschränkungen ergab die Dynamik und Orientierung des PGLa-Peptides.

Erst entstanden Berechnungsabweichungen im Bereich der Eigenabweichung der Versuche und zwar ohne oder mit Ile oder Gly Substitutionsdaten. Der Ala-d₃ Aminosäurerest war zwar weniger NMR-empfindlich als 4-CF₃-Phenylglycin, aber konnte sogar Ile oder Gly ersetzen. Das bestätigte die Zuverlässigkeit der Methode für solche amphipathische Peptide. Obwohl bei niedrigerer Peptidkonzentration die Neigungsänderung stärker als die Rotation der Helix um ihre eigene Achse war, wurden die Bewegungen des Peptides gut vom skalaren Ordnungsparameter modelliert. Die Daten von vier Ala-Substitutionen reichten aus, um eine genaue Orientierung zu berechnen. Die Ergebnisse bestätigten die zwei S- und T-Zustandsbildungen des Peptides. Bei niedrigerer Peptidkonzentration legte sich die PGLa-Helix parallel auf die Membranoberfläche, und die Lysin-Seitenketten waren vom hydrophoben Membraninneren weggerichtet (S-Zustand), wobei bei hoher Peptidkonzentration (T-Zustand) sich die Helix um ungefähr 30° gegen die Membranebene neigte.

Der Übergang zwischen den S- und T-Zuständen wurde mit einer plausiblen antiparallelen Homodimerisierung erklärt, und seine P/L-Grenze vom niedrigen Wassergehalt der Probe oder in Gegenwart von anionischen Lipiden erniedrigt. Obwohl die anionischen Lipide durch PGLa entmischt wurden, blieben die Membranen aller Proben in einer lamellaren Phase. Es wurde für PGLa keine Transmembran-Orientierung (I-Zustand) festgestellt, sogar mit dem hohen P/L=1:20. PGLa soll somit Poren mit einem anderen Mechanismus als mit dem „Toroidal Wormhole“-Modell bilden oder diese Poren sind transient und können durch diese NMR-Messungen nicht erfasst werden.

In Gegenwart eines Mag2-Äquivalents neigte sich das PGLa senkrecht (I-Zustand) in DMPC/DMPG Membranen. Für das erste Mal wurde dieser mit dem „Toroidal wormhole“-Modell kompatible Zustand genau beobachtet und beschrieben. Dieser Zustand erklärte den bekannten antimikrobiellen synergetischen Effekt. Weitere antimikrobielle Tests wiesen an, dass eine durch eine Salzbrücke stabilisierte parallele Heterodimerisierung stattfand.

Abstract

Antimicrobial peptides (AMPs) are widely spread over both animal and plant kingdoms. PGLa, a magainin family AMP, is naturally secreted in the integumentary system of a frog upon injury or hormonal stimuli. It belongs to one class of AMPs which are cationic and exhibit an amphipathic shape when folded into an α -helical structure. Some AMPs may influence the inflammatory process or the adaptive immune response of the host organism, but they are mainly expected to act on invading bacteria by membrane permeabilization. To study the action of these peptides on biological membranes, one can use solid-state NMR as it allows to monitor, in oriented lipid samples, the dynamic and orientational features of NMR-labeled peptides and lipids. Several PGLa analogues were thus synthesized carrying at a single site an Ala- d_3 residue at position 6, 8, 10, 14 in place of a native Ala, at position 9 and 13 in place of an Ile, or at position 7 and 11 in place of a Gly. Hemolytic and antimicrobial activity experiments showed that these analogues were as active as the wild type peptide.

Based on circular dichroism (CD) measurements of PGLa in the presence of liposomes and other solution state NMR studies, PGLa was modeled as being a straight regular α -helix when bound to a membrane. First its behavior was investigated in DMPC membranes in a fluid liquid crystalline state at 308 K, at a low concentration with a peptide to lipid ratio (P/L) of 1:200 and a high concentration with P/L=1:50. The orientation of the peptide could be calculated using data points from the native Ala substitutions or from the other substitutions with an error in the range of the experimental intrinsic error, confirming the reliability of the α -helix structure model. A biaxial model of motion was compared to the previously used uniaxial model and it did not lead to different results but gave more information on the anisotropic motion of PGLa. It was concluded that at low concentration PGLa lies almost flat on the surface membrane with the lysine side chains pointing up to the water phase. This is called the S-state. It has a relative strong biaxial motion indicating that the peptide is more likely to change its insertion angle rather than to reorient around its helical axis. At higher concentration, PGLa lost this biaxiality feature, probably due to peptide-peptide association. PGLa was then found to insert from the C-terminus with an angle of $\sim 35^\circ$ between the helix axis and the membrane surface, but still having the lysine side chains pointing up to the water phase. This state, the T-state, was different than the fully inserted state, the I-state, expected in the toroidal pore model of AMPs activity. It confirmed the previous analysis using the more NMR-sensitive CF_3 -Phg label. Thus, it showed those results using a convenient ^{19}F -label to be reliable, even though this label might induce disturbing effects at high concentration and

lead to deviations in the calculated orientation. The re-orientation of PGLa from the S- to the T-state was interpreted as caused by a homo-dimer formation.

Given that reliable and accurate calculations were obtained using only 4 data points from the native Ala-substitution of the central part of the peptide in a uniaxial model of motion, analyses could be carried out with several experimental conditions being varied. Specifically the influence of the presence of anionic lipids by adding DMPG to the lipid bilayer, the level of lipid hydration by using different kind of samples, and the peptide concentration with P/L ratios of 1:200, 1:100, 1:50 and 1:20 were investigated. PGLa was found to re-align from the S- to the T-state between P/L = 1:200 and 1:100 in DMPC at low hydration, and in DMPC/DMPG (3:1) at both low and high hydration. On the other hand, at high hydration in the absence of anionic lipid an intermediate state, interpreted as a fast exchange between the S- and T-state, was found between P/L = 1:100 and 1:50. It was concluded that anionic lipids or a low level of hydration favored the insertion of the peptide in the membrane permeabilizing state. However, full insertion was not found even at P/L=1:20. Though segregation of anionic lipids by PGLa was noticed, the lipid bilayers were still found to be well oriented in a lamellar phase. Thus, if PGLa is supposed to form pores according to the toroidal pore model, these pores are not seen by this NMR experiment and must be transient.

PGLa acts differently on membrane in the presence of magainin 2 (Mag2), another magainin peptide, and synergism of action against bacteria between these two peptides has been shown. Even if no detailed structure of PGLa in the presence of Mag2 is available, CD experiments of PGLa and Mag2 mixtures revealed that the peptides mainly kept an α -helical structure. Mag2 and some analogues were synthesized and mixed with ^2H -labeled PGLa analogues. From the ^2H -NMR analyses, it appeared that PGLa was close to a transmembrane state, I-state, when mixed with Mag2. This was corroborated by oriented CD measurements. Furthermore, antimicrobial assays revealed that the mutation of the Glu residue at position 19 in the Mag2 peptide by Gln suppressed the synergism, whereas lowering or swapping the charge of other residues did not. It was thus concluded that PGLa associated with Mag2 forming a parallel hetero-dimer, stabilized by a salt bridge probably between Glu-19 of Mag2 and Lys-19 of PGLa and thus forming stable pores. This is the first time that the orientation of an AMP in the functionally relevant I-state was experimentally demonstrated.

Table of contents

Aim of the study.....	i
Zusammenfassung.....	ii
Abstract.....	iii
Table of contents.....	v
List of abbreviations.....	viii
Preface.....	ix
Acknowledgments.....	xii

I. Introduction to the biology of magainin membrane active peptides 1

1. BIOMEMBRANES.....	1
1.1. Introduction.....	1
1.2. Bacterial and animal membranes.....	2
2. ANTIMICROBIAL PEPTIDES FROM THE FROG <i>XENOPUS LAEVIS</i>	4
2.1 AMPs in general.....	4
2.2. Frog AMPs.....	5
2.3. Biosynthetic pathway: origin of diversity and control of toxicity.....	5
3. MECHANISM OF ANTIMICROBIAL ACTION.....	8
3.1. Membranes as target: features of antimicrobial peptides.....	8
3.1.1. Affinity and binding to lipid membranes.....	9
3.1.2. α -helical structure and amphipathicity.....	9
3.1.3. Hydrophobicity and polar angle.....	10
3.2. Mechanism of membrane disruption.....	10
3.2.1. Action on the outer membrane of Gram-negative bacteria.....	10
3.2.2. Models for cytoplasmic permeabilization.....	11
3.3. Other functions of AMPs.....	12
3.4. Bacterial resistance against AMPs.....	13
4. CONCLUSIONS.....	14

II. Structural and dynamic information of biological compounds extracted from solid-state ^2H - and ^{31}P -NMR data analysis..... 15

1. INTRODUCTION TO SOLID-STATE NMR SPECTROSCOPY.....	15
1.1. Origin of the nuclear magnetic resonance: the Zeeman interaction.....	15
1.2. Internal nuclear magnetic interactions.....	16
1.2.1. The chemical shift interaction.....	17
1.2.2. The quadrupole interaction.....	18
1.3. Influence of motion.....	20
1.3.1. Influence of motion for ^{31}P	20
1.3.2. Influence of motion for ^2H	22
1.3.3. The Saupe order matrix and the generalized degree of order.....	24
2. STRUCTURE ANALYSIS: ORIENTATION DETERMINATION OF PEPTIDES BOUND TO A MEMBRANE.....	26
2.1. Methods of solution calculation and error assessment.....	26
2.2. Experimental section.....	28
2.2.1. Peptide structure model.....	28
2.2.2. Solid-state NMR sample preparation.....	29
2.2.3. NMR spectroscopy.....	31

III. Synthesis and characterization of labeled peptides 32

1. SYNTHESIS AND PURIFICATION OF THE PEPTIDES.....	32
1.1. Principle of solid phase peptide synthesis (SPPS) and HPLC purification.....	32

1.1.1. SPPS.....	32
1.1.2. HPLC.....	34
1.2. Materials and methods.....	35
1.3. Results.....	41
2. CIRCULAR DICHROISM (CD), ORIENTED CD (OCD) MEASUREMENTS.....	41
2.1. Principle of CD and OCD spectroscopy.....	41
2.2. Materials and methods.....	42
2.3. Results from CD experiments.....	44
3. BIOLOGICAL TESTS: HEMOLYTIC ASSAY AND MINIMAL INHIBITORY CONCENTRATION (MIC).....	46
3.1. Principle.....	46
3.2. Materials and methods.....	47
3.3. Results of MIC and HA tests.....	49

IV. Solid-state NMR analysis of the PGLa peptide orientation in membrane: a ²H-labeling strategy..... 51

1. STATING THE PROBLEM.....	51
2. MATERIALS AND METHODS.....	54
2.1. Sample preparation.....	54
2.2. NMR spectroscopy.....	54
2.3. Calculations.....	54
3. RESULTS.....	55
3.1. Biological considerations.....	55
3.2. Choice of NMR samples.....	56
3.3. ² H-NMR results.....	56
3.3.1. Helix alignment at low peptide concentration (P/L = 1:200).....	58
3.3.2. Helix alignment at high peptide concentration (P/L = 1:50).....	60
3.4. Order tensor analysis.....	61
4. DISCUSSION.....	63
4.1. Assessment of the model.....	63
4.2. Concentration-dependent re-alignment of PGLa.....	65
4.3. Comparison with previous ¹⁹ F- and ¹⁵ N-NMR results.....	67
5. CONCLUSIONS.....	70

V. Conditions affecting the re-alignment of the antimicrobial peptide PGLa in membranes as monitored by solid-state ²H-NMR spectroscopy..... 71

1. STATING THE PROBLEM.....	71
2. MATERIALS AND METHODS.....	73
2.1. Sample preparation.....	73
2.2. NMR spectroscopy.....	73
2.3. Calculation.....	74
3. RESULTS.....	74
3.1. ³¹ P-NMR study of the lipid bilayers.....	77
3.2. ² H-NMR results.....	79
3.3. Orientation of PGLa in DMPC lipid samples.....	79
3.4. Orientation of PGLa in DMPC/DMPG lipid samples.....	81
3.5. Molecular order parameter.....	82
3.6. Influence of hydration.....	82
4. DISCUSSION.....	83
4.1. Phase behavior of the lipid membrane.....	84
4.2. Peptide re-alignment under different conditions.....	86
4.3. The T-state and the pore structure.....	87
5. CONCLUSIONS.....	88

VI. Synergistic transmembrane alignment of the PGLa/Mag2 hetero-dimer..... 89

1. STATING THE PROBLEM.....	89
2. MATERIALS AND METHODS.....	90

2.1. Antimicrobial tests	90
2.2. CD/OCD measurements	91
2.3. NMR-sample preparation and spectroscopy	91
3. RESULTS	92
3.1. Antimicrobial activity of the ² H-labeled PGLa analogues	92
3.2. Antimicrobial activity of Mag2 analogues	92
3.3. Choice of lipid system	93
3.4. CD and OCD experiments	93
3.5. ³¹ P-NMR spectroscopy	96
3.6. ² H-NMR spectroscopy	97
4. DISCUSSION	99
4.1. Orientation of PGLa in the presence of Mag2	100
4.2. Hetero-dimer formation and pore structure	101
5. CONCLUSIONS	103
VII. Summary	105
References	109
List of publications	120
Curriculum vitae	121

Note to the reader. Numbers given in square brackets [] refer to citation located in the References section or to sections within the thesis if they contain capital roman digits.

List of abbreviations

μg	microgram
μL	microliter
AMP	antimicrobial peptide
aq	aqueous
Boc	t-butyloxycarbonyl
CD	circular dichroism
cDNA	complementar DNA
CF ₃ -Phg	4-trifluoromethylphenylglycine
CFU	colony forming unit
CL	cardiolipin
CPF	caerulin peptide fragment
CSA	chemical shift anisotropy
DCM	dichloromethane
DIPEA	diisopropylethylamine
DMF	dimethylformamide
DMPC	dimyristoyl-PC
DMPG	dimyristoyl-PG
DMSO	dimethylsulfoxide
DNA	deoxyribonucleic acid
DPC	dodecylphosphatidylcholine
EDTA	ethylenediaminetetraacetic acid
eq	equivalent
ES	electrospray
ESI	electrospray ionization
FAB	fast atom bombardment
FID	free induction decay
Fmoc	9-fluorenylmethoxycarbonyl
G	gram
GDO	global degree of order
GP sample	glass plate oriented sample
h	hour
ħ	Planck constant (in radians)
HA	hemolytic activity
HBTU	2-(1H-benzotriazole-1-yl)-1,1,3,3-tetramethyluronium hexafluorophosphate
L/P	lipid/peptide
LB	Luria Bertani
LC-MS	liquid chromatography-mass spectrometry

LPS	lipopolysaccharide
LUV	large unilamellar vesicle
MBHA	4-methylbenzhydryl-amide
MHz	megahertz
MIC	minimal inhibitory concentration
min	minute
mL	milliliter
MLV	multilamellar vesicle
mM	millimolar
mmol	millimole
MS	mass spectrometry
nm	nanometer
NMP	N-methyl-2-pyrrolidinone
NMR	nuclear magnetic resonance
OCD	oriented circular dichroism
PAF	principal axes frame
PC	glycerophosphatidylcholin
PE	glycerophosphatidylethanolamine
PG	glycerophosphatidylglycerol
Qc	quadrupolar coupling
REDOR	rotational echo double resonance
rf	radio frequency
RP-HPLC	reversed-phase high performance liquid chromatography
RMSD	root mean square deviation
rt	retention time
SM	sphingomyelin
SPPS	solid phase peptide synthesis
tBu	t-butyl
TFA	trifluoroacetic acid
TIS	triisopropylsilane
TOF	time of flight
v/v	by volume
w/w	by weight
wt	wild type
XPF	xenopsin peptide fragment

Preface

Through the last half century, the widespread use and often abuse of antibiotics have after an apparent era of “health miracle” lead to the emergence of several multidrug-resistant pathogenic micro-organisms, also nicknamed “superbugs”. Apart from the resistant response towards the use of antibiotics, there is an increasing and urgent need of new active compounds (www.tufts.edu/med/apua). In this view, research has focused more attention on gene encoded antimicrobial peptides (gene encoded AMPs) which are an essential part of the innate immune system. These intriguing compounds are among the most ancient and efficient components of host defense and have been identified in a large number of living species, if not in all, ranging from plants, bacteria, and animals [1]. They seem to act principally on the cell membranes of these pathogens. De novo designed peptides based on features of these natural microbicidal peptides have shown promising results even in the field of cancer therapeutic research. There is a great interest in optimizing these AMPs and getting new lead compounds. In this quest, besides random trial of synthetic compounds, one may naturally try to understand the exact molecular interactions and mechanisms of action of AMPs.

There are some practical aspects to consider in this quest. When the antibiotic target is a protein, its structure (with ligand of interest) is often investigated to obtain an optimized antibiotic. Such well resolved three-dimensional structures can be obtained from solution NMR and X-ray crystallography studies. Unfortunately, most of the potential drug targets are membrane proteins which need their membrane environment to be functionally active. This mandatory practical consideration has restricted access to structural information via X-ray crystallographic techniques. Likewise investigating solubilized non-functional membrane proteins by solution-state NMR is of limited interest. Nevertheless, the recent development of solution-state NMR of proteins in bicelles has resulted in a few newly resolved membrane protein structures, but size and stability of bicelles need to be maintained. In the case where the drug target is not a protein but a whole membrane and the “ligand” is a peptide, there are even more difficulties arising from the highly dynamic features of the ensemble. Fortunately, solid-state NMR, which allows working with viscous anisotropic samples, offers an unequalled means to get information on the dynamics, structures, distances and orientations in this kind of system [2]. Hence, the present work is concerned with the application of a solid-state ^2H -NMR method to investigate the action of the membrane active peptide PGLa, an AMP from a frog, with lipid bilayers in order to shed light on how it acts on biological membranes.

To appreciate the interest of studying a peptide from a frog, chapter I will give some biological background, not only for the sake of understanding what biomembranes and AMPs are, or how they may act together, but also to justify the choice of these peptides. Regardless of their origin, these peptides may be seen as an archetype for studying α -helical vertebrate AMP. This part is not aiming to fully review all studies on magainin peptides or AMPs as it will be an everlasting work and go beyond the purpose of this thesis, but to give an understandable overview in these fields: the biosynthetic pathway related to the host control of AMP toxicity, the peptide features needed for microbicidal activity and selectivity, and of course models for the action of membrane active peptides as it will be the main theme of the discussion.

Chapter II introduces the solid-state NMR theory applied to ^{31}P and ^2H nuclei in biological samples on the basics of established methods to study such membrane active peptides in terms of orientation. NMR sample preparation and NMR data acquisition methods are described and great attention is paid to the structure calculation and analysis on which the conclusive results are based.

Chapter III covers the “materials and methods” part of the work concerning peptide synthesis and characterization. Short and critical basics for each method are given along technical data and applied processing. For this study, peptides containing a suitable NMR label, 3,3,3- $^2\text{H}_3$ -Alanine (Ala- d_3), were chemically synthesized and highly purified. As some mutations compared to the wild type peptides were introduced, it was needed to check their biological activity and their conformation. Even if this represents an enormous part of the practical work, most of the analytical results are directly reported in this chapter to let the discussion of the following chapters be centered on the NMR results and biophysical interpretations of the problem.

Chapter IV could be a good illustration of the adage of toxicology stating that everything is a matter of concentration. A direct application of a powerful solid-state ^2H -NMR method is reported. Its non-disturbing strategic labeling with Ala- d_3 affords accurate measurements of the orientation of PGLa in a model membrane and shows a concentration dependent re-alignment. This change is discussed in terms of a cooperation process between peptides, like a dimerization mechanism, and compared with known models of membrane permeabilization. Most of the results presented in this chapter have been published in *Biophysical Journal* [3].

In Chapter V, several conditions affecting this re-alignment are screened: the peptide concentration, level of hydration and the content of anionic lipids, which abound in bacterial

membranes, are modulated. The aim is to assess whether the new previously found orientational state of the peptide is compatible with the “toroidal wormhole” model of membrane permeabilization. These results have been published in *Biochimica et Biophysica Acta* [4].

In Chapter VI, the influence of magainin 2 (Mag2), a peptide from the same family as PGLa, on membrane orientation of PGLa is studied as synergism of biological activity between these two peptides is known. The higher microbicidal potency of the mixture is thus explained through orientational analysis of the peptides and the stability of membranes defects. The NMR results presented in this chapter have been published in the *Journal of Biological Chemistry* [5].

Finally, all these interesting results on PGLa are summarized, and conclusions of the study are drawn in terms of the AMP model of action on membranes and consequences for antimicrobial peptides optimization.

Acknowledgments

Je n'aurai pu accomplir ce travail enthousiasmant si l'opportunité, la liberté et les moyens ne m'en avaient été donnés. Pour cela mes remerciements et ma reconnaissance vont d'abord à Anne S. Ulrich (Prof. Dr.).

Je pense aussi à mes collègues du groupe Bio-NMR parmi lesquels j'ai travaillé. Notamment, pour m'avoir enseigné, accompagné et supporté tout au long de ce doctorat, je tiens à remercier profondément Erik Strandberg (Dr.) et Parvesh Wadhvani (Dr.).

Je remercie également Stefanie Maurer et Sylvia Gehrlein de leur assistance pour les synthèses peptidiques, Marco Ieronimo, Nathalie Kanithasen et Deniz Tiltak de leurs enseignements pour les tests biologiques, Markus Schmidt et Stephan Grage (Dr.) pour leur support dans l'utilisation du matériel RMN, Jochen Bürck (Dr.) et Mme Mathieu pour les mesures de spectroscopie CD, Raiker Witter (Dr.) pour les measurements MAS-RMN.

De ces temps passés aggrementés, je dis encore merci à Sonja Müller (Dr.), Parvesh, Erik et Eric Kervio (Dr.) pour leurs amitiés et conseils. Mes pensées s'adressent enfin naturellement à ma famille et mes amis dont l'éloignement n'a pas été synonyme d'oubli et à Stefanie pour sa patience et son support inconditionnel.

I. Introduction to the biology of magainin membrane active peptides

It may be stating the obvious, but it is still worth noting that for any successful antibiotic development, selective toxicity towards host and pathogen cells is of fundamental concern. The following sections introduce the concept of biomembranes and a comparison between eukaryotic and bacterial membranes. The AMPs from the magainin peptides are thus described to shed light on how differences and similarities have lead naturally to their selective activity on the membranes.

1. Biomembranes

1.1. Introduction

Membranes are the fundaments maintaining life through compartmentalization of cells and homeostasis. Transport and communication between the two inter- and intracellular spaces are tightly controlled by the membrane and a number of catalytic reactions are only supported in their vicinity.

In animal and bacteria alike, lipids are the primary constituents of membranes. They are amphipathic molecules possessing highly mobile fatty acyl chains and a polar headgroup. The extensive diversity of acyl chains, whose length can vary from 6 to 30 carbon atoms, with or without double bonds, in combination with the enormous variety of headgroups, have long made it difficult to establish a logical and comprehensive classification system and nomenclature [6]. In an aqueous solution, hydrophobic forces from the acyl chain and hydrogen bonding with the headgroups often drive the formation of bilayered assemblies which maintain the hydrophobic acyl core between two polar regions at the interface towards the aqueous phase.

Membranes are commonly described using the fluid mosaic model of Singer and Nicolson [7] as depicted in figure I.1, where proteins and glycoproteins are embedded in this

lipid bilayer, either crossing its full thickness (integral proteins) or bound to the surface (peripheral protein), and where the lipids are in a fluid liquid crystalline state.

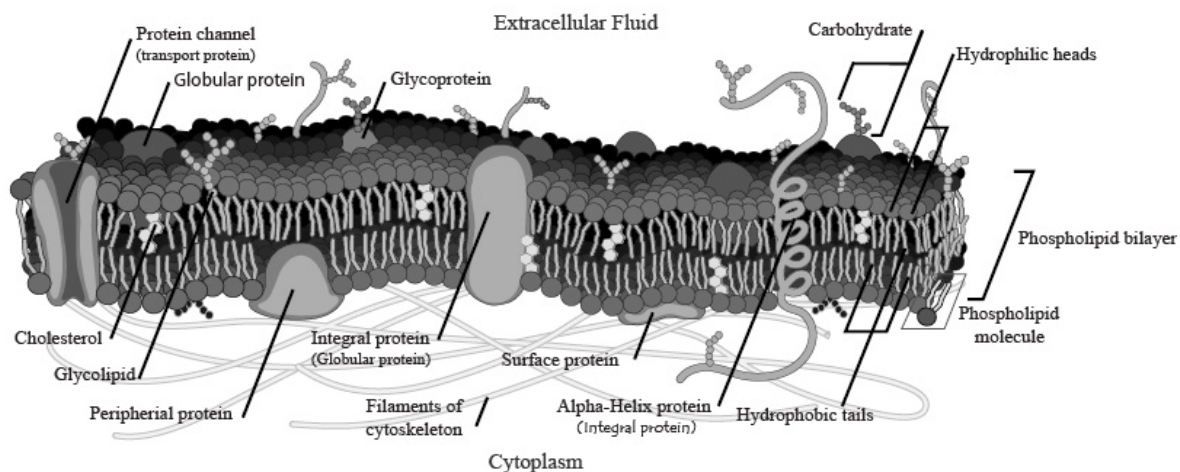


Figure I.1. The membrane mosaic fluid model according to Singer and Nicholson [7]. (Adapted from a figure in the public domain).

To refine this simple model, the prevalence of proteins in the membrane can first be considered: membrane proteins can compose up to 80% of the bacterial membrane by weight and one may wonder if lipids are not indeed the mosaic constituent in a protein fluid matrix. Lipid molecules which sustain the structure and thereby the functionality of the membrane proteins are also tightly bound and integrated to the protein surface forming around the proteic core, a first and second shells [8, 9]. Despite weak lipid–lipid interactions, small protein-stabilized lipid domains, called lipid rafts, have been unraveled and are involved in different important functions like endocytosis or signaling [10, 11]. It has been reported that lipid molecules can even be considered as receptor-like entities, shown by correlating the binding response of the antimicrobial peptide polymyxin B to a membrane directly to the concentration of lipid-II [12].

1.2. Bacterial and animal membranes

Apart from the hydrophobic core of the membrane, where the length and unsaturation of acyl chains influence especially the fluidity and the matched embedding of the proteins, lipid headgroups are the classical recognition sites for sorting out membrane constituents.

They vary in size, charge, and polarity and their composition constitutes the most important difference between eukaryotic and prokaryotic membranes as depicted in Figure I.2

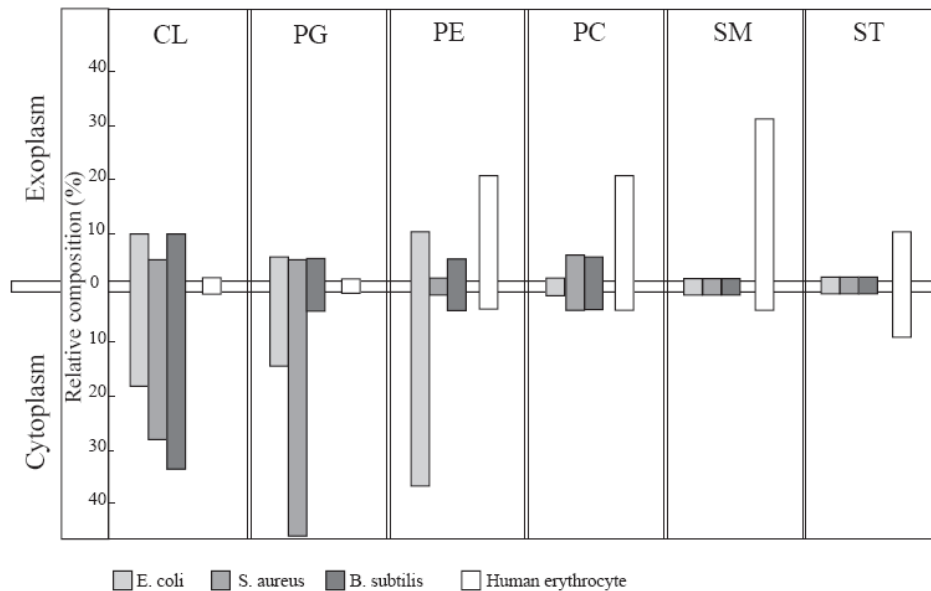


Figure I.2. Asymmetric lipid composition of cytoplasmic membranes from several bacteria compared to human erythrocytes. Cardiolipin (CL), glycerophosphoglycerol (PG), glycerophosphoethanolamine (PE), glycerophosphocholine (PC), glycerophosphoethanolamine (PE), sphingomyelin (SM), sterol (ST). (Adapted from [13]).

Prokaryotic cytoplasmic membranes contain a high proportion of anionic lipids such as glycerophosphoglycerols (PG), cardiolipins (CL or di-PG), whereas these lipids are hardly found in mammalian cytoplasmic membranes. On the other hand, eukaryotic membranes possess a high proportion of zwitterionic lipids like glycerophosphoethanolamines (PE), glycerophosphocholines (PC), sphingomyelin (SM or ceramide phosphocholines) and the sterol lipids which are important for the dynamics and integrity of the lipid layers [14, 15].

Bacterial membranes are also characterized through a highly asymmetric lipid charge distribution raising the well-known transmembrane potential. This electrical potential is necessary for several energy-dependent catalytic or transport processes. As illustrated in Figure I.3, two membrane architectures prevail in bacteria. In Gram-negative bacteria, an outer membrane, rich in PG, lipopolysaccharide (LPS) and magnesium, followed by a 2 nm thick peptidoglycan wall protects the cytoplasmic membrane. By Gram-positive bacteria, the cytoplasmic membrane is directly surrounded by a 20 to 40 nm thick peptidoglycan wall.

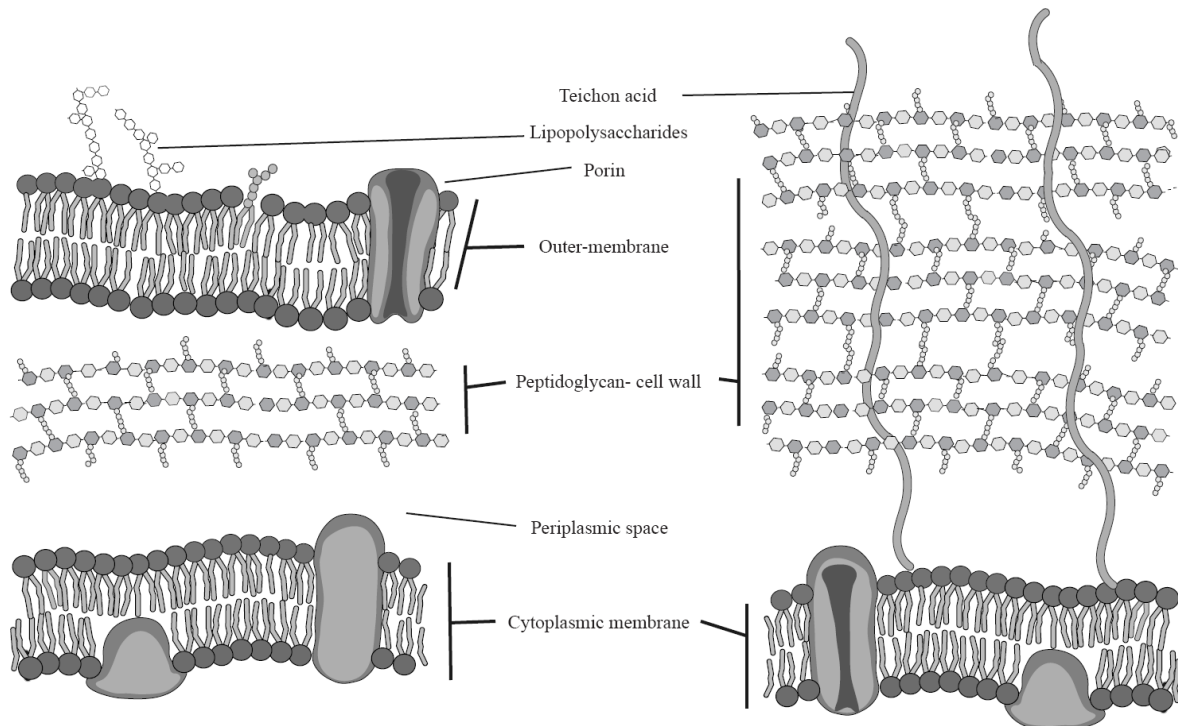


Figure I.3. Gram-positive (left part) and Gram-negative (right part) bacterial membranes.

2. Antimicrobial peptides from the frog *Xenopus laevis*

2.1 AMPs in general

Eukaryotic AMPs in their mature state contain generally between ten and forty residues and can be grossly classified in the following three groups according to their structure and composition [16]:

- linear peptides which are mostly constituted of one or two predominant α -helical domains, for example in the cecropin, magainin, and bombinin peptide families.
- peptides with intramolecular cysteine residues which mostly link several β -strands, as for example protegrins or defensins.
- peptides containing one or two residues in abundance, especially tryptophan, arginine and/or proline.

Nowadays, about one thousand gene-encoded AMPs from eukaryotes have been reported and most of them are deposited in the database of Tossi at the university of Trieste (www.bbcm.univ.triest.it/~tossi). The two first above-mentioned classes are certainly the most common. These AMPs generally possess several positively charged residues under

physiological conditions. This noticeable feature appears essential to tackle pathogens as detailed in part 3.

2.2. Frog AMPs

Historically, secretions of frog and toad integument were intensely studied as they contain a lot of active peptides and alkaloids (see [17] for a review). For examples, the peptide caerulein acts in the same way as the mammalian intestinal peptide hormone gastrin to contract smooth muscles, and the peptide xenopsin is the counterpart of the mammalian neurotransmitter neurotensin. The microbicidal properties of frog peptides have been known since 1970s and the discovery of the peptide bombinin from the skin of *Bombina variegata* [18]. Unfortunately, it also exerts toxicity to mammalian cells. Only in the late 1980s, Zasloff et al. noticed that *Xenopus laevis* frogs survived surgery and their wounds were healing well despite a non-sterile environment. Two peptides, magainin 1 (Mag1) and magainin 2 (Mag2) were isolated and their antimicrobial properties established [19]. Along with the findings of the AMP cecropin from insects [20] and the α -defensins from rabbits a few years before, it has started a new era of interest for animal AMPs as part of the innate immune system.

For the frog species *Xenopus laevis*, more than ten peptides having antimicrobial properties have been identified (Table I.1). They are all part of the magainin family. The Peptidyl-glycyl-leucyl-amide (PGLa) peptide, first predicted from a cDNA library [21], is found to be a major component of dorsal skin exudate [22], and alike the xenopsin peptide fragment (XPF) it has been shown to act against bacteria, fungi and protozoa [23]. PGQ is found in the intestinal track with the other caerulein peptide fragment (CPF), XPF, Mag1, and Mag2 peptides [24]. All exert activity against a wide spectrum of pathogens (Table 1.2).

2.3. Biosynthetic pathway: origin of diversity and control of toxicity

In *Xenopus laevis*, these peptides are localized in both the external and the internal [24] integumentary system and stored in granular multinucleated cells as well as in mammalian-like Paneth cells in the small intestine [25]. The epithelial surface is a strategic place as these peptides are part of the first line defence against any microbial invasion by forming a “chemical barrier”. In this localization, they are also less susceptible to exert

Table 1.1 Magainin peptide family: names and sequences of the antimicrobial peptide from the African frog *Xenopus laevis*.

Peptide	Full name	Sequence	Reference
CPF 1	Caerulein peptide fragment 1	GFASF LGKAL KAALK IGANA LGGAP QQ	[19, 26-28]
CPF 2	Caerulein peptide fragment	GFASF LGKAL KAALK IGANM LGGAP QQ	[19, 26-28]
CPF 3	Caerulein peptide fragment 3	GFASF LGKAL KAALK IGANM LGGTP QQ	[19, 26-28]
CPF 4	Caerulein peptide fragment 4	GFGSF LGKAL KAALK IGANA LGGSL QQ	[19, 26-28]
CPF 5	Caerulein peptide fragment 5	GFGSF LGLAL KAALK IGANA LGGAP QQ	[19, 26-28]
CPF 6	Caerulein peptide fragment 6	GFGSF LGKAL KAGLK IGTNF LGGAP QQ	[19, 26-28]
CPF 7	Caerulein peptide fragment 7	GLASL LGKAL KAALK IGANA LGGSP QQ	[19, 26-28]
CPF 8	Caerulein peptide fragment 8	GLASL LGKAL KAGLK IGTHF LGGAP QQ	[19, 26-28]
CPF 9	Caerulein peptide fragment 9	GLASL LGKAL KATLK IGTHF LGGAP QQ	[19, 26-28]
CPF 10	Caerulein peptide fragment 10	GLASF LGKAL KAALK IGAHL LGGAP QQ	[19, 26-28]
Mag1	Magainin 1	GIGKF LHSAG KFGKA FVGEI MKS	[19, 29]
Mag2	Magainin 2	GIGKF LHSAK KFGKA FVGEI MNS	[19, 29]
LPF	Levonin peptide fragment	GWASK IGQTL GKIAK VGLQG LMQPK	[30]
XPF	Xenopin peptide fragment	GWASK IGQTL GKIAK VGLKE LIQPK	[19, 27, 28]
PGLa	Peptidyl-glycyl-leucyl-amide	GMASK AGAIA GKIAK VALKA L-NH ₂	[22]
PGQ	Peptidyl-glycyl-glutaminy-acid	GVLSN VIGYL KKLGT GALNA VLKQ	[24]

Table 1.2. Examples of the wide-spectrum activity of magainin peptides against pathogens.

Peptide	Strain	Ref.	MIC (µg/mL)
Mag2	<i>E. coli</i> (D31)	[19]	5
	<i>K. pneumoniae</i>		10
	<i>C. albicans</i>		80
	<i>C. albicans</i> (14053)	[23]	200-500
XPF	<i>E. coli</i> (25922)	[23]	10-50
	<i>S. aureus</i>		100-200
	<i>C. albicans</i>		200-500
PGLa	<i>E. coli</i> (25922)	[23]	10-50
	<i>S. aureus</i> (25923)		50-100
	<i>C. albicans</i> (14053)		100-200
PGQ	<i>E. coli</i> (25922)	[24]	62-250
	<i>K. pneumoniae</i> (13883)		120-250
	<i>C. albicans</i> (14053)		250-500
	<i>S. aureus</i> (29213)		250-500
CPF	<i>E. coli</i> (25922)	[24]	16-31
	<i>K. pneumoniae</i> (13883)		31-62
	<i>C. albicans</i> (14053)		125-250
	<i>S. aureus</i> (29213)		16-31

toxicity due to the relatively inert surrounding. The cells release storage vesicles by a holocrine mechanism involving the rupture of the glands under mechanical or hormonal stimuli [31, 32].

All the peptides listed in Table 1 are naturally synthesized as prepropeptides. The prepropeptides of Mag1, Mag2, and PGLa have only an antimicrobial function whereas XPF, CPF, and LPF are fragment of, respectively, the xenopsin, caerulein, and levitide propeptides which are secreted among these other functional peptides. All of them have nevertheless a conserved nineteen residues signal peptide. The prepropeptide of PGLa is maybe the simplest as it contains only one sequence of PGLa. In comparison, the prepropeptide of Mag1 and Mag2 is predicted to be 303 residues long. The consequent propeptide contains one Mag1 sequence and five Mag2 sequences interleaved with almost identical acidic spacer sequences [33] as depicted in Figure I.4. These spacers are also well conserved in the other propeptides. The propeptides stored in the secretory vesicles are processed through post-translational proteolysis. This lysis is specific to basic residues and release spacers and functional peptides. The acidic spacers certainly inhibit the AMPs by compensating the cationic charges of the peptides, a relevant feature for bacterial membrane disruption (vide infra). Other prepropeptide genes may have derived from an ancestor gene similar to the one encoding PGLa and given repeated units by exon shuffling [34]. This leads partially to the AMP diversity which may also have been driven by positive selection [35].

	Start <u>MFLGLFICSLIAVICANALPQPEASA</u>	26
DEDMDE	REVRGIGKFLHSAGKFGKAFVGEIMKSKRDAEAVGPEAFA	72
DEDLDE	REVRGIGKFLHSAKKFGKAFVGEIMNSKRDAEAVGPEAFA	128
DEDLDE	REVRGIGKFLHSAKKFGKAFVGEIMNSKRDAEAVGPEAFA	174
DEDLDE	REVRGIGKFLHSAKKFGKAFVGEIMNSKRDAEAVGPEAFA	210
DEDFDE	REVRGIGKFLHSAKKFGKAFVGEIMNSKRDAEAVGPEAFA	256
DEDLDE	REVRGIGKFLHSAKKFGKAFVGEIMNSKRDAEAVDDRRWV	302
E end		

Figure I.4. Prepropeptide sequence for Mag1 and Mag2 peptides deduced from cDNA inserts. The signal peptide is underlined. It is also conserved in the expression of other antimicrobial peptide like PGLa or CPF. The sequences in grey boxes are the acidic peptides found in the skin exudates and are assumed to play the role of acidic spacers between AMPs to stabilize the storage vesicles. The sequence of Mag1 and the five of Mag2 are depicted in bold. (Adapted from [33]).

The exudate extracted from the dorsal dermal glands of *Xenopus laevis* has been shown to constitute a complex mixture of over thirty polypeptides derived from these few precursors [27]. Indeed mature peptides are released among some other specific peptidase

[29]. This extravesicular metalloprotease called magaininase lyses all peptides with a specific amphipathic secondary structure, independent of the amino acid sequence [36]. Within a few minutes peptides are cleaved and a mixture of tens of peptide fragments is left. This is one reason why antimicrobial properties of specific peptides were not sooner discovered. It is assumed that the release of peptidase is a mean of detoxification, as AMPs are also hemolytic at higher concentrations.

3. Mechanism of antimicrobial action

3.1. Membranes as target: features of antimicrobial peptides

There is plenty of evidence that action of AMPs on membranes leads to bacterial death or proliferation inhibition. Protein-free liposomes leak upon addition of Mag1 [37], Mag2 [38, 39] and PGLa [40-42]. To show that no specific membrane receptors are involved, *all-D* amino acid Mag2 has been synthesized and tested against bacteria [43, 44]. These studies reveal that peptides from the D- and L-forms of the amino acids have the same microbicidal potency. The selectivity and activity of the peptides on lipid membranes originate from several interdependent physicochemical parameters like the charge, the conformation or the hydrophobicity of the peptide and lipid mixture as depicted in Figure I.5.

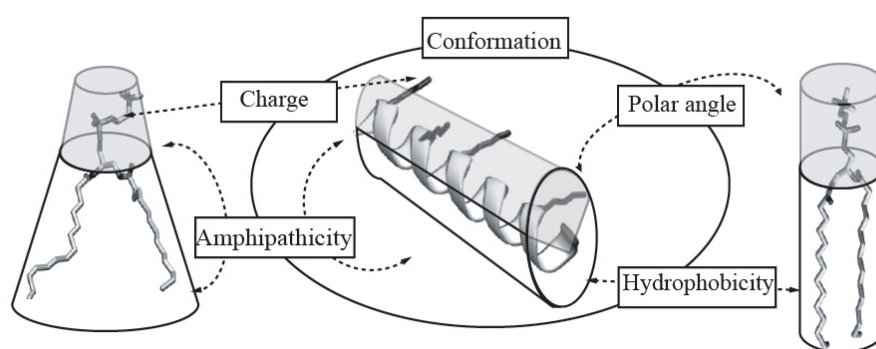


Figure I.5. Inter- and intra- correlation of several physicochemical parameters of lipid and peptide driving the selective affinity of AMPs and their interaction with lipid membranes. In the middle part, an α -helical peptide with lysine side chains (depicted in black) is schematically depicted by a surrounding cylinder with two domains: a polar and charged surface (grey colored) and a hydrophobic surface (white colored). On both side, two different lipid molecules are also schematically depicted by simple geometrical forms.

3.1.1. *Affinity and binding to lipid membranes*

Bacterial membranes contain a lot of negatively charged lipids, namely CL, PG, and LPS (vide supra). As PGLa has a charge of +5 and Mag2 a charge of +3/+4 at physiological pH, the affinity of the cationic AMPs toward bacteria is driven by electrostatic interactions. The influence of this electrostatic interaction is shown between PG and Mag1 [39, 45], Mag2 [39, 46] and PGLa [47-49]. Modification of the electrostatic properties of the peptide modulates their activity. The addition of a poly-lysine or a poly-arginine chain to Mag2 enhances the microbicidal potency without increasing the hemolytic activity [50]. However, an increase of the charge above +5 in Mag2 analogues leads to a decrease of permeabilization property [51] or an increase in their hemolytic ability [52]. The linearity of Mag2 also favors membrane binding, as a cyclic analogue shows lower binding probably due to disadvantageous charge dispatching [53].

3.1.2. *α -helical structure and amphipathicity*

Apart from their high content of cationic residues, a critical feature of magainin family AMPs is the amphipathicity they exhibit when folded to an α -helical structure. This folding arises from contact with other amphiphilic compounds. Isothermal titration calorimetric experiments show that even if anionic charges are necessary to attract the peptides (PGLa) to the membrane surface, they do not play a role in the formation of the secondary structure [49]. CD measurements show that these peptides seem to be unstructured in aqueous solution but have 60% to 80% α -helical content in the presence of anionic liposomes [47, 49, 54]. Raman spectroscopy [38] and Fourier transform infrared spectroscopy [46] give similar results. Solution state NMR reveals that Mag2 forms an α -helix between the 3rd and 22nd residue in TFE [55], and with a slight bend in dodecylphosphatidylcholine (DPC) micelles [56], and that PGLa forms an α -helix between the 6th and 20th amino acid in DPC micelles [57]. The amphipathicity is relevant for the pairing with the lipids and the action on membrane. Indeed, peptides with a reversed sequence of magainin derivatives have an increased bacterial activity, probably due to an enhanced helicity, and hence an enhanced amphipathicity [58, 59]. Figure I.6 depicts the amphipathic feature of the α -helical peptides Mag2 and PGLa. All hydrophobic residues are located on one face of the helix whereas lysine side chains are all located on the opposite face.

3.1.3. Hydrophobicity and polar angle

The overall hydrophobicity of the peptides correlates with their higher affinity to zwitterionic lipids [60]. Therefore, an increase in hydrophobicity is often followed by an increase of the hemolytic potency [61]. The polar angle, which arises from the distribution of polar residues on one side of the peptide helix as depicted in Figure 1.6, is relevant for the membrane binding and permeabilization process. Magainin derivatives with a larger polar angle have better binding potency to lipid vesicles but the permeabilizing activity decreases with a lower anionic lipids content [62].

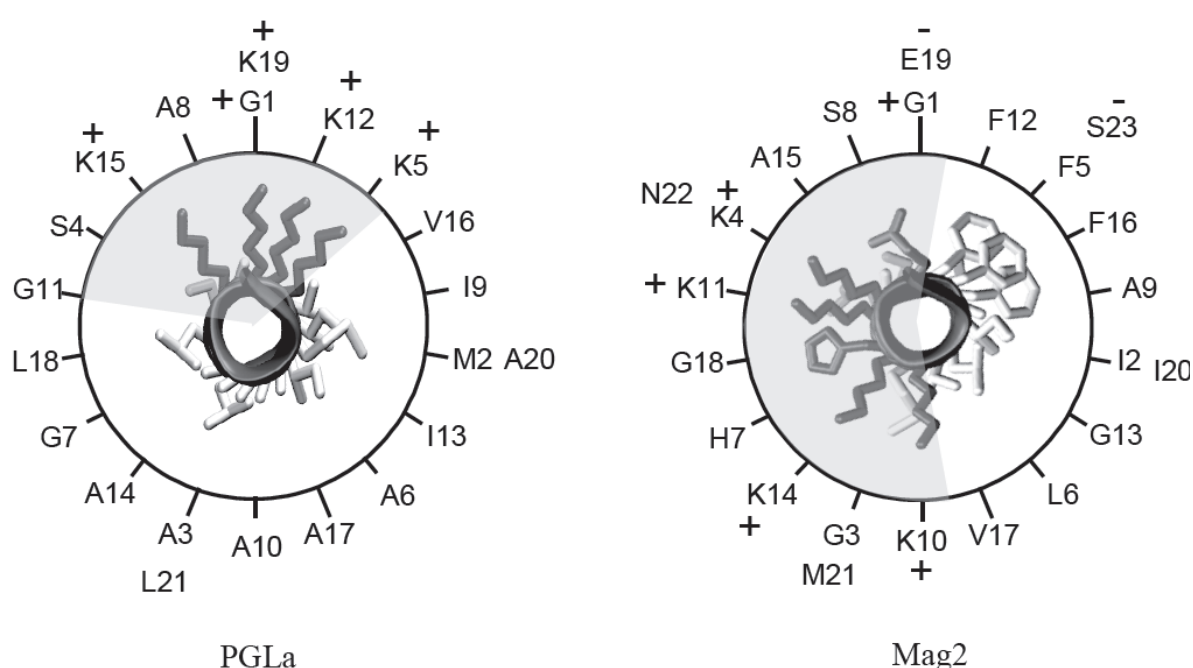


Figure 1.6. Helix axial view of Mag2 and PGLa. Lysine residues are depicted in black color whereas hydrophobic residues are in white. In this projection view, the distribution of polar residues around the helix axis defines the polar angle depicted in grey. One can see that the polar angle of Mag2 is almost twice as large as the polar angle of PGLa.

3.2. Mechanism of membrane disruption

3.2.1. Action on the outer membrane of Gram-negative bacteria

The recent development of atomic force microscopy allows to observe the action and the dynamics of AMPs on live bacteria with better than 0.1 μm resolution, and on a time scale of bacterial cell division. *E. coli* bacteria have been observed upon addition of PGLa or Mag2 above their minimal inhibitory concentration in solution [63-65]. An increase in the surface roughness and the formation of small outer membrane protovesicles were observed. PGLa

exerts an effect similar to that in the presence of EDTA, by competing with Mg^{2+} ions and sequestering them from the LPS shell, which is consequently destabilized [51]. Most damage appeared to first take place at the apical ends of the bacteria which are rich in CL [63]. Bacteria also lose their pili after a few minutes [51].

Even though the interaction of AMPs with the outer membrane is relevant to an increased permeability, it does not directly lead to bacterial killing. The death of the bacteria, which means the loss of capability of growing or dividing in favorable conditions, is attributed to leakage through the cytoplasmic membrane under the action of AMPs, as monitored by K^+ ion efflux from *E. coli* cytoplasm in the presence of Mag2 [66].

3.2.2. Models for cytoplasmic permeabilization

As mentioned, the relevant target of AMPs is the cytoplasmic membrane. The leakage of this membrane has been described according to three different processes reviewed in the general Shai-Matsuzaki-Huang model as depicted in Figure I.7. In the first step of this model, the peptides, just after secretion, are usually unstructured in the aqueous environment. However under certain conditions, the AMPs can also aggregate or assemble together before binding to the membrane. For example, Mag2 forms periodic filaments in aqueous buffer of low pH and high ionic strength [67] and the peptide distinctin is shown to form defined dimers in an aqueous phase to minimize the contact of hydrophobic residues with water [68].

After binding to the membrane and folding into a helix, at low concentration the peptides lie on the surface as shown for PGLa ([IV] and reference therein). A local thinning of the membrane may occur as shown with in-plane neutron scattering for Mag2, alamethicin, and melittin (see [69] for a review and references therein). After reaching a “threshold” peptide concentration, defects can appear on the membrane in different manners according to three different models:

The carpet model: locally, a high concentration of peptides on the membrane surface induces defects and the loss of membrane integrity in a detergent-like manner, with possible formation of micelles. Cecropin and melittin are assumed to follow this mechanism.

The barrel-stave pore model: the gathering of several monomers leads to the re-orientation of the peptide assembly to a transmembrane orientation and a pore is formed. The tightly packed peptide assembly forms a barrel-like structure spanning the membrane. This pore structure has been shown to occur for alamethicin.

The toroidal wormhole model: the peptides assemble with intercalated anionic lipid headgroups to compensate for the charge repulsion [49] and form pores [70-72]. The direct involvement of lipids in the pore structure leads to a toroidal-shaped hole. Mag2 and Mag1 are expected to follow this mechanism. They are shown to re-orient above a threshold concentration as seen by OCD and form pores [72], but with a larger radius than for alamethicin. As a consequence of this pore formation and de-assembly, Mag2 enhances the lipid translocation rate [73]. This can dissipate the electric potential and thus uncouple the respiration of cells [74]. PGLa is also expected to reorient [75] and to form pores [49]. These steps will be discussed in more detail in the present study.

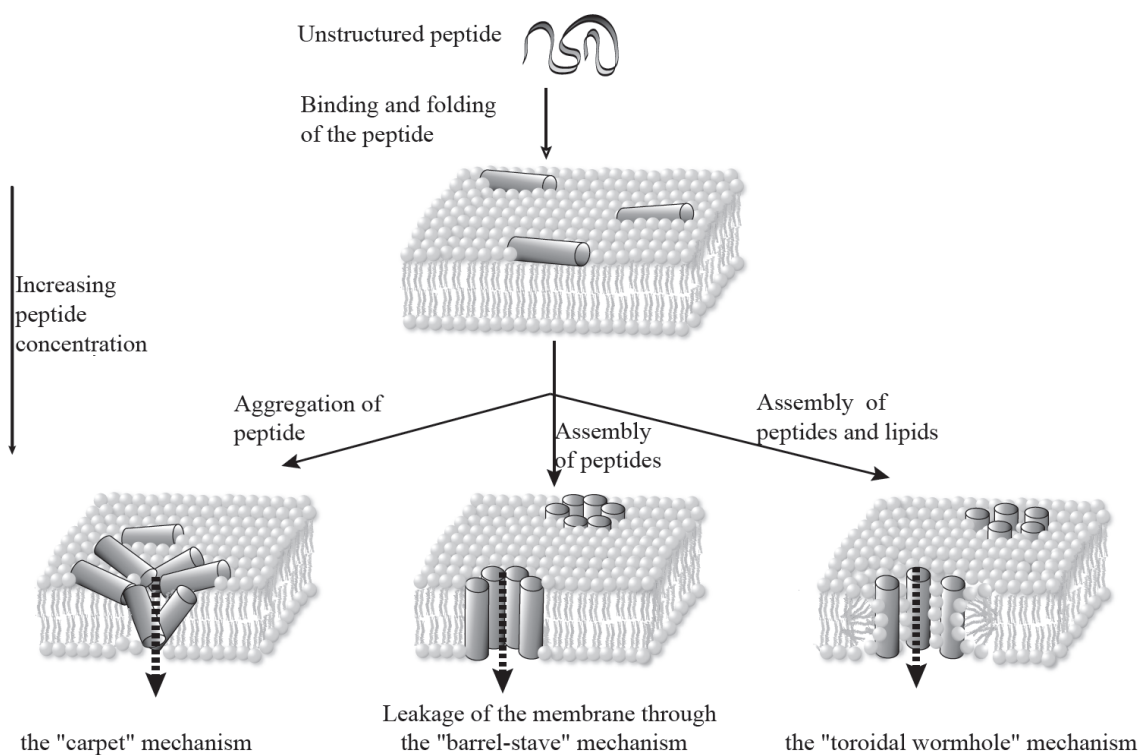


Figure I.7. Depiction of the Shai-Huang-Matsuzaki model for cytoplasmic permeabilization.

3.3. Other functions of AMPs

The role of AMPs has recently been reconsidered. Their functions are much more complex than a simple direct disturbing effect of pathogen membranes. Indeed, this common membrane disordering and permeabilization process has been shown not to be the only possible microbicidal mechanism. As for example the buforin peptide from the toad *Bufo bufo* is found to inhibit bacterial growth through DNA binding [76]. Besides their microbicidal

functions, AMPs also influence the adaptive immune system. For example, α - and β -defensins are known to attract dendritic cells. Magainin related peptides have also some features illustrating the concept of host defense peptides, a term which is nowadays preferred rather than AMP [77, 78]. In this view, the cationic amphipathic peptides are also able to activate the immune system of the host organism. Mag2-amide is found to induce the degranulation of mast cells of rat and the release of histamine, an important compound to induce inflammatory response. This release is a secretory process and is not related to membrane perturbation of the cells. Paradoxically, the high affinity of Magainin 2 and its derivatives peptides for LPS [79, 80] may limit any excess of the host immune response. Pexiganan or MSI-78, a potent Mag2 analogue, has been seen to prevent septic shock in rat models of Gram-negative septic shock [81, 82].

3.4. Bacterial resistance against AMPs

One might think that bacteria could hardly develop resistance against AMPs contrary to commercial antibiotics, as neither a protein receptor nor a DNA motif is usually triggered by AMPs but rather an interaction directly with the whole membrane. In fact, it appears that the plethora of cationic antimicrobial peptides is the consequence of a co-evolution between defender organisms and microbes [83]. There is now an increasing number of reports on the evolution which has shaped the diversity of AMPs. In other words, bacteria are able to acquire resistance [84] as new host defense peptides are selected. For example, the constitution of LPS of *B. bronchiseptica* gives the bacteria a lower affinity to AMPs like Mag2-amide and offers significant shielding [85]. The resistance can also be induced when cationic peptides displace Mg^{2+} from the membrane. This Mg^{2+} depletion induces the PhoP/PhoQ mechanism of several bacteria [86]. As one of the consequences, the lipid composition of the membrane is changed and this minimizes the affinity of the peptide to the membrane. For *Salmonella*, the same mechanism is shown to enhance the production of outer membrane endopeptidases. For bacteria in a dormant state, a reduced membrane potential induces a lower self-uptake force for AMPs. In spite of these mechanisms, the development of resistance against AMPs seems to be a much slower process than against conventional antibiotics [87]. This indicates that the membrane keeps being the foremost relevant target in effective antibiotic development.

4. Conclusions

Gene encoded AMPs are of utmost relevance for the immune system. Compared to the cascade of reactions hailed by the acquired immune system for defense, cationic AMPs exhibit remarkable advantages. Not only are they relatively fast and produced at “low cost” by cells at a site of potential invasion, but even more, they act selectively, efficiently and quickly against a wide spectrum of pathogens through by tackling a relevant target, the pathogen membrane.

Because the membranes of pathogens are a strategic target, one may still develop and optimize news AMPs. However, due to the diversity of membrane constituents and AMPs, any exact mechanisms of interaction have been difficult to describe and still need to be more specifically characterized, as there are plenty of influencing parameters, such as the hydrophobicity, the amphipathicity, or the charge. In the quest of elaborating the mechanism of membrane action, the Mag2 peptide has certainly been the most extensively studied AMP, and a toroidal wormhole model of membrane permeabilization has been proposed as a paradigm for this kind of AMPs [88]. However, the “toroidal wormhole” mechanism is only a model and may not apply to all cationic AMPs. Especially for PGLa little is known on the structure of the membrane pores it could induce. Though it belongs to the same family of magainin peptides, it has different features and antimicrobial properties and may act in a different way.

II. Structural and dynamic information of biological compounds extracted from solid-state ^2H - and ^{31}P -NMR data analysis

In this study, peptides and lipids are the biological compounds of interest. Fortunately, they can be advantageously studied by NMR under experimental conditions close to the conditions of their natural environment. This chapter introduces the basic NMR theory involved in the investigation.

1. Introduction to solid-state NMR spectroscopy

1.1. Origin of the nuclear magnetic resonance: the Zeeman interaction

Nuclear magnetism originates from non-zero spin angular momentum I , integer or half-integer of a nucleus, and from the dipolar magnetic moment μ collinear to it:

$$\mu = \gamma \hbar I \quad (\text{i})$$

where γ is the magnetogyric ratio of the nucleus and \hbar the Planck constant in unit of radian (usually omitted). It is concerned with the behavior of large assemblies of such nuclei leading to a net macroscopic magnetization M :

$$M = \sum \mu \quad (\text{ii})$$

When a uniform magnetic field B is applied, classical electromagnetism gives an equation of motion for a torque, and this leads to:

$$\frac{dM}{dt} = M \times B \quad (\text{iii})$$

The solutions of the equation are the magnetization vectors which precess around B at a frequency $\omega_L = \gamma B$, the Larmor frequency. From the quantum mechanical description, this interaction is called the Zeeman interaction, and its Hamiltonian writes:

$$\hat{H}_{Zeeman} = -\gamma \hat{I} B \quad (\text{iv})$$

If the magnetic field B_0 of the spectrometer is taken along the z axis of a Cartesian frame, $B_0 = (0, 0, B_0)$, the spin operator \hat{I}_z have $2I+1$ eigenstates hence $2I+1$ associated energy levels which are separated by $E_{I,m+1} - E_{I,m} = \gamma B_0$ (in frequency units). From this, it is clear that a

stronger magnetic field allows better energy separation transition between two states. Populations of these states follow a Boltzmann statistical law of distribution. So to enhance the magnetization, the quantity which is expected to be measurable, first, as many identical nuclei as possible have to be considered; second, a high magnetic field has to be used to enhance the energy difference. One sees the difficulty of having a bulk sample to be placed in a homogenous magnetic field of high strength.

If an additive small magnetic field \mathbf{B}_{RF} , perpendicular to \mathbf{B}_0 , is induced with a coil on the sample with an oscillation frequency at or near the Larmor frequency, it can be shown with the same equation (iii) that \mathbf{M} can flip by an angle which depends on the time of the irradiation. This is the resonance phenomenon. After this radio-frequency pulse, the frequency at which the spins flipped, or energy was absorbed, can be measured through the coupling of the sample with the same coil. This reveals the resonance frequency.

1.2. Internal nuclear magnetic interactions

Clearly, the surroundings of the nucleus are neither inert with the external magnetic field nor isotropic. The magnetic field experienced by the nucleus will be different from the external field because of shielding from electron (chemical shielding), and secondly, the considered nuclear spin will be coupled with other particle spins (spin-spin dipolar coupling, J-coupling) or multipole electromagnetic moment (electric quadrupole coupling). Therefore the frequency of resonance will be modified according to its environment and its orientation in the external magnetic field. Description of the surroundings (nuclei in the neighbourhood, orientation of the bonds) is deduced from theoretical knowledge on these interactions.

The NMR interactions of two typical nuclei for biological studies with spin $\frac{1}{2}$ and 1, namely ^{31}P and ^2H are now considered. The first one is naturally found in DNA and, more interestingly here, in phospholipids in biomembranes. The second is a natural isotope of hydrogen but of small natural abundance. Through chemical synthesis, a peptide can be specifically enriched at a defined position [III].

Under a strong external magnetic field, the internal interactions of these nuclei induce generally small changes in the system, and perturbation theory can be used to treat them as first order perturbation of the Zeeman interaction, giving the axis of the external magnetic field B_0 as a quantization axis:

$$\hat{H}_{total} = \hat{H}_{Zeeman} + \hat{H}_{internal} \quad (\text{v})$$

For ^{31}P , the main internal interaction is the chemical shift, whereas for ^2H , the quadrupole coupling is at least one order stronger than the others. These two interactions are now described for static nuclei in a uniform magnetic field \mathbf{B}_0 .

1.2.1. The chemical shift interaction

The chemical shift originates from the electron cloud surrounding the nucleus. The external magnetic field \mathbf{B}_0 induces electrons to circulate around it (diamagnetism) or to mix, in some case, electronic states (paramagnetism). These phenomena respectively reduce and augment the field felt at the nucleus, hence the frequency of resonance. It is clear that the distribution of electrons around the nucleus is not isotropic and reflects the positions of adjacent chemical bonds. However when considering fast random motions or rather re-orientations, as for nucleus in gas or liquid samples, the electron distribution around the nucleus is viewed as spherically averaged and can be considered as isotropic. This is the origin of the isotropic chemical shift denoted σ_{iso} . Having \mathbf{B}_0 as the axis of quantization, the anisotropic part of the interaction tensor to be considered is usually given with a symmetric traceless cartesian second-rank tensor σ . The tensor becomes diagonal in some frame where it can be graphically represented by an ellipsoid volume whose principal axes align with the axes of the frame. This frame is naturally called the principal axes frame (PAF) as depicted in Figure II.1. Then only four other parameters are needed to describe it: δ_σ , the width of the interaction anisotropy, η_σ , its asymmetry (between two defined axes), and two polar angles, θ and φ , to define the orientation of \mathbf{B}_0 with regard to the PAF. Normally three successive rotations with angles α, β, γ , denoted Euler angles, should be used to describe any re-orientation of a Cartesian frame, but as any rotation around \mathbf{B}_0 is being undifferentiated, two are enough.

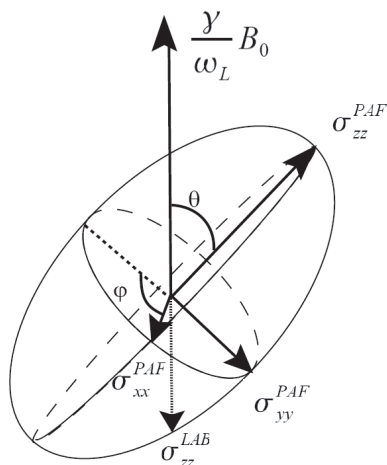


Figure II.1. A second rank symmetric tensor with positive eigenvalues is represented by a tensor ellipsoid where the lengths of the principal axes are functions of the respective eigenvalues σ_{xx}^{PAF} , σ_{yy}^{PAF} , σ_{zz}^{PAF} .

$$\sigma_{xx}^{PAF} = \sigma_{iso} - \delta_{\sigma} \frac{1 + \eta_{\sigma}}{2} \quad \text{(vi)}$$

$$\sigma_{yy}^{PAF} = \sigma_{iso} - \delta_{\sigma} \frac{1 - \eta_{\sigma}}{2}$$

$$\sigma_{zz}^{PAF} = \sigma_{iso} + \delta_{\sigma}$$

Only the component of σ along \mathbf{B}_0 will be quantized, and one has to express the tensor in the laboratory frame (LAB) defined by \mathbf{B}_0 :

$$\hat{H}_{CS} = -\gamma \hat{I}_z \sigma_{zz}^{LAB} B_0 \quad \text{(vii)}$$

Using the Euler rotation matrix $R(\alpha, \beta, \gamma)$ with the two polar angles relative to \mathbf{B}_0 , as shown in Figure II.1, σ^{LAB} can simply be written:

$$\sigma^{LAB} = R^{-1}(0, \theta, \varphi) \sigma^{PAF} R(0, \theta, \varphi) \quad \text{(viii)}$$

and:

$$\sigma_{zz}^{LAB} = \sigma_{iso} - \frac{1}{2} \delta_{\sigma} (3 \cos^2 \theta - 1 + \eta_{\sigma} \sin^2 \theta \cos 2\varphi) \quad \text{(ix)}$$

Hence, the observed chemical shift (CS) is given by:

$$\omega_{CS}(\theta, \varphi) = -\gamma \sigma_{zz}^{LAB} B_0 = -\omega_L (\sigma_{iso} - \frac{1}{2} \delta_{\sigma} (3 \cos^2 \theta - 1 + \eta_{\sigma} \sin^2 \theta \cos 2\varphi)) \quad \text{(x)}$$

1.2.2. The quadrupole interaction

For a spin I , only multipole moments of the electrostatic charge distribution of $2I$ th order exist. In other words, the charge distribution in nuclei of spin $>1/2$ rises an electric quadrupole moment that interact with the electric field gradient. Noticeable is that this interaction does not need an external magnetic field to occur. So has been developed the nuclear quadrupolar resonance (NQR). But in the case of a deuteron in an aliphatic bond, the quadrupole moment is not very strong, and within the high field approximation, the perturbation theory can still be applied giving \mathbf{B}_0 the axis of quantization and only perturbation of the first order must be considered. Its Hamiltonian writes:

$$\hat{H}_Q = \hat{I} \mathbf{Q} \hat{I} \quad \text{(xi)}$$

with \mathbf{Q} being the interaction tensor containing the electric field gradient. Of course the electric field gradient gives no isotropic component, and the tensor can be described in the same way as the anisotropic part of the above mentioned chemical shielding tensor. The components of \mathbf{Q} in the PAF are given as:

$$Q_{xx}^{PAF} = -\delta_Q \frac{1 + \eta_Q}{2}$$

$$Q_{yy}^{PAF} = -\delta_Q \frac{1 - \eta_Q}{2} \quad (\text{xii})$$

$$Q_{zz}^{PAF} = \delta_Q$$

When expressed in the LAB frame with θ and φ the two polar angles as defined in Figure II.1, the component of interest becomes:

$$Q_{zz}^{LAB} = \frac{1}{2} \delta_Q (3 \cos^2 \theta - 1 + \eta_Q \sin^2 \theta \cos 2\varphi) \quad (\text{xiii})$$

Aliphatic bonds are usually axially symmetric, which gives the main principal axis aligned along the C-²H bond, an asymmetry parameter η_Q of zero and a typical value of 125 kHz for δ_Q . ²H has a spin $I=1$ and two transitions are therefore observed. The Zeeman level is split consequently into two with a shift of ν_{Q+} and ν_{Q-} , $\nu_{Q\pm}$ being:

$$\nu_{Q\pm} = \pm \frac{1}{2} \delta_Q (3 \cos^2 \theta - 1) \quad (\text{xiv})$$

The quadrupole splitting is defined by:

$$\Delta \nu_Q = \nu_{Q+} - \nu_{Q-} \quad (\text{xv})$$

From a quadrupole splitting value, one can then directly extract the possible orientation of the C-²H bond with regard to \mathbf{B}_0 . Obviously, for $\arccos \sqrt{2/3} < \theta < \pi/2$, the sign of $\Delta \nu_Q$ can not be known from a single experiment.

In summary, for both interactions, possible orientations of bonds are directly deduced from the shift of the Zeeman frequency. However, biologically active molecules are usually not static and any motion on the time scale of the interaction frequency or higher must be taken into account. Similarities between these interactions should be noticed as well as their symmetry, with $\eta=0$, giving the frequency shift or splitting generated from one angle $\theta \in [0, \pi/2]$ only. Sufficient information is easily extracted from one experimental value considering uniaxially symmetric systems like phospholipid bilayers as shown below. In contrast, for diluted compounds of less symmetry, one may need to use several constraints. The next section deepens the analysis of solid-state NMR data leading to the structural information correlated with the dynamic aspects.

1.3. Influence of motion

1.3.1. Influence of motion for ^{31}P

As described in the first chapter, a functional phospholipid biomembrane is usually in a fluid liquid crystalline phase that leaves the ^{31}P nucleus free to rotate quickly around an axis parallel to the local membrane normal. A tensor which is averaged over the time scale of the CSA interaction strength is then created as depicted in Figure II.2.

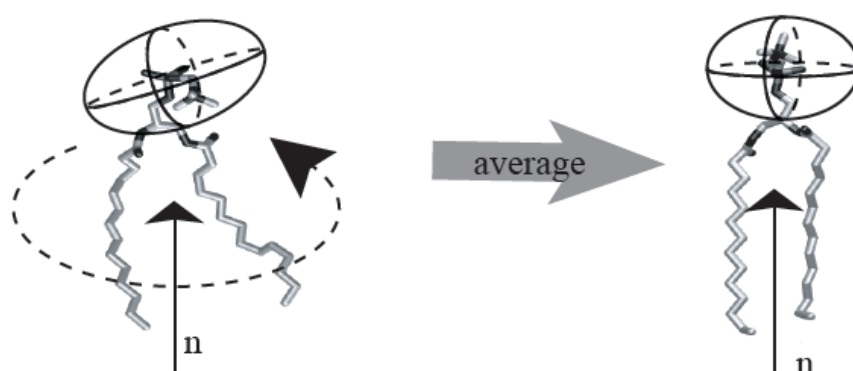


Figure II.2. Within a phospholipid bilayer, the motion of the ^{31}P nucleus can be considered as a fast rotation around the local membrane normal n . The tensor of interaction is as a consequence averaged, giving a new principal axes system aligned with the axis of rotation, hence n .

Using the same Euler rotation tools as above and knowing the polar angles of the tensor with respect to the axis of rotation, the new averaged tensor can be easily calculated. Noticeable is that under this fast rotation, the asymmetry parameter for the new tensor vanishes and the main axis of the PAF aligns with the axis of rotation with a component value given by equation (vi). It follows that ω_{CS} depends solely on polar angle θ between this new principal axis (which is collinear to the local membrane surface normal) and \mathbf{B}_0 . The orientation of the membrane normal is of interest, so measuring the components of the averaged tensor in the liquid crystalline state is fully satisfying. The result of this interaction can now be represented with a typical orbital $\frac{1}{2}(3\cos^2\theta - 1)$ which vanishes for $\theta_m \approx 54.7^\circ$. This angle is called the magic angle.

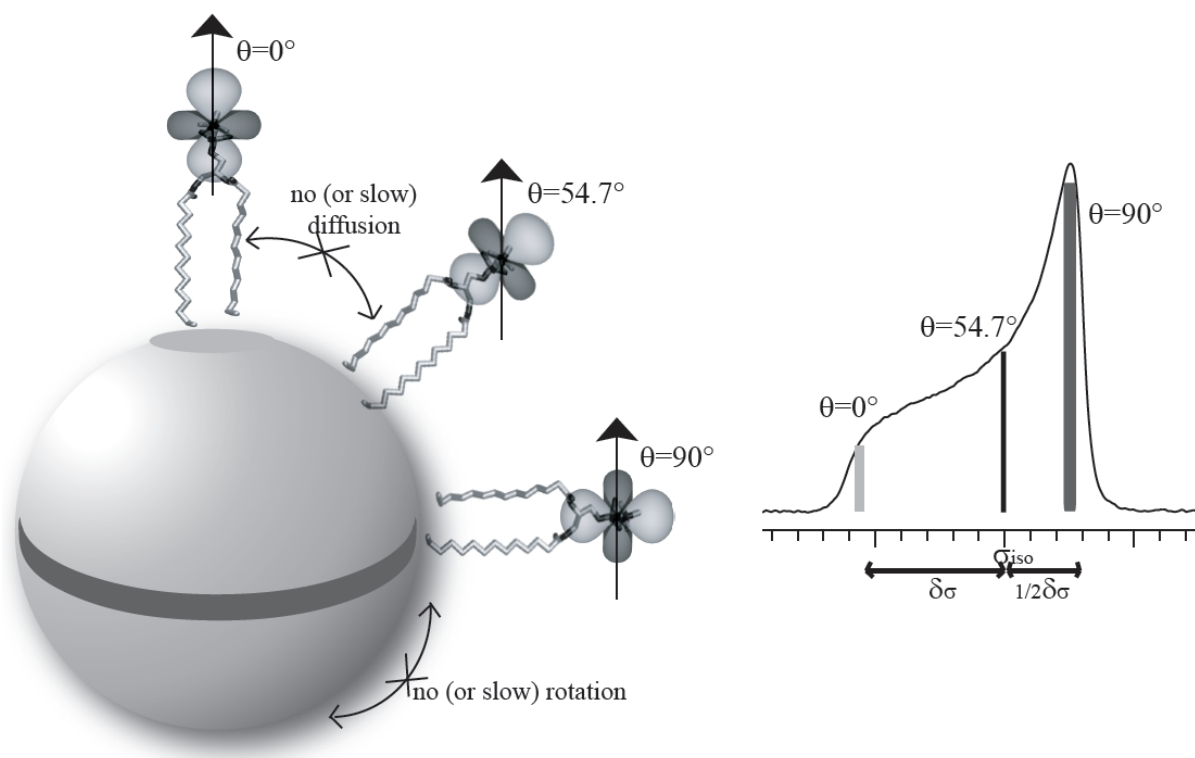


Figure II.3. Lipid molecules composing a large vesicle can be considered as distributed over a spherical surface which does not re-orient and on which lipid molecules have no translational motion. The resulting NMR spectrum is the summation of all individual contributions. The equatorial lipid population contributes the intense signal at the highest shielding ($\theta=90^\circ$). The few lipids at the poles ($\theta=0^\circ$) give a small contribution at the lowest shielding. The lipids oriented with $\theta=54.7^\circ$ give the signal at the isotropic chemical shift.

However, in a membrane, lipids also diffuse in any direction of the surface plane and the whole membrane itself can be subject of re-orientation motions. Interpretation of NMR spectra is then more complicated. In a simple example of lipids distributed over a large sphere as found in large liposomes, given the high curvature radius, their re-orientation after a surface translation (in the timescale of the NMR interaction) is negligible. As diffusion of a particle depends on its size and the viscosity of its environment, a large liposome in a concentrated mixture will not be given the chance of fast re-orientation, and this rotation can also be neglected. Hence the NMR spectrum is obtained by summation of all lipid molecule contributions over the whole surface as illustrated in Figure II.3.

In contrast, small diluted lipid assemblies in solution, like micelles, have fast re-orientation motions, and the anisotropy obviously vanishes. Another situation where the anisotropy is also reduced to zero occurs when the surface topology has a high curvature as in a cubic phase, because in this case, the diffusion of lipids on the liquid crystal surface induces fast isotropic re-orientation. And at last but not least, such anisotropy averaging is also achieved if an external mechanical rotation is applied to the sample around an axis at the

magic angle with respect to \mathbf{B}_0 . A direct application is extensively developed under the name of magic angle spinning (MAS) NMR spectroscopy.

Finally, neglecting other local fluctuations of the membrane surface, there is still a molecular tumbling felt at the nucleus as a result of some random re-orientations. It also contributes to averaging of the anisotropic tensor by some factor. This is often modeled by a scalar factor S_{mol} , or a molecular order parameter, which has a value ranging from 1 in the absence of tumbling, to 0 for fast isotropic tumbling as for small solutes in non-viscous media.

1.3.2. Influence of motion for ^2H

Regarding a deuteron, the same treatment above developed can be followed. Starting from the interaction tensor in its PAF, successive individual or integrated Euler rotations, corresponding to either simple frame transformation or to a tensor averaging, reveal the final contribution to the Zeeman perturbation.

Figure II.4 describes the successive transformations from a deuteron frame to a molecular frame which allow to interpret the NMR signal. The interaction tensor of the deuteron is symmetric around the $\text{C}_\beta\text{-}^2\text{H}$ axis (which generate its principal axis frame D-PAF). The methyl group of 3,3,3- d_3 -alanine undergoes a fast rotation around the $\text{C}_\alpha\text{-C}_\beta$ bond, which can be modelled by discrete hopping of each deuteron between the three equivalent sites. The three deuterons being equivalent, only one has to be explicitly considered. It follows that the tensor is averaged over the $\text{C}_\alpha\text{-C}_\beta$ bond. The angle between $\text{C}_\alpha\text{-C}_\beta$ and any $\text{C}_\beta\text{-}^2\text{H}$ is, in such methyl group, $\alpha = 109.5^\circ$. The averaged tensor Q_{average} obtained can be written in the frame of the methyl rotation axis (giving also the new principal axis frame M-PAF):

$$Q_{\text{average}}^{M\text{-PAF}} = \frac{1}{2}(3\cos^2\alpha - 1)Q^{D\text{-PAF}} = -\frac{1}{3}Q^{D\text{-PAF}} \quad (\text{xvi})$$

Thus from equations (xiv) and (xv), the splitting becomes:

$$\Delta\nu_Q = -\frac{1}{3}\delta_Q(3\cos^2\theta - 1) \quad (\text{xvii})$$

The maximum splitting which can then be measured for a deuterated methyl group is $\Delta\nu_Q = 84$ kHz.

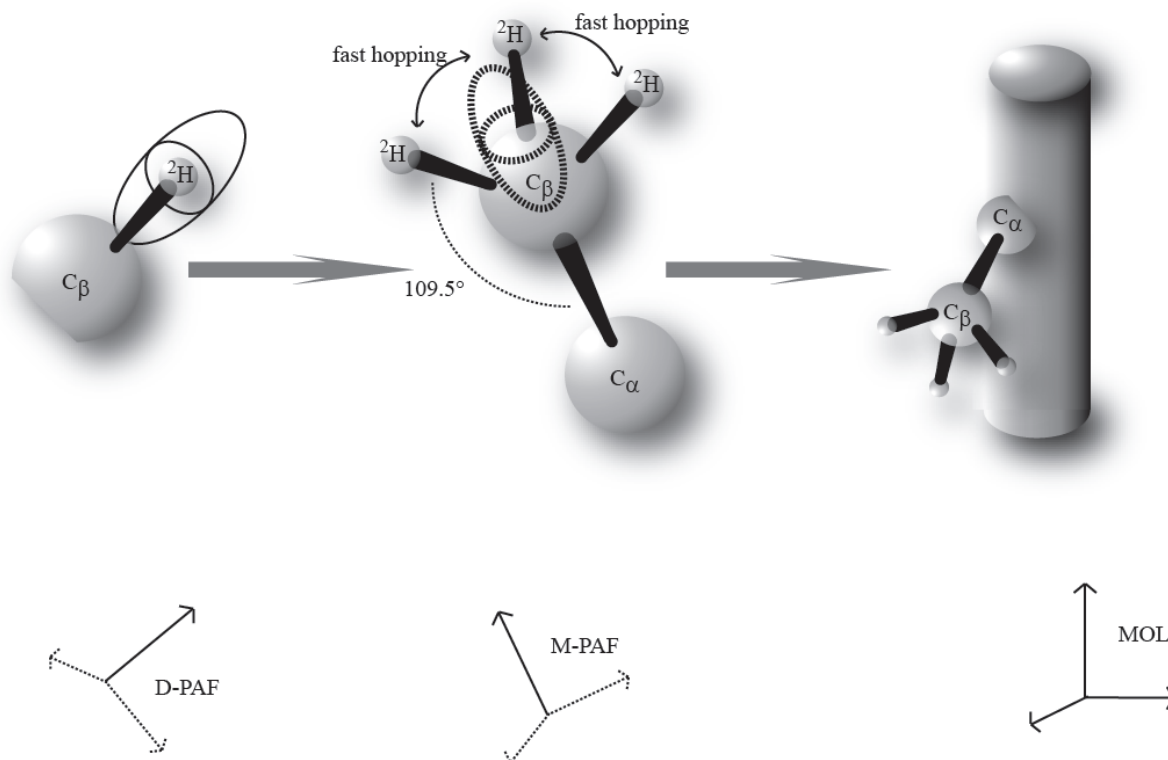


Figure II.4. The quadrupole interaction tensor is aligned along the C_β - ^2H bond which defines the deuteron principal axes frame (D-PAF). The fast long-axial rotation of the methyl group along the C_α - C_β bond creates a new averaged tensor. This tensor is aligned along the C_α - C_β axis giving the methyl principal axes frame (M-PAF). It can be expressed in a different frame like a molecular frame (MOL) in which the orientation of B_0 is also expressed.

The quadrupole tensor is usually expressed in a molecular frame where all atom coordinates are defined. For the model of a rigid body, the coordinates of C_α and C_β are fixed, and so is the orientation of the bond. The tensor can be expressed in the molecular frame (MOL) by a simple rotation. The orientation and motion of this molecular frame relative to the laboratory frame defined by B_0 is now to be determined. If the molecules are static and randomly distributed as it is the case of a powder, then their orientation can be viewed as distributed over a sphere and a typical powder pattern is obtained (as depicted in Figure II.5.) following the same principle of summation as previously described in Figure II.3.

If now each molecule is allowed to rotate fast around an axis of fixed orientation in the molecular frame, the NMR signal for one molecule becomes:

$$\Delta \nu_Q = \frac{1}{2} (3 \cos^2 \xi - 1) \delta_Q (3 \cos^2 \theta - 1) \quad (\text{xviii})$$

where ξ is the angle between the axis of rotation and B_0 , and θ is the angle between C_α - C_β and the axis of rotation as it can be deduced from equations (xvi) and (xviii), and δ_Q is now the quadrupolar constant for the fast hopping methyl group, thus 1/3 of the deuteron quadrupolar constant as seen from equation (xvii).

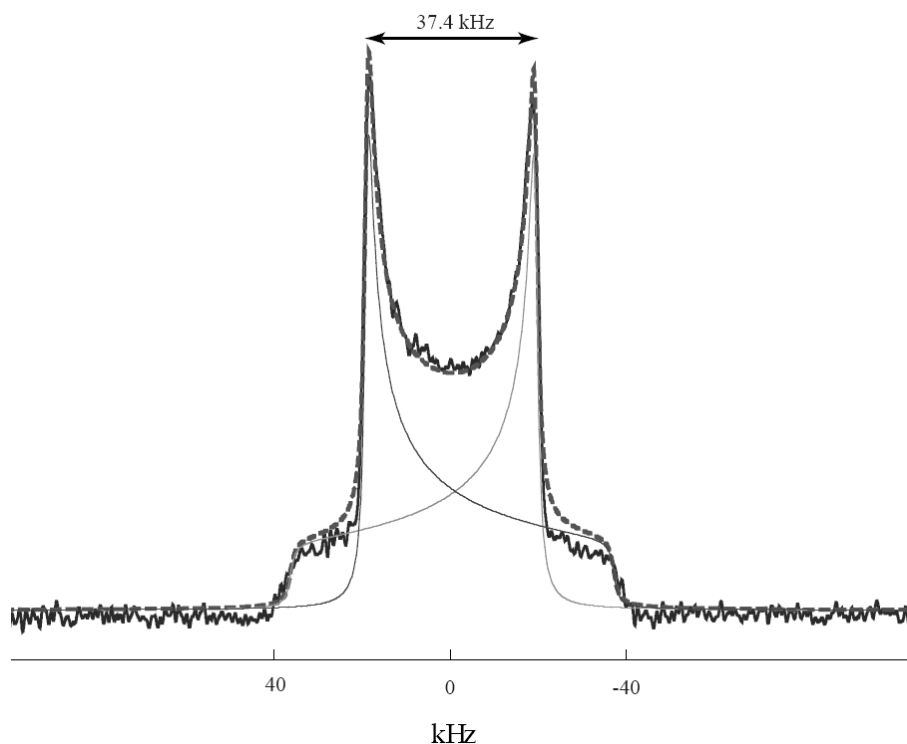


Figure II.5. Experimental ^2H -NMR powder spectrum (thick solid line) of polycrystalline 3,3,3- d_3 -alanine. Due to the two opposite transitions of the spin 1, the spectra can be seen as the sum (dashed line) of two CSA powder spectra with opposite δ_σ (thin solid lines).

When $\xi = 0^\circ$, the effect of this fast rotation is not seen, whereas when $\xi = 90^\circ$, $\Delta\nu_q$ is reduced by a factor of $-1/2$. If the axis of rotation aligns with the surface normal of a sphere, molecules at the equatorial position will produce the higher signal from which θ can be deduced. A remarkable example is when the molecule is a rigid peptide bound on the surface of a membrane but is still allowed to rotate around the membrane normal.

As for lipids, further motional averaging can reduce the splitting. This is described by the same global molecular order parameter S_{mol} .

1.3.3. The Saupe order matrix and the generalized degree of order

Analysing NMR data of a solute in a uniaxial liquid crystalline phase consists of getting the interaction components along B_0 which contain all the order parameters of the system. An order parameter is a measure of the degree of spatial restriction of the motion. Indeed this notion was intuitively introduced in two similar kinds of models: the continuous fast rotational diffusion of a lipid phosphorus head group and the fast discrete hopping of the deuteron in a methyl group, both motions being restricted to a cone. The homogeneous fast diffusion of a peptide in a cone around the axis given by the membrane normal was also

envisaged by equation (xviii). These orders reduce the width of the anisotropy by a constant positive or negative factor.

On top of these orders, the molecular order parameter S_{mol} was defined as the empirical value containing all other motions which reduce the anisotropy of an interaction by a constant absolute factor. In other words, S_{mol} is often considered as the random isotropic deviation of a molecular vector from a director (B_0).

However, the peptides in this study do not have any symmetry, even if their overall amphipathic cylindrical shapes make it appear so. Their motion when bound to a membrane may be highly anisotropic and complex. The S_{mol} parameter is clearly applicable only for spherical compounds, but one has to remember that zero anisotropy contribution can also originate from motion around an axis near the magic angle. Indeed the splittings $\Delta\nu_Q$ has to be evaluated as:

$$\Delta\nu_Q = \delta_Q \langle 3\cos^2\theta - 1 \rangle \quad (\text{xix})$$

The angular brackets express a time average and gather all variations of θ , the angle between B_0 and the C_α - C_β bond. In a molecular frame of the rigid molecule the angles α_i of the bond C_α - C_β with regard to the axis i are known whereas the angles β_i , between B_0 and the axis i , are the ones containing the ordering of the molecular orientation as depicted in Figure II.6. Equation (xix) can be then rewritten as:

$$\Delta\nu_Q = \delta_Q \sum_{i,j=x,y,z} S_{ij} \cos\alpha_i \cos\alpha_j \quad (\text{xx})$$

Using the Kronecker function δ_j^i ($\delta_j^i = 1$ if $i=j$, $\delta_j^i = 0$ otherwise), the S_{ij} parameters are defined by:

$$S_{ij} = \frac{3}{2} \langle \cos\beta_i \cos\beta_j \rangle - \frac{1}{2} \delta_i^j \quad (\text{xxi})$$

Given the uniaxial quantization B_0 , they constitute only a 3×3 matrix called the Saupe order matrix. It is a symmetric, real, traceless matrix. It possesses five independent components and can be expressed in a frame where it becomes diagonal with the three elements S_{xx} , S_{yy} , S_{zz} . An asymmetry or rhombicity parameter can be defined as previously by $\eta = (S_{xx} - S_{yy})/S_{zz}$. Thus the determination of the order matrix elements gives not only the orientation information of the molecule but also affords two order parameters. These parameters express the motional averaging along the direction of highest order S_{zz} , and η the asymmetry in motion about this axis or the rhombicity. When $\eta = 0$, the molecule is said to undergo a uniaxial motion, and when $\eta \neq 0$ a biaxial motion.

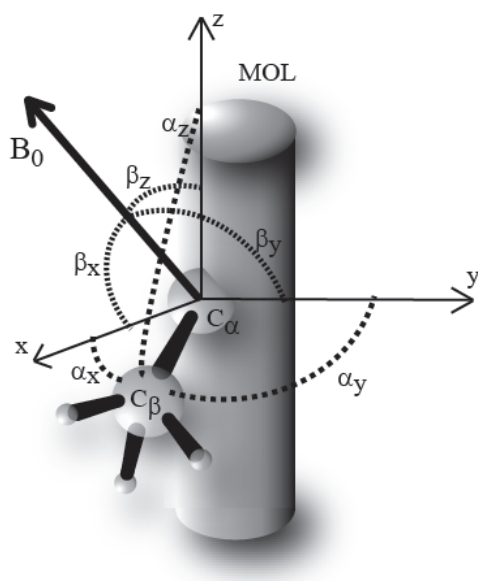


Figure II.6. In a frame (MOL) of a rigid molecule, the angles α_x , α_y , and α_z , describing the position of the interaction tensor with respect to the x, y, and z axes are known. Experimental measurements yield probabilities for the angles β_x , β_y , and β_z , defining B_0 within the molecular frame or the ordering of the molecule.

One can then define a global degree of order GDO to have a simple scalar description of the overall motion of the system with:

$$GDO = \sqrt{\frac{2}{3} \sum_{ij} S_{ij}^2} \quad (\text{xxii})$$

In the special case of a uniaxial motion of the molecule, i.e. $\eta = 0$, the GDO simply becomes equivalent to the previously mentioned order parameter S_{mol} .

2. Structure analysis: Orientation determination of peptides bound to a membrane

2.1. Methods of solution calculation and error assessment

Let us consider a peptide bound to a lipid bilayer, folded in a defined secondary structure, and labeled with one 3,3,3-d₃-alanine residue (Ala-d₃). The orientation and the motion of this peptide in the membrane are of interest. This desired information, as presented in Figure II.7, has to be extracted from NMR measurements of several labeled peptides. To some extent, to be discussed later in the case of PGLa, the peptide backbone can be considered as a rigid body. Hence, the deuterated methyl group is directly attached to the rigid peptide backbone and can rotate freely around the C_α-C_β bond. Having set a molecular frame for this peptide, the orientation of the interaction tensor from the methyl in its frame is fully known and can be related to the laboratory frame through NMR measurements depending on

its motion. In a first simple motional model, one can assume that the whole molecule undergoes isotropic wobbling, whereas in a more sophisticated biaxial motion model, the re-orientation with respect to B_0 of the C_α - C_β bond, hence the re-orientation of the peptide in the rigid body assumption, will not be equivalent in all directions.

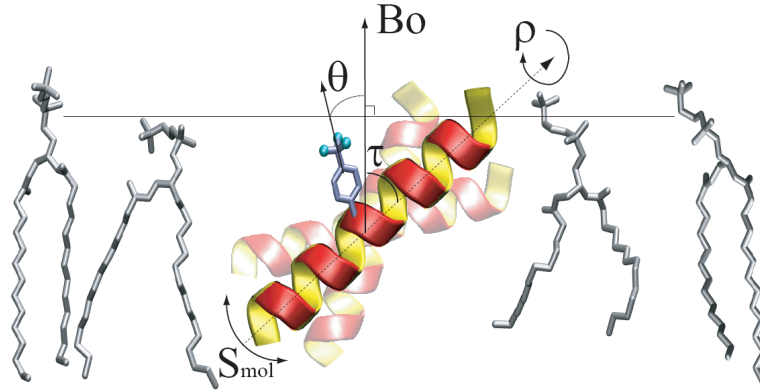


Figure II.7. From NMR measurements of $\Delta\nu_q < \theta >$ of several labeled residues, the orientation of the peptide bound to the lipid membrane can be determined. It is defined by motional averaging parameters contained in S_{mol} and two polar angles τ and ρ . τ is the tilt relative to the membrane surface normal and ρ is the rotation angle around the helix axis. (Molecules are generated using the VMD software [89]).

In the first model, the angle θ_i between the C_α - C_β bond of the residue i and B_0 is considered. It is expressed as a function of τ and ρ . The entire molecule is also subject to wobbling motions leading to a narrowing effect of the splitting contained in the S_{mol} parameter which reduces all splittings with a constant factor. The value of $\Delta\nu_q^i$ from a peptide labeled at the residue i is then given by:

$$\Delta\nu_Q^i = S_{mol} \delta_Q (3 \cos^2 \langle \theta_i(\tau, \rho) \rangle - 1) \quad (\text{xxiii})$$

For each labeled residue, splittings are calculated ($\Delta\nu_Q^i(\text{calc})$) as a function of $(S_{mol}, \tau, \rho) \in [0,1] \times [0,\pi] \times [0,\pi]$, and these splittings can be compared with experimental values ($\Delta\nu_Q^i(\text{exp})$). Using a least-square deviation method, a solution ensemble of (S_{mol}, τ, ρ) within a defined error range is given by minimizing the RMSD function evaluated as:

$$RMSD = \sqrt{\frac{1}{N} \sum_i^N (\Delta\nu_Q^i(\text{exp}) - \Delta\nu_Q^i(\text{calc}))^2} \quad (\text{xxiv})$$

Although solution ensembles are obtained even with one experimental value, a minimum of four data points are required to get interpretable results because, apart from the fact that there are three unknown parameters, the sign of $\Delta\nu_Q$ is often not known.

The second way is based on solving the equation (xx), hence determining the Saupe order matrix. As there are five independent matrix elements, at least five $\Delta\nu_Q^i$ values from five non-collinear C_α - C_β bonds are needed to fully determine the matrix. Also here, the missing sign of the splitting must be taken into account. If more values are available a singular decomposition (SVD) method can be used to solve the equations. This gives the best solution in an RMSD sense.

The first model has been implemented in a small but efficient FORTRAN program written by E. Strandberg [3, 4, 90]. The second approach was integrated with a C language program, essentially for residual dipolar coupling analysis under the name of Orderten_SVD [91, 92]. It was later developed further and supplemented with a graphical user interface to form the Redcat software [93]. It can be used for any NMR tensor interaction with zero asymmetry parameter. It also allows getting solutions in a defined subspace if the system is under-determined. Both afford graphical means to view the solution ensemble and to assess the accuracy of the fit to experimental data.

2.2. Experimental section

2.2.1. Peptide structure model

In the whole study, the PGLa molecule was modeled as a regular α -helical peptide as deduced from an α -helical poly-alanine model structure constructed in SYBYL with the torsion angles $\varphi=-58^\circ$ and $\psi=-47^\circ$. The angles describing the orientation of the C_α - C_β bond of Ala-d₃ are $\varepsilon_{//}=121.1^\circ$ and $\varepsilon_{\perp}=53.2^\circ$. $\varepsilon_{//}$ is the angle between C_α - C_β and the helix axis. In the plane perpendicular to the helix axis and passing by C_β , ε_{\perp} is the angle between the projection of C_α - C_β in this plane. The peptide molecular frame is defined with the helix axis aligned along the z axis and the vector from the helix axis to the C_α atom of the lysine residue at position 12 defines the y axis. Thus the two angles describing the orientation of the peptide in the laboratory frame are τ , the angle between B_0 and the z axis if the molecular frame and ρ , the azimuthal rotation around the z axis of the molecular frame as depicted in Figure II.8.

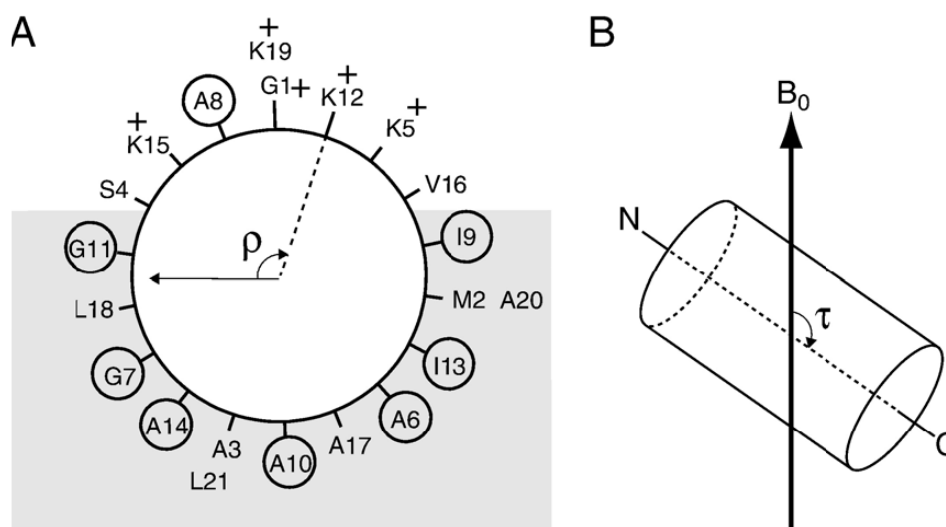


Figure II.8. (A) Helical wheel projection of PGLa. Charged lysine residues and the N-terminus are marked with +, and residues labeled with Ala- d_3 [III.1] are marked with circles. The grey box represents the hydrophobic domain. The ρ angle is defined by the rotation of the peptide around the helix axis. (B) The helix tilt angle τ is defined as the angle between the peptide long axis and the membrane normal, which in oriented samples is aligned parallel to the external magnetic field B_0 . In the figure $\tau=125^\circ$. (Adapted from [3])

2.2.2. Solid-state NMR sample preparation

A word on the samples

This study deals with the interaction of peptides with lipid membranes, and the relative orientations of the molecules of interest. The investigated samples should consequently display orientational information. For solid-state NMR spectroscopy (in a static mode), there are mainly two possibilities for preparing such samples.

One is to let the features of the lipids shape the topology of the membrane. It is driven by the minimization of water-hydrophobic chain contact and curvature strain. For example, when some lipids like DMPC are mixed with a small amount of water, multilamellar vesicles (MLVs) are spontaneously formed. Typically a hydration of 50% w/w is used and is more than enough for a complete hydration of the lipid head groups [94]. MLVs consist of onion like structured vesicles of high radius interleaved with thin water layers, and with excess water inbetween the MLVs. Their relative motions are then limited.

Another way to prepare the sample is to use a macroscopic support for the orientation. A usual example is the “sandwich” like sample. When lipids are deposited between two planar glass plates and are slowly hydrated, they form multi-layers which align their surfaces with the glass plates. Other solid supports have also been reported to be used, for example arrays of nano-tubes in an alumina matrix [95].

The second method has the advantage of providing all lipid bilayers with a uniform orientation, hence greatly simplifying the interpretation of NMR spectra. The membrane surface can be oriented at wish with respect to the magnetic field of the spectrometer. One disadvantage is the filling of an significant part of the NMR coil with glass plate material, reducing the amount of membrane sample that can be measured. In contrast, the first method allows a much higher effective sample volume. Unluckily, in the latter case the NMR signal has to be interpreted with respect to the topology of the vesicles which makes the analysis more complicated and less informative.

Sample preparation

List of materials and reagents

Dimyristoylphosphatidylcholine (DMPC)	Alexis Biochemicals (Lausen, Switzerland) or Avanti Polar Lipids (Alabaster, AL, USA)
Dimyristoylphosphatidylglycerol sodium salt (DMPG)	“
Deuterium-depleted water	Acros (Geel, Belgium)
Methanol (UV grade)	Merck (Darmstadt, Germany)
Chloroform (UV grade)	“
Thin glass plates (18 mm×7.5 mm×0.08 mm)	Marienfeld Laboratory Glassware (Lauda-Königshofen, Germany)

The appropriate amounts of peptides and lipids were co-dissolved in a mixture of methanol/chloroform (1:3). Occasionally a small amount of water was added to samples containing DMPG. Non-oriented MLV samples were prepared as lipid dispersions. Typically, 2 mg of peptide were co-dissolved with an appropriate amount of lipid, and the solution was dried under vacuum overnight to remove all traces of solvents. Deuterium-depleted water was added to obtain a hydration of normally 50% (w/w of total sample), or in some specified cases either 40% (w/w) or 75% (w/w). The hydrated mixture was vigorously vortexed and freeze–thawed several times to yield homogeneous multilamellar vesicles. The MLV samples were packed in a polyethylene bag and sealed.

Samples oriented on glass plates (GP samples) were prepared by depositing aliquots of the peptide/lipid solution in methanol/chloroform onto thin glass plates. Typically, 2.5 mg of peptide were mixed with almost 20 mg of lipids and diluted in 200 μ L methanol/chloroform solution to prepare samples with a P/L=1:20 (and distributed over 15 glass plates), and 2 mg of peptide with almost 35 mg lipid for P/L=1:50 (spread on 24 glass plates). The samples were dried overnight under vacuum, stacked and covered with an additional clean plate. The stack was hydrated for 36 h at 45°C in a humidity chamber over a saturated solution of K₂SO₄ in deuterium-depleted water, giving a relative humidity of 96%. The hydrated sample was

wrapped in parafilm, packed into a polyethylene bag and sealed. All samples were stored at -20°C prior to measurements.

2.2.3. NMR spectroscopy

List of NMR spectrometers and software

Bruker Avance 500 MHz wide bore NMR spectrometer	Bruker BioSpin (Rheinstetten, Germany)
Bruker Avance 600 MHz wide bore NMR spectrometer	“
Topsin 1.3 Data acquisition and processing software	“

^{31}P -NMR experiment were performed at a frequency of 202.5 MHz or 242.9 MHz, using a Hahn echo sequence with phase cycling [96] with a 7 ms 90° pulse, 30 μs echo time, 2 s relaxation delay time, 100 kHz spectral width, 4096 data points, and proton decoupling using tppm20 [97]. Additional ^{31}P -NMR experiments were performed at 121 MHz with a Bruker probe head for 5mm sample rotors. Typically, 128 to 512 scans were collected, and spectra were processed by left-shifting the free induction decay to start at the echo maximum, zero filling to 16,384 data points, and a 100 Hz exponential multiplication before Fourier transformation.

^2H -NMR experiments were performed at 76.77 MHz or 92.12 MHz using a quadrupole echo sequence [98] with a 4.5 ms 90° pulse, an echo delay of 30 ms, an 80 ms relaxation delay time, 250 kHz spectral width, and 2,048 data points. Between 300,000 and 1,000,000 scans were collected. Acquisition was started before the echo and the time domain data was left-shifted to get the free induction decay starting at the echo maximum before further processing by zero filling to 16,384 data points and a 400 Hz exponential multiplication followed by Fourier transformation.

During all the experiments, the temperature was controlled by a heated dry air flow and kept at 308 K.

III. Synthesis and characterization of labeled peptides

NMR spectroscopy deals with nuclei of spin $I > 0$. In biological compounds, such nuclei are naturally present (^{31}P , ^{13}C , ^1H of spin $\frac{1}{2}$, ^{14}N of spin 1), or alternatively can be incorporated in order to enhance the NMR signal or to get specific information. Nuclei, at defined sites, can be substituted or enriched by NMR-active isotopes (^1H by ^2H , ^{12}C by ^{13}C , ^{14}N by ^{15}N), or be replaced by a different nucleus (^1H by ^{19}F). These substitutions either provide more NMR-sensitive nuclei, or overcome the natural abundance background. Sometimes a whole side-chain of a residue can be mutated to incorporate the NMR-active nucleus of interest. As explained in the next section, Ile and Gly can be replaced by a deuterated Ala in a peptide for NMR purposes. These mutations have to be “silent” in terms of biological properties of the peptide. Some biological tests allowing to evaluate the biophysical modifications on structure and function of the peptides are also described.

1. Synthesis and purification of the peptides

1.1. Principle of solid phase peptide synthesis (SPPS) and HPLC purification

1.1.1. SPPS

The usually used solid phase peptide synthesis is a methodology initiated by Merrifield in 1963 [99]. The concept does not reflect what really occurs as it is not a true heterogeneous phase contact reaction. In fact, solute reagents react on a growing peptide chain which is linked to a pseudo-solid, indeed solvent-swollen, polymer matrix. The beauty of the idea resides in the possibility to use very large excess of reagents and to wash out by-products by a simple filtration step of the polymer beads, hence boosting the kinetics of the reaction and avoiding long lasting chromatographic purification protocols. For a Fmoc (9-fluorenylmethoxycarbonyl) strategy [100], successive cycles of Fmoc-deprotection with piperidine and Fmoc-protected amino acid coupling to the freshly deprotected N-terminus with interleaved suitable washing/filtration steps constitute the core of SPPS as depicted in Figure III.1.

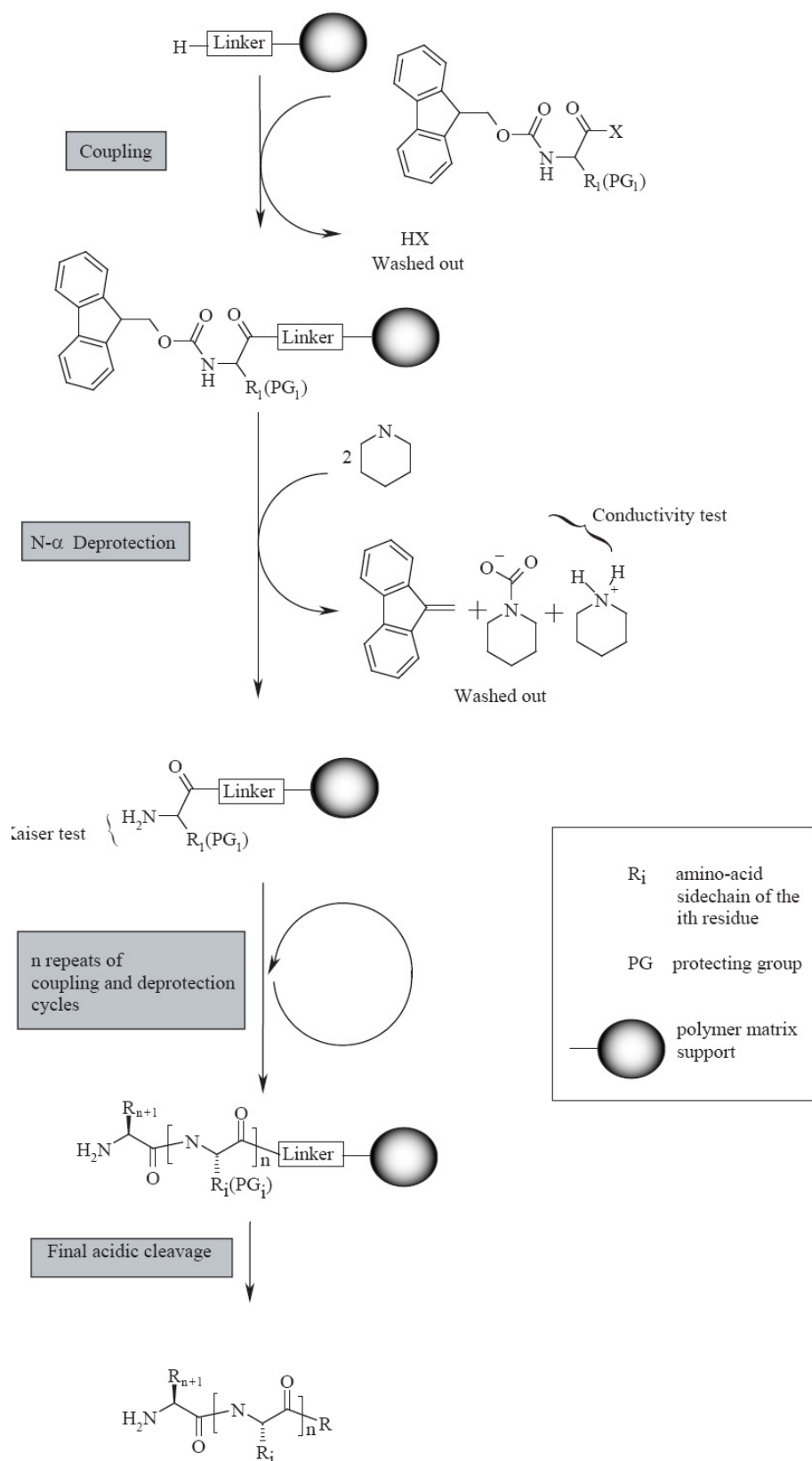


Figure III.1. SPPS cycle for a N- α -Fmoc protection strategy.

A final acidic cleavage procedure releases the peptide from the resin. Suitable choices of the peptide-resin linker and of the amino-acid side chain protecting groups allow different synthesis strategies to obtain peptides where some functional orthogonal groups could be kept protected for further chemical processing.

Problems arise if coupling or deprotection reactions are not quantitative or if orthogonal protecting groups does not stand ongoing reaction conditions as they should. Depending on the peptide sequence, steric hindrance from bulk amino acid, folding of the peptide, and badly swollen matrix are also source of difficulties. This may lead to deletion in the sequence or to a dendritic growth of the peptide and produce a final mixture of undesired peptides. Given that long reaction times are undesirable because racemization processes are then much more likely to occur, one has to use efficient coupling reagents and effective solvents in an optimized procedure. After a coupling step, an efficient capping of the unreacted free NH_2 groups may overcome some of the problems. Furthermore, to ensure completion of the coupling or deprotection reactions, diverse monitoring methods are also used:

- A colorimetric method: the Kaiser Test where free NH_2 groups are unraveled by the blue color of Ruhemann's purple.
- A conductivity method: piperidine-carbamate salts released from Fmoc deprotection change the resistivity of the solution (see Figure III.1).

1.1.2. HPLC

Even when the process is optimized for a successful SPPS, the crude product released from the final cleavage step may often be a mixture containing not only the desired peptide, but also protecting group by-products, scavengers from the cleavage solution and unwanted peptides (*vide supra*). Fortunately, development of highly pressurized liquid chromatography or high performance liquid chromatography (HPLC) systems equipped with a so called reversed-phase (RP) column can drastically enhance the efficiency of peptide separation and purification. Micrometer-sized silica based beads tightly packed in a shielded column which gives rise to an increased surface contact and high theoretical plate numbers. High pressure pumps able to reasonably flush this column with constant flow, limiting any diffusion of eluted compounds has sharpened the separation resolution. Highly hydrophobic alkyl or phenyl chains coating the silica beads and polar eluent are used, which is in reverse to the principles of standard chromatography. This coating constitutes a stationary apolar phase whereas the mobile phase has a variable polarity which is controlled through solvent mixing.

The retention time in the column is driven by the composition of this mobile phase which switches off at will the hydrophobic affinity of the compounds toward the stationary phase. When purifying ionic or acidic products one has to use adjuvant to stabilize the pH and chasing out other counter-ions which would give different physical behaviors of the eluted products.

RP-HPLC coupled with mass spectrometry unit has now for years been the tool of choice for peptide and protein analysis and purification.

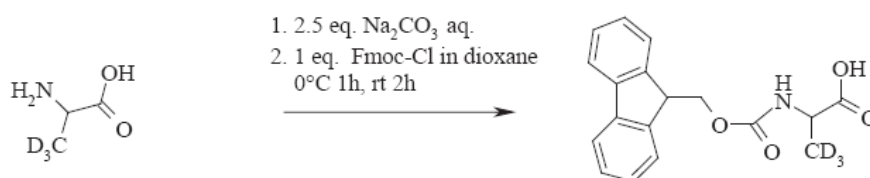
1.2. Materials and methods

List of reagents

Acetonitrile (ACN) HPLC grade	Fischer Scientific (Leicestershire, UK)
Acetonitrile (ACN)	Fluka (Buchs, Switzerland)
2 Cl-Triyl chloride resin	Iris Biotech (Marktretwitz, Germany)
Diethylether	Merck (Darmstadt, Germany)
Dimethylformamide (DMF)	“
Ethanedithiol	“
Ethylacetate	“
Fmoc-L-Asn-OH	Iris Biotech (Marktretwitz, Germany)
Fmoc-Cl	“
Fmoc-L-Glu(OtBu)-OH	“
Fmoc-Gly-OH	“
Fmoc-L-His(trt)-OH	“
Fmoc-L-His(boc)-OH	“
Fmoc-L-Ala-OH	“
Fmoc-L-Leu-OH	“
Fmoc-L-Ile-OH	“
Fmoc-L-Lys(Boc)-OH	“
Fmoc-L-Met-OH	“
Fmoc-L-Phe-OH	“
Fmoc-L-Ser(tBu)-OH	“
Fmoc-L-Val-OH	“
Glass beads (150-212 μm)	Sigma-Aldrich (Seelze, Germany)
2-(1H-benzotriazole-1-yl)-1,1,3,3-tetramethyluronium hexafluorophosphate (HBTU)	Iris Biotech (Marktretwitz, Germany)
HCl (1M)	Merck (Darmstadt, Germany)
Hydroxybenzotriazol (HOBt) anhydrous	Iris Biotech (Marktretwitz, Germany)
L-Alanine-3,3,3- d_3	Cambridge Isotope Laboratories (Andover, MA, USA)
Methanol (MeOH)	Fischer Scientific (Leicestershire, UK)
MgSO_4	Roth (Karlsruhe, Germany)
Na_2CO_3	Roth (Karlsruhe, Germany)
Piperidine	Roth (Karlsruhe, Germany)
Fmoc-Rink-amide MBHA resin	Iris Biotech (Marktretwitz, Germany)
Trifluoroacetic acid (TFA)	Sigma-Aldrich (Seelze, Germany)
Triisopropylsilane (TIS)	Sigma-Aldrich (Seelze, Germany)

List of devices and softwares

Peptide Synthesizer 433A	Applied Biosystems (Foster City, CA, USA)
SynthAssist Software Version 2.0	Applied Biosystems (Foster City, CA, USA)
5 mL manual SPPS reaction columns	ABIMED Analysentechnik, (Langenfeld, Germany)
Lyophilizer Christ Alpha 2-4	Martin Christ (Osterode, Germany)
HPLC/MS Agilent 1100 Capillary LC System	Agilent (Palo Alto, CA, USA)
ESI-TOF mass spectrometer	Bruker Daltonics (Bremen, Germany)
HPLC pumps PU 2087Plus	Jasco (Tokyo, Japan)
HPLC diode array detector MD-2010	Jasco (Tokyo, Japan)
HPLC analytical C18 column VYDAC CAT.#218TP54	Vydac (Hesperia, CA, USA)
HPLC preparative C18 column VYDAC CAT.#218TP1022	Vydac (Hesperia, CA, USA)

Synthesis of *N*- α -Fmoc-L-3,3,3- d_3 -Alanine according the procedure of Carpino et al. [101]Figure III.2. Synthesis of *N*- α -Fmoc-L-3,3,3- d_3 -alanine.

Typically, L-3,3,3- d_3 -alanine (1 g, 10.85 mmol, 1.0 eq.) was completely dissolved in an aqueous solution of Na₂CO₃ (10% v/v, 27.12 mmol, 2.5 eq.). The resulting solution was cooled in an ice bath to 0°C. Fmoc-Cl (10.74 mmol, 1.0 eq.) previously dissolved in dioxane (10 mL), was added dropwise to the stirred reaction mixture. The mixture was stirred for 1 h at 0°C and an additional 2 h at room temperature. The reaction mixture was poured into H₂O (800 mL) and extracted with diethyl ether (2×100 mL) to remove small amounts of 9-fluorenylmethanol and dibenzofulvene. The aqueous phase was cooled in an ice bath to 0°C and subsequently acidified to red Congo pH paper with concentrated HCl. The resulting white precipitate was extracted with ethyl acetate (2×200 mL). The ethyl acetate extract was washed with water (200 mL), dried over MgSO₄. The solvent was rotary evaporated in vacuum until a white solid product remained. The product was identified with FAB-MS and analysed by HPLC using an analytical column with standard analytical method (vide infra). HPLC chromatogram of commercial *N*- α -Fmoc-L-alanine was used for referencing.

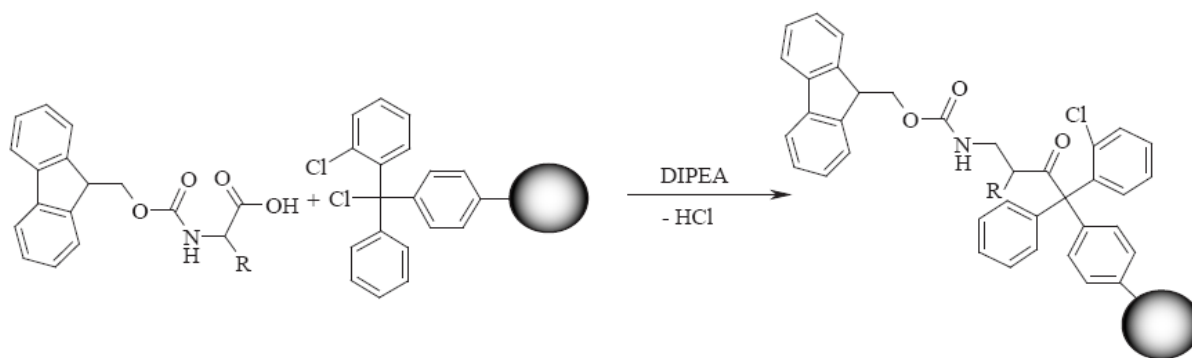
Loading of the trityl resin

Figure III.3. Loading of the 2-chlorotrityl resin.

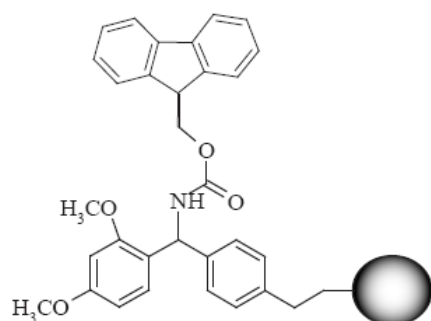
2-Chlorotrityl resin was used for the synthesis of Mag2, Mag1, and Mag2(E19Q) peptides. Typically, Fmoc-Ser(tBu)-OH (1 g, 2.61 mmol, 1 eq. to resin) and DIPEA (0.41 μ L, 10.5 mmol, MW 129.2, d 0.78, 4 eq.) were dissolved in dry DCM (10 mL). A few drops of DMF were added to help for the dissolution of the amino-acid. The mixture was added to 2-Chlorotrityl chloride resin (1.8 g, 1.41 mmol/g initial chloride loading, 1 eq.) which was pre-swollen in DCM. The mixture was gently stirred at rt for 2 h and filtered. The resin was then washed with a DCM/MeOH/DIPEA (17:2:1) solution (2 \times 10 mL) to substitute the remaining chloride on the resin. This was followed with sequential washes once each with DCM (10 mL), with DMF (10 mL), with DCM (2 \times 10 mL), and finally with MeOH (10 mL). The resin was then dried overnight in vacuum over KOH and submitted to resin loading determination protocol.

Resin loading determination

Resin loading is measured by a simple concentration determination using a UV method based to quantify released Fmoc groups. An estimated 5 μ mol of Fmoc-Ser loaded on the resin was weighed (estimated loading 1mmol/g) and submitted to deprotection for 20 min in piperidine in DMF solution (20% v/v, 1 mL) with intermittent shaking. The resin was allowed to settle down and the solution was transferred to silica-UV cells. The absorbance was read on a UV-vis spectrometer at 280 nm and the blank was set with piperidine in DMF solution. Three measurements were done and averaged. The loading was estimated according the formula:

$$\text{mmol/g} = \text{Abs}/(1.65 \times \text{mg of resin})$$

Loading of the Rink amid MBHA resin



The commercially available Rink amid MBHA resin was obtained as a Fmoc protected derivative and was used for the synthesis of PGLa and Mag2-amide peptides. After swelling the resin in DCM, a Fmoc-deprotection (vide infra) of the linker amino group was carried with suitable washing steps, the coupling of the first amino acid follows the same procedure as for amino acid coupling (vide infra).

Figure III.4. Rink amide MBHA resin

SPPS procedure

The peptides listed in Table III.1 were synthesized by automated or manual synthesis. For the manual synthesis, an ABIMED reaction column equipped with filter at the bottom outlet, a top cap for the N₂ inlet and a magnetic stir-bar was mounted on a magnetic stirring system. Sufficient amount of the dry preloaded resin was poured into the reaction vessel and suspended in NMP. Successive steps of deprotection and coupling as described below were carried out to follow the respective peptide sequences (see Table III.1) and interleaved with NMP washing steps.

Amino acid activation and coupling

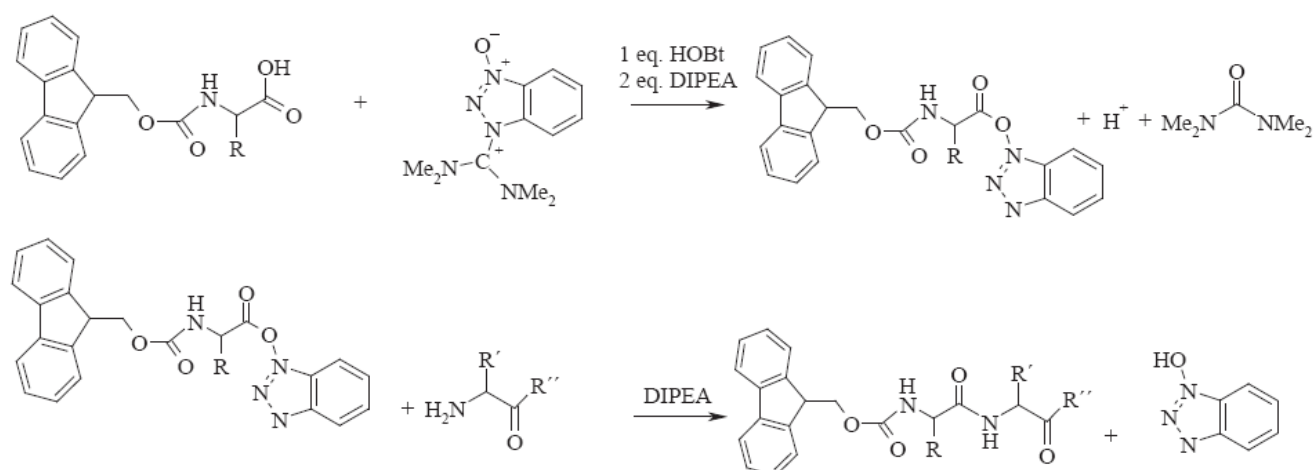


Figure III.5. Amino acid activation and coupling using a HBTU/HOBt protocol.

A stock solution of HOBt/HBTU (0.45 M) was prepared in DMF by pouring anhydrous HOBt (13.5 g, 0.1 mol, MW 135.1) into a 250 mL graduated vessel. DMF (to 200 mL) was added to dissolve HOBt. To the clear solution, HBTU (37.9 g, 0.1 mol, MW 379.3) was added. The solution was allowed to stir until HBTU was fully dissolved.

Typically, the N- α -Fmoc protected amino-acid (Fmoc-Aaa-OH, 1 mmol, 4 eq. relative to the resin loading in a 250 μ M scale synthesis and 10 eq. relative to the resin loading in a 100 μ M scale synthesis) was dissolved with the HOBt/HBTU in DMF solution (2.1 mL, 0.95 eq. relative to the Fmoc-Aaa-OH). DIPEA (330 μ L, 2 eq. relative to the Fmoc-Aaa-OH) was added to allow the activation of the Fmoc-Aaa-OH. The activated amino acid solution was then poured on the resin in the reaction vessel and allowed to couple for 2 h upon continuous gentle stirring. The reaction solution was then flushed out and the resin washed several times with NMP. In the case of manual synthesis, completion of the reaction was assessed using the Kaiser test: absence of any blue coloration was considered as successful coupling.

Fmoc deprotection

A stock solution of piperidine in NMP (20% v/v) was prepared. Piperidine solution (2 mL) was added to the resin (250 μ M scale synthesis) and mixed continuously for 5-10 min through vortexing of the reaction vessel (automated synthesis) or for 30 min under gentle N₂ purging through the resin (manual synthesis). The resin was then washed with NMP (2 \times 5 mL) and the residual NMP flushed out with N₂ stream. Completion of the deprotection was monitored by change of the conductivity of piperidine-carbamate salt adduct in the filtered solution (automated synthesis) or by performing Kaiser-test (manual synthesis). The deprotection step was repeated if the conductivity change was more than 5% or if the Kaiser test was not sufficiently blue. After completion of the Fmoc-deprotection, the resin was again washed with NMP.

Cleavage of the peptide from the resin

After completion of a synthesis, the resin was thoroughly washed successively with NMP, DCM and finally MeOH. The resin was then dried in vacuum overnight. The protected peptides were cleaved at rt with a TFA/TIS/H₂O/EDT (94:2.5:2.5:1 v/v) cleavage solution (25 mL for a 250 μ mol scale synthesis) for 3-4 h with occasional gentle shaking. The resin was filtered over glass wool and washed with a few mL of cleavage solution. The filtrate was concentrated under a N₂ stream until clear yellowish oil remained. The residual oil was precipitated with cold diethylether and centrifuged. The supernatant solution was removed

and the residue was dissolved in a mixture of water and acetonitrile 1:1 (v/v) and lyophilized. The identity of the peptides was confirmed with LC-MS.

Purification of the crude peptides

List of HPLC solutions

Solution A	water/acetonitrile 9:1 (v/v), 5 mM HCl
Solution B	water/acetonitrile 1:9 (v/v), 5 mM HCl

Table III.1. List of peptides.

Peptide	Labeled position	Sequence	Synthesis Scale ^a
PGLa (wt)	-	GMASK ⁵ AGAIA ¹⁰ GKIAK ¹⁵ VALKA ²⁰ L-NH ₂	250 μM (A-M)
PGLa6	A6	GMASK ⁵ Ala-d ₃ GA ¹⁰ IAGK ¹⁵ IAKVALKA ²⁰ L-NH ₂	250 μM (A)
PGLa7	G7	GMASK ⁵ AAla-d ₃ A ¹⁰ IAGK ¹⁵ IAKVALKA ²⁰ L-NH ₂	250 μM (A)
PGLa8	A8	GMASK ⁵ AGAla-d ₃ IA ¹⁰ GK ¹⁵ IAKVALKA ²⁰ L-NH ₂	250 μM (A)
PGLa9	I9	GMASK ⁵ AGAAla-d ₃ A ¹⁰ GK ¹⁵ IAKVALKA ²⁰ L-NH ₂	250 μM (A)
PGLa10	A10	GMASK ⁵ AGAIAla-d ₃ GK ¹⁵ IAKVALKA ²⁰ L-NH ₂	250 μM (A)
PGLa11	G11	GMASK ⁵ AGAIA ¹⁰ Ala-d ₃ -K ¹⁵ IAKVALKA ²⁰ L-NH ₂	250 μM (A)
PGLa13	I13	GMASK ⁵ AGAIA ¹⁰ GKAla-d ₃ AK ¹⁵ VALKA ²⁰ L-NH ₂	250 μM (A)
PGLa14	A14	GMASK ⁵ AGAIA ¹⁰ GKIAAla-d ₃ K ¹⁵ VALKA ²⁰ L-NH ₂	250 μM (A)
Mag1	-	GIGKF ⁵ LHSAG ¹⁰ KFGKA ¹⁵ FVGEI ²⁰ MKS	250 μM (A)
Mag2 (wt)	-	GIGKF ⁵ LHSAK ¹⁰ KFGKA ¹⁵ FVGEI ²⁰ MNS	100 μM (A-M)
Mag2-amide	-	GIGKF ⁵ LHSAK ¹⁰ KFGKA ¹⁵ FVGEI ²⁰ MNS-NH ₂	250 μM (A)
Mag2(E19Q)	-	GIGKF ⁵ LHSAK ¹⁰ KFGKA ¹⁵ FVGQI ²⁰ MNS	100 μM (A)

^a (A) stands for automated synthesis using the Applied Biosystems synthesizer.

(M) stands for manual synthesis using ABIMED reaction column

Table III.2. Table of HPLC methods.

	Analytical method		Preparative method	
Column	Analytical		Preparative	
temperature	35°C		35°C	
Flow rate	1.5 mL/min		15 mL/min	
Injection	n.d.		1 mL of a 10 mg crude peptide dissolved in 1mL solution A	
Gradient	Time	Solvent A (%)	Time	Solvent A (%)
	0	100	0	85
	2	100	15	70
	22	0	15.5	30
	22.5	0	16	30
	23	100	16.5	85
	25	100	17	85

The fluffy white powder obtained after the cleavage procedure was then analyzed by analytical HPLC-MS (for details see Table III.2). After identification of the desired peptide the preparative purification was performed as follows: typically, the crude peptide was dissolved in solution A and purified on a preparative column as described in Table III.2. The collected preparative HPLC fraction containing the desired peptide was then frozen and lyophilised. After lyophilization, the white powder was re-analyzed by HPLC-MS and stored in a dry sealed vial at -20°C.

1.3. Results

Synthesis of N- α -Fmoc-L-3,3,3- d_3 -Alanine

The product was obtained as white solid in high yield (91%) and purity (95% HPLC). The product was used without further processing for the synthesis of ^2H -labeled peptides.

Synthesis of the peptides

All synthesis and purification successfully led to the production of pure peptides. Typical yield of the crude peptides were ~70% (w/w) and typical purity was ~70% for PGLa derivatives and ~50% for Mag2 derivatives. This difference was probably due to the use of a different resin and the sequence of Mag2 which may have a higher propensity to aggregate during the synthesis. Double coupling procedure followed by systematic AcOH capping steps allowed to increase the yield. The final yield of the peptides was 30~50% in purity above 95%. These peptides were stored at -20°C in sealed vials before use.

2. Circular dichroism (CD), oriented CD (OCD) measurements

2.1. Principle of CD and OCD spectroscopy

Circular dichroism (CD) is an excellent and simple (in a practical sense) UV spectroscopic method that has been extensively used to study the secondary structure of peptides and proteins. It allows fast determination of the conformational state of the peptide in different environmental conditions giving that its concentration in the measured solution is accurately determined. A disadvantage is that results express only an averaged structure in time and space. It has also to be remembered that there is no theory for the secondary

structure determination. This is an empirical method based on deconvolution of the measured CD spectrum using an empirically obtained basis set from proteins with known secondary structure. Several algorithms, using different basis set and deconvolution processing, are normally used to get the averaged conformation with higher accuracy.

The main principle of CD is an asymmetric absorption of left and right handed circularly polarised light by a chiral, hence optically active, molecule. The slight adsorption difference results in an elliptically polarised light. For a protein, UV adsorption arises mainly from the $n \rightarrow \pi^*$ and $\pi \rightarrow \pi^*$ electronic transition of the amide bonds. The presence of an adjacent C_α chiral center is responsible for the dichroism effect. The energy of the transition is modulated by the conformation of φ and ψ torsion angles. In the special case of helical peptides where the carbonyl bonds are almost parallel to the helix axis and the amide bond perpendicular to it, the band intensities are predicted to be dependent on the helix orientation with respect to the incoming beam [102, 103]. The orientation of helical peptides in oriented membranes can be estimated. This is the oriented circular dichroism (OCD) spectroscopy. As an example, application of OCD is shown for the antifungal peptide alamethicin [104, 105].

Setting α as the angle between the probing light beam and the helix axis, the intensity of the absorption band is, according to theory, proportional to $\sin^2(\alpha)$ for the bonds that are parallel polarized and $\cos^2(\alpha)$ for the bonds that are perpendicularly polarized. As this absorbance may be model dependent, to determine the orientation of an α -helix by OCD one usually needs two normalized spectra from samples where the orientation of the peptide is different and well-known. Usually, sample with low and very high concentration of peptide are used. But it is also possible to use the spectra of the corresponding LUV samples. In a way similar to the zero-averaging of the anisotropic contribution of the NMR signal, the spectrum from LUV corresponds to the isotropic orientation distribution (or orientation distributed over a sphere) and is equal to the contribution of peptides being 1/3 parallel to the optical axis (equivalent to transmembrane orientation) and 2/3 perpendicular to the optical axis (equivalent to the surface state) [105]. Results from OCD applied to PGLa and Mag2 are shown and discussed in Chapter VI.

2.2. Materials and methods

List of peptides

PGLa (wt), PGLa7, PGLa9, PGLa11, PGLa13, Mag2 (wt)
--

List of reagents and devices

Dimyristoylphosphatidylcholine (DMPC)	Alexis Biochemicals (Lausen, Switzerland) or Avanti Polar Lipids (Alabaster, AL, USA)
Dimyristoylphosphatidylglycerol sodium salt (DMPG)	Alexis Biochemicals (Lausen, Switzerland) or Avanti Polar Lipids (Alabaster, AL, USA)
CD spectropolarimeter	Jasco J-810 spectropolarimeter (Jasco Corp., Tokyo, Japan)
Extruder Avanti Mini Extruder	Avanti Polar Lipids (Alabaster, AL, USA)
Methanol (UV grade)	Merck (Darmstadt, Germany)
Chloroform (UV grade)	Merck (Darmstadt, Germany)

DMPC/DMPG-LUVs preparation and CD measurements

Appropriate amount of DMPC and DMPG were weighed and co-dissolve in a chloroform-methanol solution (3:1 v/v) to form a stock solution of DMPC/DMPG in a 3:1 molar ratio. 0.25 μmol of each peptide above listed were weighed and dissolved with lipid stock solution (25 μL) to give a peptide/DMPC/DMPG 1:75:25 mixture. Solvents were evaporated under a gentle stream of N_2 and the sample was dried under vacuum overnight. Lipid dispersions were formed by addition of phosphate buffer (2 mL, 10 mM, pH 7.4). The resulting dispersion was subject to ten cycles of thoroughly vortexing - cooling (0°C) - warming (40°C). The LUVs were obtained by extrusion of the homogenised dispersion with twelve passes through a polycarbonate filter with 100 nm diameter pores (Avanti mini extruder) and keeping the extruder temperature above 40°C . Under these conditions, vesicles of uniform and constant diameter are expected to form already after five passes [106].

CD spectra were recorded in quartz cells (0.1 cm path length) at 35°C , three scans were averaged, and the baseline of the peptide-free LUV sample was subtracted. From these spectra, the secondary structure contents of the peptide were evaluated by three different methods (CONTIN [107], CDSSTR [108], SELCON3 [109]). The structure contents were average between the results of two of these algorithms giving similar outputs with reliable fits.

OCD measurements

OCD samples were prepared according to the single substrate method as described by Ludtke et al. [110]. Briefly, the mixture of lipid/peptide codissolved in methanol/chloroform solution was deposited on the measurement quartz glass windows. Solvent was allowed to evaporate and was then fully removed under vacuum. The window was mounted in the home-made measurement cell and the sample was hydrated under humid atmosphere of 96.0 % relative humidity using a saturated K_2SO_4 solution. Multilayers of lipids oriented parallel to

the windows are then obtained. The measurement cell, similar to the one described by Chen et al. [111], was mounted on the CD spectropolarimeter, placing the measurement window perpendicular to the probing beam. The sample was kept under the same humid atmosphere at 35°C. The sample was rotated in the plane of beam incidence to give eight measurements at different rotations which were averaged to reduce sample artefacts. These measurements were repeated three times to get a final average spectrum.

2.3. Results from CD experiments

CD experiments were performed on PGLa (wt), Mag2 (wt) and analogues of PGLa. PGLa analogues where Ala was replaced by Ala-d₃ were not expected to change the structural and functional properties of the PGLa (wt) and were therefore not included. Figure III.6 shows the CD spectra obtained for the peptides.

The CONTIN and SELCON3 methods gave similar content results, which were averaged and are shown in Figure III.7. The helical content of PGLa (wt) was slightly higher than expected from previous experiments under similar conditions (66% according to [75]). The helical contents of the labeled PGLa were lower than for PGLa(wt) and thus closer to this former value. The higher value found for PGLa (wt) can be due to uncertainties in the concentration determination even though all curves in the high wave length range were well overlapping. Given these small experimental uncertainties, all labeled peptides showed very similar helicity and the effect of mutation seemed to be negligible in terms of peptide structure. The content of turn is found to be around 12%. Mag2 showed similar features as the PGLa analogues. The results were found to be consistent with solution NMR structures of Mag2 [112] and PGLa [57], respectively.

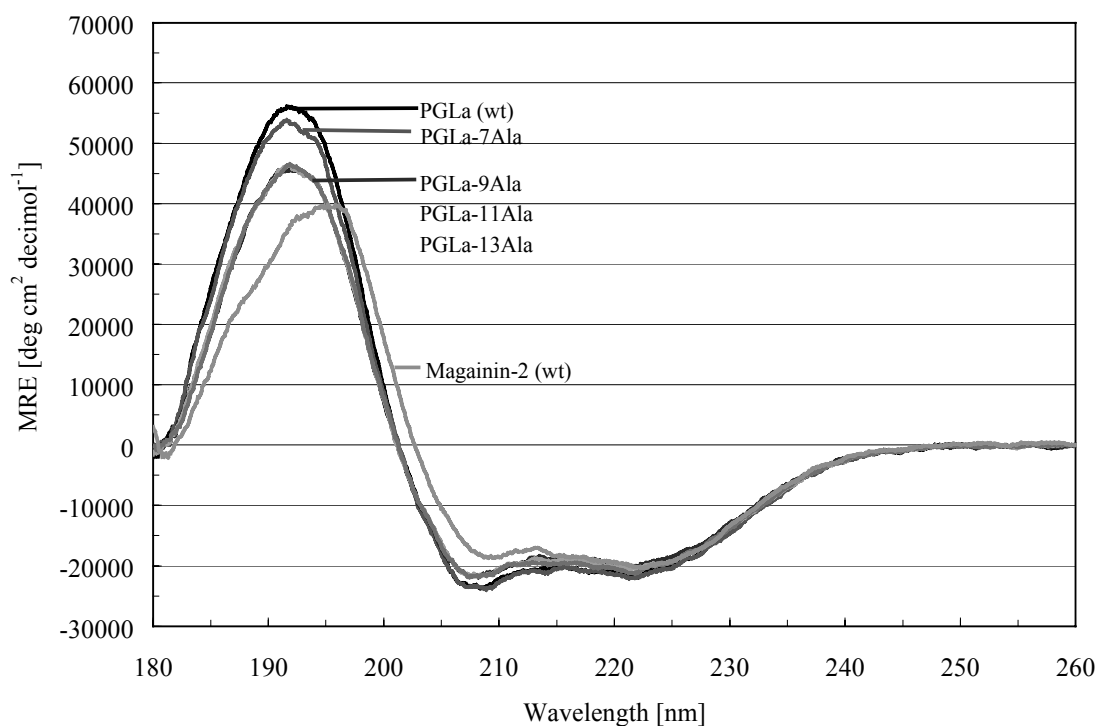


Figure III.6. CD spectra of PGLa analogues and Mag2 in the presence of DMPC/DMPG (3:1) LUVs.

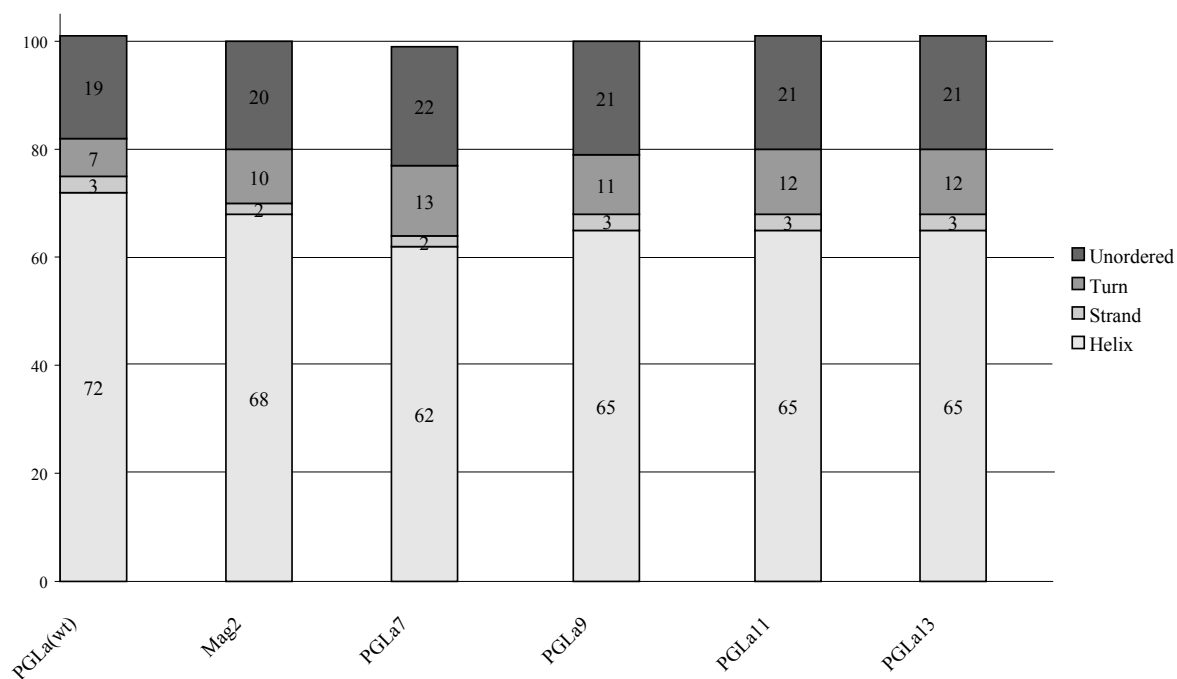


Figure III.7. Bar diagram showing the secondary structure content estimations of the peptides in the presence of DMPC/DMPG LUVs as calculated from the CONTIN and SELCON3 methods.

3. Biological tests: Hemolytic assay and minimal inhibitory concentration (MIC)

3.1. Principle

Minimal inhibitory concentration (MIC) determination is the method of choice to estimate the microbicidal potency of a substance. Similarly, toxicity is often assessed by hemolytic activity (HA) test on human red blood cells. The results obtained by these tests are not absolute and have to be considered only inside one set of experiment. Even if both of these methods may suffer from difference of standardization between different research groups, the main problems arise intrinsically from the nature of the probing “reagents”. On the one hand, bacteria are living organisms whose kinetics of growing has to be tightly controlled. First, the conditions for growing bacteria directly influence their membrane composition hence the action of AMPs, and second, the control of the bacterial concentration, measured in colony forming unit (CFU), is a difficult step due to their living nature. On the other hand, the erythrocytes are fragile cells, and processing (washing, centrifugation, buffering) or aging influence the disruptibility of their membranes [113].

For both type of tests, dilution series of an antimicrobial stock solution are mixed with living bacteria or diluted erythrocyte cell stock solutions and allowed to incubate. For the MIC determination, a visual test of the solution turbidity indicates the concentration range for which bacterial growth is inhibited. For HA, UV measurement of the released haemoglobin, compared with negative and positive controls, determines the percentage of lysed erythrocytes. The resolution is limited by the choice of dilution series which often give rise to logarithmic concentration scale. The temperature for these experiments is often set to the human body temperature but the potency of AMPs is clearly temperature dependant [114].

One has to be very critical to the obtained toxicity potency results. As described in the first chapter, the studied AMPs are found not in blood vessel but in the epithelial surface, hence other cell types than erythrocytes are exposed to them in the host organism. AMPs are also able to intervene in other immune reaction cascades. To fully compare the activity between two peptides, it is normally necessary to determine at least two inhibition parameters [115].

3.2. Materials and methods

List of reagents

Tris	Applichem (Darmstadt, Germany)
HCl	Roth (Karlsruhe, Germany)
DMSO	Sigma-Aldrich (Steinheim, Germany)
Triton X-100	Roth (Karlsruhe, Germany)
Erythrocyte (perempted citrate phosphate dextrose-stabilized blood bags with erythrocyte suspensions of healthy human donors)	Municipal Hospital blood bank (Karlsruhe, Germany)
0.1 M NaOH	Merck (Darmstadt, Germany)
Agar-Agar	Roth (Karlsruhe, Germany)
Bacto Tryptone: Pancreatic Digest of Casein	Becton, Dickinson and Company (Sparks, MD, USA)
Yeast Extract	AppliChem (Darmstadt, Germany)
NaCl	Fischer Scientific (Leicestershire, UK)

List of devices

Centrifuge 3-18K	Sigma (Osterode am Harz, Germany)
Centrifuge Mikro 20	Hettich Zentrifugen (Tuttlingen, Germany)
Incubator Cobas Eia	Roche (Basel, Switzerland)
Water Bath Type 1004	Roche (Basel, Switzerland)
Flat-bottom 96-well microliter plates	Nunc (Roskilde, Denmark)
Incubator Shaker Model G25	New Brunswick Scientific (Edison, NJ, USA)
Spectrophotometer Smart Spec 3000	Bio-Rad (Hercules, CA, USA)

List of phosphate-buffered Solutions

T172E	172 mM Tris	adjusted to pH 7.4 with HCl at 4°C
T172W	172 mM Tris	adjusted to pH 7.4 with HCl at 37°C
Triton solution	0.2% Triton X-100 in T172W	

List of bacterial strains

<i>Escherichia coli</i> DH5 α
<i>Akinetobacter hebeiensis</i> DSM 586

List of growth media

(All media were autoclaved at 120°C)

LB Medium	NaCl	10 g/L	adjusted to pH 7.4 at 25°C with NaOH
	Bacto Tryptone	10 g/L	
	Yeast Extract	5 g/L	
LB Medium without Salt	Bacto Tryptone	10 g/L	adjusted to pH 7.4 at 25°C with NaOH
	Yeast Extract	5 g/L	

MIC determination (according to Strandberg et al. [116])

Cavities of microplates were filled with 50 μL salt free LB medium. Peptides and their mixtures were dissolved in salt free LB medium to afford 256 μM peptide concentration stock solutions. For each peptide stock solution, quadruple two-fold dilution series were prepared as follows: first 50 μL of peptide stock solution was poured in a first-row cavity and mixed. The following cavity in a row was diluted and mixed to half with 50 μL of solution from the preceding cavity. The two last columns were left for negative and positive controls. Bacteria were grown in LB medium at 37°C and a shaking at 230 rpm. Aliquots were collected in their mid-logarithmic growth phase. The aliquots were further diluted in salt free LB medium to afford an approximated 10^6 CFU bacteria concentration (estimated from internal optical density measurement standards). 50 μL were then dispensed in each cavity except for the last column left for negative control. Microplates were capped and incubated for 18 h at 37°C. Turbid solution in a cavity indicated bacterial growth, whereas limp solution was a sign of bacterial growth inhibition. The MIC value was then taken as the lowest peptide concentration inhibiting bacterial growth.

Hemolytic test

A volume of erythrocyte solution was washed twice by suspending the erythrocyte in 9-fold excess of T172E, centrifuging the suspension at 600 g, at 4°C, for 10 min and removing the supernatant. Ice-cooled T172E buffer was finally added to afford a 10-fold diluted erythrocyte suspension. This stock cell suspension was kept on ice during the whole experimental procedure. The peptides were weighed and dissolved in T172W buffer to give a 2.0 μM concentrated stock solution for each peptide. Two-fold dilutions series, ranging from 2000 μM to 62.5 μM , were prepared by successive suitable aliquot and dilution with equal amount of T172W buffer. A positive control vial was half-filled with 0.2% Triton solution instead of peptide solution and a negative control vial was half-filled with T172W buffer. Prior to the hemolysis test of each series, a volume of the above mentioned erythrocyte stock suspension was further 20-fold diluted with preheated T172W buffer and incubated for five min in a water bath at 37°C. Thereafter appropriate volumes were dispensed in each reaction vial of the series, affording a final two-fold dilution series. The vials were further incubated with gentle shaking at 37°C for 20 min before a 10 min 20,000 g centrifugation to pellet cells. Absorption of the released haemoglobin was then measured at 540 nm and three measurements were averaged. Measurements of the positive and negative controls defined

respectively the 100% and 0% hemolysis values and allowed to calculate the percentage of hemolysis due to the peptide.

3.3. Results of MIC and HA tests

The analogues of PGLa were Ala-d₃ replaced a non native Ala were tested against two Gram-negative bacterial strains and compared to the PGLa (wt) and Mag2. Results are depicted in Figure III.8. All analogues showed similar activity as PGLa(wt) though PGLa13 seemed to be less active for both strains.

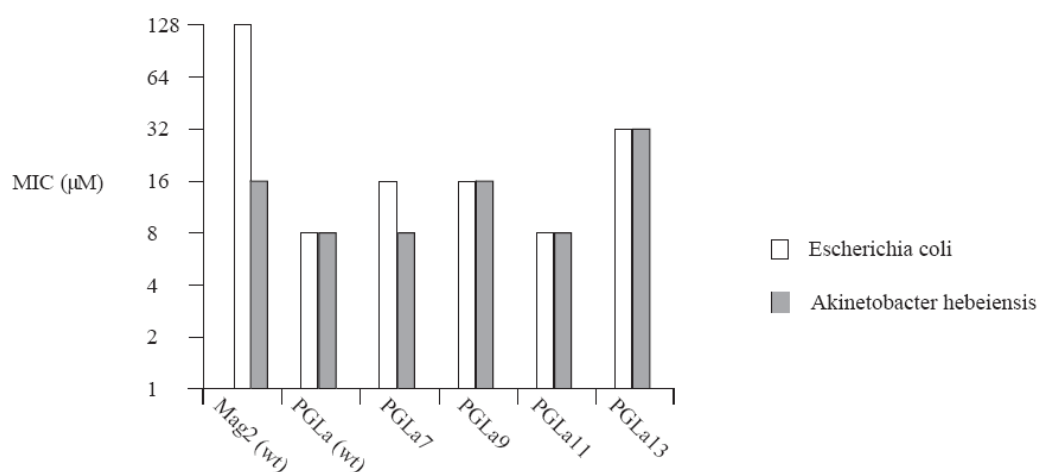


Figure III.8. MIC determination of PGLa analogues against *E. coli* and *A. hebeiensis*

The HA of the PGLa (wt) and the PGLa analogues are showed in Figure III.9. The tests revealed strong correlation of hemolysis with the hydrophobicity of the peptide. These results are consistent with other HA analysis [23, 113]. PGLa13 and PGLa9 having a Ile residue replaced by an Ala-d₃ are less hydrophobic and showed lower hemolytic activity than PGLa (wt). On the opposite, PGLa7 and PGLa11 having a Gly residue replaced by an Ala-d₃ are more hydrophobic and showed a stronger hemolytic activity than PGLa(wt). This correlates well with the fact that erythrocyte outer membrane leaflets are mainly composed of zwitterionic lipids. Hence the main force behind the peptide membrane affinity is the hydrophobicity.

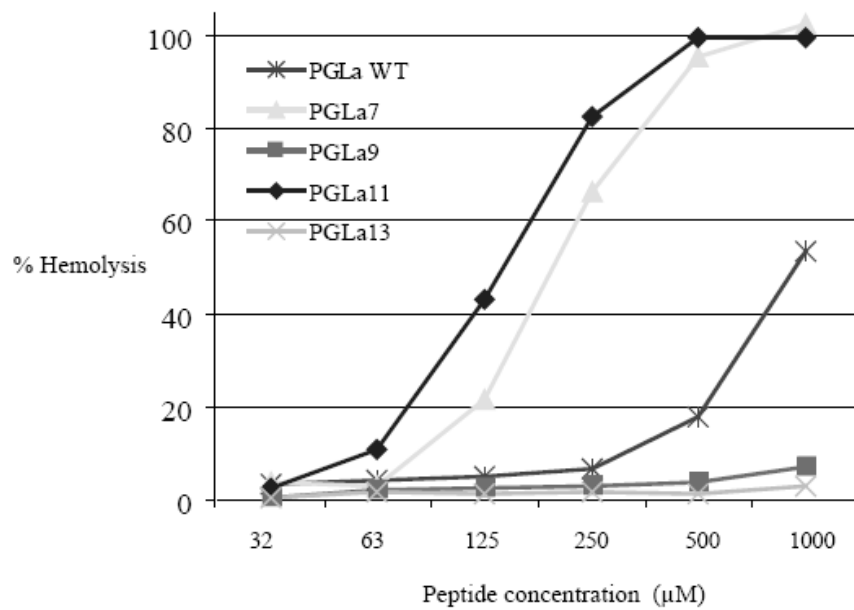


Figure III.9. Hemolytic activity of PGLa and PGLa analogues against human erythrocytes.

IV. Solid-state NMR analysis of the PGLa peptide orientation in membrane: a ^2H -labeling strategy

Except for the order tensor analysis, the results presented in this chapter have been published as [3] in Biophysical Journal by E. Strandberg, P. Wadhvani, P. Tremouilhac, U.H. Durr, and A.S. Ulrich in 2006.

Because of the high biological relevance of membrane active peptides [I], it is important to find an effective method of investigation for these peptides in membranes. As clearly indicated [II], one very powerful method is solid-state NMR spectroscopy. It can give dynamic and structural information at the molecular level of biological systems close to natural conditions. The availability of NMR information in such sample can be advantageously controlled, for example, by specific isotope incorporation via peptide synthesis [III]. This part of the thesis is a direct application of the whole methodology described in Chapter II. Thanks to solid-state NMR analysis of deuterated labeled analogues of the antimicrobial peptide PGLa, the behavior of the peptide in membranes can be accurately described and related to a biological model of its action, given that the disturbing effects of labels are discriminated and model for motions is adapted. These aspects are here discussed together with a comparison with another ^{19}F -labeling strategy.

1. Stating the problem

For peptides of known rigid structures, several orientational constraints can be easily measured from NMR labels directly attached to the peptide backbone. It is usually achieved through isotopic enrichment of ^{15}N and ^{13}C nuclei in the peptide backbone. This replacement does not generally change the chemico-physical properties (from a biological point of view) of the molecule. The same applies for ^2H replacing ^1H in the methyl group of an alanine (Ala) residue. The methyl group is effectively directly attached to the C_α , which is part of the backbone. However, all of these three nuclei are quite insensitive labels compared to ^1H (^1H , ^2H , ^{15}N , and ^{13}C have, respectively, a magnetogyric ratio γ of 26.8, 4.1, -2.7, and $6.7 \cdot 10^7 \text{ rad s}^{-1}$

$^1\text{T}^{-1}$). For ^{13}C and ^{15}N nuclei covalently bond to protons, the cross-polarization (CP) signal enhancement technique can partly overcome this problem. However, it may have some drawbacks. The optimal conditions need to be found for efficient polarization transfer and proton decoupling. First of all, such conditions are not always found for small dynamic system, and a direct pulsing method may be necessary [117]. Secondly, cross polarization implies long and high-power pulses that may overheat the sample and make the temperature control harder [118]. On the other hand, for ^2H , the signal is easily acquired by a simple solid echo experiment, with relatively short recycling time (0.1 to 0.5 s as opposed to usually at least 2 s for CP experiments or up to 5 s for a direct pulsing on ^{15}N). Thus ^2H -NMR in a selective labeling strategy can afford several advantages if no natural background deteriorates the signal.

Another strategy to get orientational constraints takes advantage of the non-conventional (for natural compounds) ^{19}F -NMR [48]. The ^{19}F nucleus has a gyromagnetic ratio of $25.2 \cdot 10^7 \text{ rad s}^{-1} \text{ T}^{-1}$ and is almost as sensitive as ^1H . Having almost the same van der Waals radius as ^1H , ^{19}F nuclei can be used to replace protons. Another benefit is that ^{19}F , in contrast to ^1H , has no natural background in biological samples. By-passing the induced difference of chemical properties, a promising technique using 4- CF_3 -phenylglycine (CF_3 -Phg) has been developed [119]. The analysis deduced from the fluorinated methyl group of this residue follows the same principle as the one from a deuterated methyl group, even if for ^{19}F , the NMR interaction is the homo-nuclear dipolar coupling. Short experiments on several labeled peptides allow to get the orientation of a peptide in a membrane. This technique has been successfully applied on PGLa (vide infra).

PGLa has been reported to bind to lipid membranes and to adopt an α -helical structure ([III.2] and references in [I.3.1]). The α -helical segment extends at least from residue 6 to 20 in micelles, as shown by solution ^1H -NMR [57]. In the same study, solid-state ^{15}N -NMR experiments have revealed that PGLa aligns with its helix axis parallel to the membrane surface though no accurate tilt or rotation angles are measured. Using the above mentioned CF_3 -Phg labeling strategy, for the first time, the accurate rotation coordinates have been determined, showing PGLa lying parallel to the surface with its lysine side chains pointing up to the water layer [119]. When a defined threshold concentration is reached, the peptide tilt in the membrane increases by almost 30° [75]. These results not only confirm previous experiments using PGLa analogues labeled at one position with 4-F-phenylglycine [120] but also give a more accurate orientation. This re-alignment is in agreement with the biological interpretation following the two-state model of Huang [121]. Nevertheless, at high

concentration, the peptide is not found in a transmembrane orientation (I-state) but just obliquely inserted in the membrane in a so called tilted state (T-state). It has been postulated that this T-state originates from a homo-dimerization process as these peptides are likely to form dimers [122-125]. However, one complication with the ^{19}F labeling scheme is that the implied mutations are likely to modify the hydrophobicity, hydrophobic moment and/or polar angle of the peptide. These features are important parameters for interaction with lipids [I] or for self-packing aggregation in a membrane environment [126]. Although the biological functions of the mutants are checked, slight changes still occur. Furthermore, the dimer interface may be potentially destroyed through these labeling disturbances. Consequently, the fitting of data are to be assessed in view of these mutant modifications, which can severely disturb the peptide behavior.

In this respect, considering the abundance of Ala residues in the sequence of PGLa, the Ala- d_3 amino acid is a suitable NMR label. Indeed replacing Ala by Ala- d_3 is obviously not disturbing the peptide, and replacing glycine (Gly) or isoleucine (Ile) by Ala is expected to induce minor changes in the above mentioned peptide features. The GALA (geometric analysis of labeled alanine) approach then helps to extract orientational constraints for determining the alignment. This method has already been successfully applied for several transmembrane model peptides, the WALP peptides [90, 127]. However, in contrast to the WALP studies where the investigated peptides are quite symmetrical molecules, the present problem deals with peripherically bound amphipathic peptides, and several parameters have to be critically evaluated.

Practically, in the present study, several PGLa analogues, having at a single site either an Ala, Ile, or Gly residue substituted by Ala- d_3 [III.1.3], were used to extract orientational constraints of the peptide in DMPC lipid bilayers in a liquid crystalline state and at two different peptide concentrations. The substituted residues were all located in the middle part of the peptide which is expected to be α -helical when bound to a lipid membrane [III.2.3.]. The PGLa analogues used were biologically tested and found to be similarly active as the wild type [III.3.3]. From these measured constraints and a model for the peptide structure the exact orientation of PGLa was calculated. The reliability of the model and the calculation methods as well as the suitability of the residue replacements were assessed. The obtained orientational and dynamics information were critically discussed and compared with previous results from ^{19}F -NMR analysis [75, 119] to evaluate the respective advantages of the two strategies.

2. Materials and methods

2.1. Sample preparation

In this part, the pure, PGLa6, PGLa7, PGLa8, PGLa9, PGLa10, PGLa11, PGLa13, PGLa14 peptide stocks synthesized previously [III.1], were used after LC-MS control. Sample preparations followed the general method described in [II.2.]. In this study, MLV and GP samples containing PGLa carrying an Ala-d₃ at a single site in DMPC bilayers were prepared as listed in Table IV.1. The set of MLV samples had a P/L of 1:200 and was hydrated with deuterium depleted water for a total amount of 50% (w/w). The corresponding set of GP samples had a P/L=1:50 and were hydrated at a relative humidity of 96%.

2.2. NMR spectroscopy

General methods for ²H- and ³¹P-NMR data acquisitions are described in [II.2.2.2]. GP samples were fit in the NMR coil with the normal of the plates parallel to the magnetic field. Experiments were carried out at 308K.

2.3. Calculations

The PGLa peptide was modeled as a standard α -helix, as described previously [II.2.2.3]. The orientational analyses were done using in parallel the two methods described in chapter section II.2.1. First, an axially symmetric order tensor for the peptide was assumed and used to determine the three parameters τ , ρ and S_{mol} whose accuracy was assessed by RMSD determination. The value of the MLV sample splittings were multiply by a factor of 2 in the calculations to remove the effect of MLVs, compared to GP samples.

Secondly, calculations were done using the Redcat software [93] as described in [II.2.1]. At least 6 absolute quadrupole splittings were entered and error analyses were systematically done to sign the values. The full order matrix was then determined. For the sake of comparison, the order induce by the MLVs was removed by multiplication by factor a of -2 of the order matrix after calculation. This analysis provide the principal values of the order tensor S_{xx} , S_{yy} , S_{zz} (with the convention $S_{zz} > S_{xx} > S_{yy}$) and the set (α, β, γ) of Euler

angles which transform molecular coordinates into the principal axes frame of the order matrix. The relation $\beta = \tau$, the tilt angle of the peptide and $-\gamma = \rho$, the azimuthal rotation angle, were used to compare the two methods. Due to the four-fold degeneracy from the symmetry of the system, the values of τ and ρ were both taken in the range of 0 to 180°. For the sake of homogeneity between the two model, the global degree of order (GDO) [128] as defined in [II.1.3.3], is given under the name of S_{mol} .

Table IV.1. Sequences of the peptides used and quadrupole splittings (in kHz) measured in PGLa-Ala-d₃/DMPC samples.

Peptide	Labeled position	Sequence	P/L=1:200 a	P/L=1:200 b	P/L=1:50 c
PGLa wt	-	GMASKAGAIAGKIAKVALKAL-NH ₂			
PGLa6	A6	GMASK Ala-d ₃ GAIAGKIAKVALKAL-NH ₂	7.8	15.6	18.2
PGLa7	G7	GMASKA Ala-d ₃ AIAGKIAKVALKAL-NH ₂	4.8	9.6	2.5
PGLa8	A8	GMASKAG Ala-d ₃ IAGKIAKVALK AL-NH ₂	8.6	17.2	42
PGLa9	I9	GMASKAGA Ala-d ₃ AGKIAKVALKAL-NH ₂	2.6	5.2	30.0
PGLa10	A10	GMASKAGAI Ala-d ₃ GKIAKVALKAL-NH ₂	7.5	15.0	30.3
PGLa11	G11	GMASKAGAIA Ala-d ₃ KIAKVALKAL-NH ₂	18.5	37	52.1
PGLa13	I13	GMASKAGAIAGK Ala-d ₃ AKVALKAL-NH ₂	13.2	26.4	20.1
PGLa14	A14	GMASKAGAIAGKI Ala-d ₃ KVALK AL-NH ₂	13.3	26.6	21.5

^a MLV samples: splittings measured from the edges (90° peaks) of the Pake powder pattern.

^b MLV samples: splittings measured from the edges (90° peaks) of the Pake powder pattern, and multiplied by a factor of 2 to correspond to the 0° signal.

^c GP samples aligned with the bilayer normal parallel to the magnetic field.

3. Results

3.1. Biological considerations

From biological tests and CD secondary structure determinations [III.2, III.3], the labeled peptides showed slight differences compared to wild type PGLa but neither striking changes in helical content nor in the MIC were observed and no labeled peptides were discarded from the analysis.

3.2. Choice of NMR samples

As described in the previous chapter, two kinds of samples can be used, multilamellar vesicles (MLVs) samples or oriented glass-plates (GP) samples. Equation II.xviii shows also that in the case of peptides rotating fast around the membrane normal, the splitting between the highest horns of the powder like spectrum directly depends on the angle between the peptide and the membrane normal. To compensate for the low sensitivity of ^2H -NMR, bulk sample like MLVs are prepared for low peptide concentration (P/L=1:200). The orientation of the lipid membranes was checked by ^{31}P -NMR and appeared to be well oriented, as identical and typical powder patterns with zero rhombicity were obtained for MLV samples, and identical narrow single peak in the low field were acquired for GP samples.

3.3. ^2H -NMR results

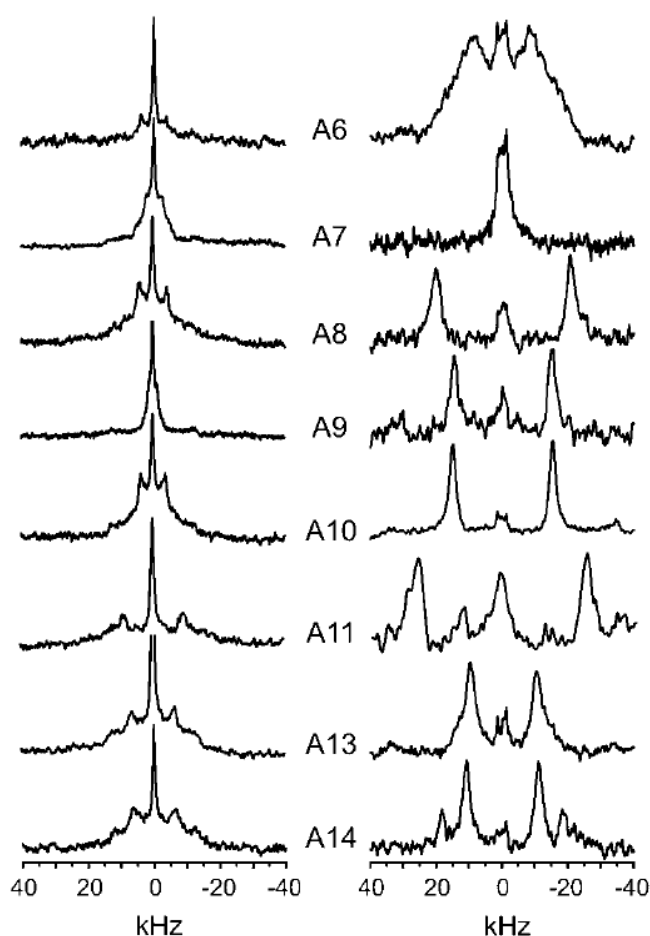


Figure IV.1. ^2H -NMR spectra of PGLa labeled with Ala- d_3 in eight different positions (as numbered) and reconstituted in DMPC at P/L=1:200 (left panel), and 1:50 (right panel). The samples with low peptide concentration were prepared as multilamellar lipid dispersions and show Pake patterns, whereas all samples with high concentration were prepared as macroscopically oriented membranes and show sharp splittings. (Adapted from [3]).

Figure IV.1 gathers ^2H -NMR spectra for the eight labeled positions and the two peptide concentrations. At low concentration (P/L=1:200), typical Pake patterns were observed. From the horn of spectra, different splittings for all samples were measured. This was a clear indication of a specific orientation of the peptide with no long-axial rotation. The isotropic peak was attributed to residual deuterons from the water. A less intense broad splitting of 26 kHz was revealed by peptide-

free samples to be a signal from natural abundance deuterons from the lipids (data shown in [V]). In contrast, for GP samples only a single splitting was observed together with the isotropic peak for each sample, indicating also a well defined orientation of the peptide.

Table IV.1 gathers the observed splitting for each spectrum. In the hypothesis of fast axial rotation of the peptide along the membrane normal, the splitting from a MLVs sample has to be doubled for comparison with data of a GP-sample. Indeed, to remove the averaging induced using the main splitting from the MLV samples, a factor of -2 should be used [II.xviii] but as the sign of the quadrupole splitting cannot be directly determined from the spectra, absolute values are used. It is clear that splittings changed with the peptide concentration, which indicated a different orientation of the peptide as a function of concentration.

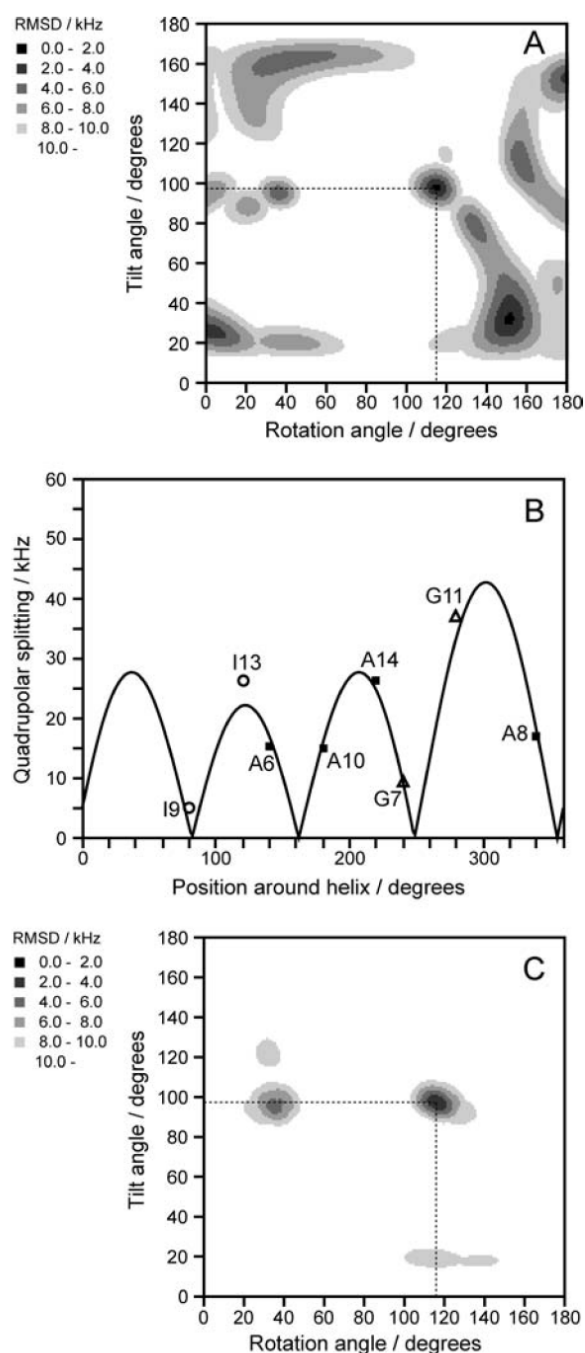
Table IV.2. Best-fit orientation parameters (τ , ρ , S_{mol}) and RMSD error assessment for PGLa in DMPC in a model with an uniaxially symmetric ordering tensor.

P/L system and NMR label	List of labeled residues used in the analysis	τ ($^{\circ}$)	ρ ($^{\circ}$)	S_{mol}	RMSD (kHz)
P/L = 1:200					
Ala-d ₃ (unsigned splittings)	A6 A8 A10 A14	98	115	0.66	1.3
	A6 G7 A8 A10 G11 A14	98	115	0.69	1.4
	A6 A8 I9 A10 I13 A14	98	114	0.68	2.2
	G7 I9 G11 I13	96	118	0.72	1.3
	A6 G7 A8 I9 A10 G11 I13 A14	98	115	0.70	2.0
Ala-d ₃ (unsigned splittings)	A6 G7 A8 I9	98	111	0.52	0.7
	G7 A8 I9 A10	100	113	0.57	1.2
	A8 I9 A10 G11	102	116	0.61	1.8
	I9 A10 G11 I13	98	112	0.78	0.6
	A10 G11 I13 A14	97	115	0.72	1.2
P/L = 1:50					
Ala-d ₃ (unsigned splittings)	A6 A8 A10 A14	126	110	0.75	0.5
	A6 G7 A8 A10 G11 A14	127	109	0.74	1.0
	A6 A8 I9 A10 I13 A14	124	112	0.78	0.9
	G7 I9 G11 I13	128	112	0.77	0.4
	A6 G7 A8 I9 A10 G11 I13 A14	126	111	0.78	1.2
	A6 G7 A8 I9	124	113	0.82	0.5
	G7 A8 I9 A10	128	111	0.76	0.7
	A8 I9 A10 G11	126	111	0.77	0.8
	I9 A10 G11 I13	128	113	0.76	0.8
A10 G11 I13 A14	127	110	0.79	1.1	

3.3.1. Helix alignment at low peptide concentration ($P/L = 1:200$)

As the substitution of ^1H by ^2H is not expected to induce noticeable structural changes, the analysis was first carried out using only the four values of the labels at native Ala positions: A6, A8, A10, A14. The degeneracy due to the use of the absolute values of the splittings for the calculation led to multiple solutions below a RMSD of 2 kHz as seen from the RMSD plot depicted in Figure IV.2.A. However, a relatively good fit within the experimental uncertainties was found with a RMSD of 1.3 kHz. It shows a peptide orientation with the helix axis lying almost parallel to the membrane surface at a tilt angle $\tau = 99^\circ$ and with the lysine side chains pointing to the water phase at a rotation angle $\rho = 115^\circ$. This alignment corresponds to the peptide being in the S-state. τ being larger than 90° indicated that the C-terminus of the peptide was inserted slightly deeper into the membrane. The corresponding order parameter S_{mol} was 0.66. Overall, this alignment was consistent with a previous ^{19}F -NMR analysis using the CF_3 -Phg label [119]. Another way of assessing the quality of the fits makes use of the quadrupolar wave plot as depicted in Figure IV.2.B. In this plot, one can see that no data points deviated from the best fit simulated curve.

Figure IV.2. (A) RMSD plot for PGLa/DMPC at 1:200, using only the ^2H -NMR data from the four non-perturbing positions A6, A8, A10, and A14. (B) Quadrupolar wave plot, with the curve fitted only to the four native Ala positions (filled square). The experimental splittings from two Ile positions (open circles) and two Gly positions (filled triangles) are also shown, with residue numbers given next to the data points. (C) RMSD plot calculated from all eight labeled Ala- d_3 positions, showing a unique minimum that confirms the best-fit solution from panel A. (Adapted from [3]).



To refine the calculations, $^2\text{H-NMR}$ data from the Ile or Gly substitutions were included. In a first analysis, only Gly changed to Ala- d_3 at position 7 and 11 and the native Ala substitutions data were used. A very similar solution defined by an RMSD of 1.4 kHz and giving $\tau = 98^\circ$ and $\rho = 115^\circ$ was found. When Ile changed to Ala- d_3 at position 9 and 13 and the native Ala substitutions data were used, the best solution had a higher RMSD of 2.2 kHz, but the orientation of the peptide was found to be identical, with $\tau = 98^\circ$ and $\rho = 114^\circ$. In both cases the molecular order was similar with, $S_{\text{mol}} = 0.69$ and 0.68 , respectively. Interestingly, if only Gly and Ile substitutions data were used a solution was found as good as the one revealed by using only native Ala substitutions, with an RMSD of 1.3 kHz. In this analysis the orientation of the peptide was relatively similar with $\tau = 96^\circ$ and $\rho = 118^\circ$, though S_{mol} had a slightly higher value of 0.72 . The quadrupolar waves of these systems showed clearly that, in no cases, did the data points of the Gly or Ile substitutions deviate significantly from the best-fit curve. It could be concluded that, at this peptide concentration, the replacement of a Gly or Ile residue in the middle of the peptide by an Ala residue had no influence on the structure or the orientational state of the peptide.

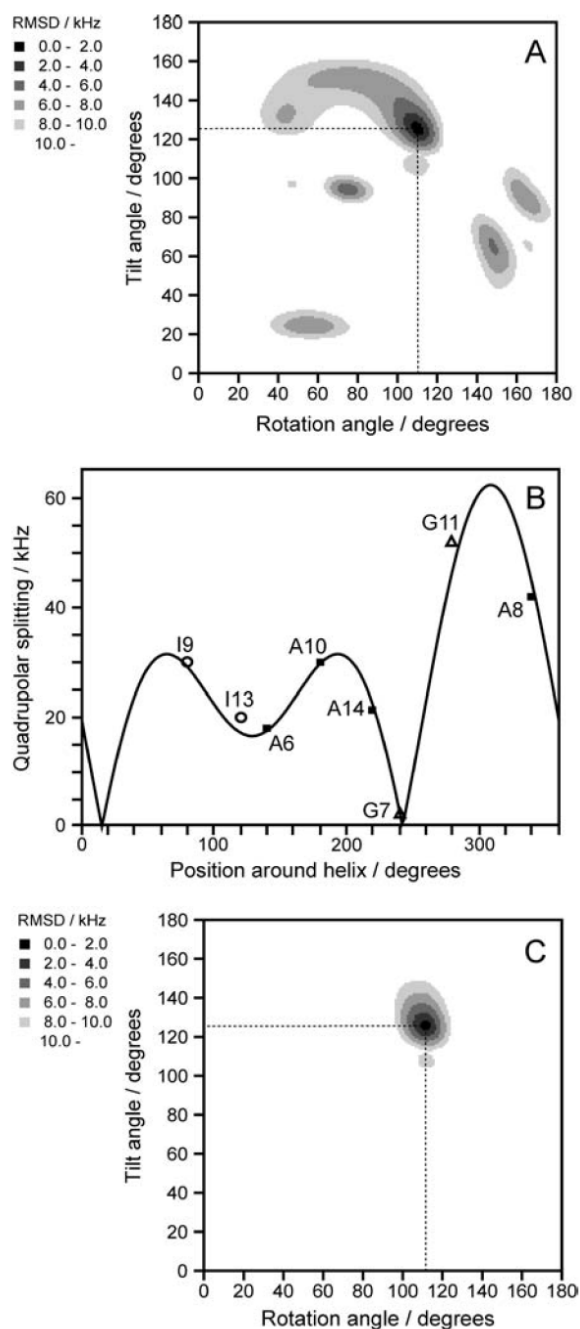
Another analysis was thus carried out using all eight data. As seen from the resulting RMSD plot in Figure IV.3.A and IV.3.C, all secondary shallow minima disappeared and only one unique solution was left giving $\tau = 98^\circ$, $\rho = 115^\circ$ and $S_{\text{mol}} = 0.70$ with an RMSD of 2.0 kHz. The overall orientation of the peptide was thus defined. The analysis gave also the signs of the experimental splittings, as it can be seen from the quadrupolar wave plot where any splitting greater than $0.5 \times \Delta\nu_{\text{Q}}^{\text{max}} \times S_{\text{mol}} \approx 30$ kHz should be positive.

To assess the hypothesis of the helical peptide being straight and rigid between the 6th and 14th residue, a systematic analysis was carried out using different sets of 4 consecutive labels. In the five cases, similar orientations for all segments were found with τ ranging from 97° to 102° and ρ from 111° to 116° . In all but one case the fits were better than the one using only the four native Ala substitutions data with RMSD values ranging from 0.6 to 1.2 kHz. The last case still gave a relatively good fit with a RMSD of 1.8 kHz. More interesting was the value of S_{mol} which clearly increased progressively from 0.52, for the segment between the A6 and A9 residue, to 0.72 for the A10-A14 segment. It could be concluded that for this part of the peptide, the model of straight α -helix was consistent with the data, and that the peptide was more mobile at the N-terminal end.

3.3.2. Helix alignment at high peptide concentration ($P/L = 1:50$)

In the analysis at $P/L=1:50$, the same data combinations were used as for the low concentration analysis (see Table IV.2). It appeared from the best fit using only the four data points from the native Ala substitution, that PGLa was tilted deeper into the membrane with $\tau = 126^\circ$, whereas the azimuthal angle stayed almost the same with $\rho = 110^\circ$. The motion appeared to be more restricted with $S_{\text{mol}} = 0.78$. The error for this solution was even lower than the intrinsic experimental uncertainties with an RMSD of 0.5 kHz. The tilt was almost 30° steeper than at low concentration, though the lysine side chains were still pointing to the water phase. This result was consistent with the previous ^{19}F -NMR analysis, though in this study the azimuthal rotation was slightly reduced by 15° [75].

Figure IV.3. (A) RMSD plot for PGLa/DMPC at 1:50, using only the ^2H -NMR data from the four non-perturbed positions A6, A8, A10, and A14. (B) Quadrupolar wave plot, with the curve fitted only to the four native Ala positions (filled square). The experimental splittings from two Ile positions (open circles) and two Gly positions (filled triangles) are also shown, with residue numbers given next to the data points. (C) RMSD plot calculated from all eight labeled Ala- d_3 positions, showing a unique minimum that confirms the best-fit solution from panel A. (Adapted from [3]).



At higher peptide concentration, direct contact between peptides could occur. Thus, the same analysis approach was used to assess whether Ile or Gly substitution with Ala could modify the structural or orientational properties of PGLa. The analysis using two supplementary data points from either Ile substitutions or Gly substitutions revealed similar orientations. The analysis using only non-native Ala substitutions also gave well defined result with an RMSD of 0.4 kHz. It was similarly concluded that the non-native Ala

substitutions affected neither the structural nor the orientational features of PGLa at this concentration. Like in the low peptide concentration case, the use of the eight data points selected out all secondary minima from the analysis using only the 4 native Ala substitution data points as depicted in Figure IV.3.

The orientational analysis was also carried out using different sets of 4 consecutive labels. For all segments between the 6th and the 14th residue, a similar orientation was found with τ ranging from 124° to 127° and ρ ranging from 110° to 113°. In contrast to the low concentration case, the segments appeared to have almost the same molecular order as each value was in the range of 0.76 to 0.82. For all segments, solutions were well defined with RMSD values of 1.1 kHz or below.

3.4. Order tensor analysis

The replacement of Ile or Gly by Ala residue did not seem to induce any structural or orientational changes and therefore 8 useful data points were available for the analysis. In the previous section, a model with 3 parameters was used, and 4 data points were enough to get a good and accurate fit. To refine this simple motional model, and given that more than 5 data points were available for each system, a full order tensor determination was carried out at both high and low peptide concentration. Using at least five data points, it afforded the principal values of the order tensor in the principal axis frame which are defined by the highest order S_{zz} , and the rhombicity $\eta=(S_{xx}-S_{yy})/S_{zz}$, and the transformation bringing the molecule in the principal axes frame of the order tensor. The analysis was done using different combination of at least 5 data points as listed in Table IV.3

First of all, the same orientations in terms of τ , ρ for PGLa were found as in the previous model. At P/L=1:200, the S_{mol} values were comparable with the above described analysis and showed likewise a slight increase from the C terminus to the N terminus around a mean value of 0.68. At P/L=1:50, S_{mol} was also more constant around a mean value of 0.76.

The main advantage of this analysis is that the rhombicity of the order tensor could be determined. At low peptide concentration, the rhombicity was $\eta = 0.30$. The positions of the principal axes are depicted in Figure IV.4. At high concentration, however, the tensor became symmetric with an almost vanishing rhombicity of $\eta = 0.05$. This revealed that motions were axially symmetric around the main alignment director.

Table IV.3. Best-fit orientation parameters (τ , ρ , S_{mol}) and RMSD error assessment for PGLa in DMPC from the determination of the full order tensor.

P/L ratio	List of labeled residues used in the analysis	τ (°)	ρ (°)	S_{mol}	RMSD (kHz)	S_{xx}	S_{yy}	S_{zz}	η
1:200	A6 G7 A8 A10 G11 A14	102	114	0.67	1.0	-0.18	-0.46	0.64	0.43
	A6 A8 I9 A10 I13 A14	99	114	0.68	2.0	-0.23	-0.43	0.66	0.30
	A6 G7 A8 I9 A10 G11 I13 A14	99	113	0.68	1.7	-0.24	-0.43	0.67	0.29
	A6 G7 A8 I9 A10	101	114	0.59	<1	-0.20	-0.38	0.59	0.31
	G7 A8 I9 A10 G11	99	113	0.70	<1	-0.25	-0.44	0.70	0.27
	A8 I9 A10 G11 I13	98	113	0.71	<1	-0.24	-0.46	0.70	0.31
	I9 A10 G11 I13 A14	99	113	0.70	<1	-0.20	-0.48	0.68	0.40
1:50	A6 G7 A8 A10 G11 A14	127	110	0.79	0.8	-0.36	-0.43	0.79	0.09
	A6 A8 I9 A10 I13 A14	126	110	0.78	0.6	-0.36	-0.42	0.78	0.07
	A6 G7 A8 I9 A10 G11 I13 A14	127	114	0.78	1.0	-0.37	-0.41	0.78	0.04
	A6 G7 A8 I9 A10	124	110	0.78	<1	-0.37	-0.41	0.79	0.05
	G7 A8 I9 A10 G11	125	111	0.77	<1	-0.37	-0.40	0.77	0.06
	A8 I9 A10 G11 I13	125	111	0.77	<1	-0.33	-0.43	0.76	0.13
	I9 A10 G11 I13 A14	128	110	0.78	<1	-0.37	-0.41	0.78	0.04

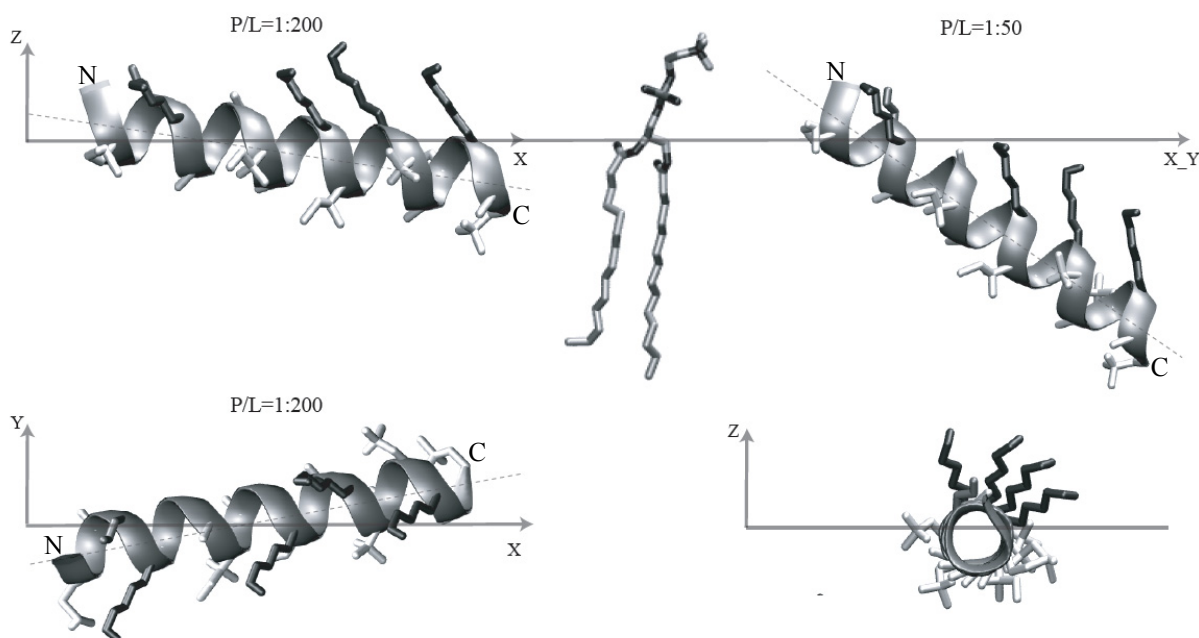


Figure IV.4. Position of the principal axes of the order tensor. The normal to the lipid membrane surface give the main director along the z axis and thus the mean bilayer surface is in the xy -plane. Top panels: the figures show the tilt of the peptide into the membrane at both low and high concentration. A DMPC molecule is also depicted for the sake of visualizing the monolayer thickness. Top left panel: at low peptide concentration, PGLa lies almost flat along the membrane surface. The presence of long hydrophobic side chains toward the C-terminus opposed to the short polar residues toward the N-terminus make the N-terminus

peptide tilt slightly more inside the membrane. Top right panel: at high peptide concentration, PGLa tilt is deeper into the membrane. Bottom-left panel: the x axis of the order tensor in its principal axis frame can be located at low peptide concentration being almost aligned along the helix axis. This shows that the peptide is more likely to pitch (oscillation of tilt of the peptide) than to list (rotational oscillation of the peptide around its helical axis). Bottom right panel: the view from the helix axis shows the list (the azimuthal rotation around the helix axis) of PGLa.

The analysis also gives the distribution of parameters as depicted in histograms in Figure IV.5 for η . The most probable value is close to the value with minimum RMSD given in Table IV.3.

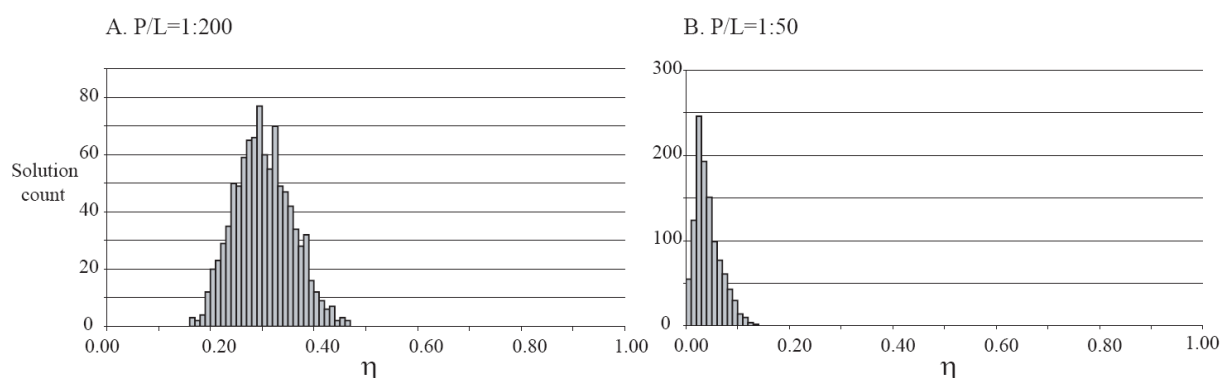


Figure IV.5. Histogram plots of the rhombicity $\eta = (S_{xx} - S_{yy})/S_{zz}$ for ~ 1000 solutions with $\text{RMSD} < 1.5$ kHz using the eight data points. (A) $P/L=1:200$. (B) $P/L=1:50$.

4. Discussion

In this study, the orientation and motion of the antimicrobial peptide PGLa incorporated at different concentrations in DMPC membrane were determined using solid-state ^2H -NMR on selectively Ala- d_3 labeled peptides. The reliability of the models was first assessed. A concentration-dependent re-alignment of the PGLa was thus discovered and is explained in terms of a cooperative process between peptide molecules. Finally, the presented result allowed to discuss the accuracy and some practical aspects of a previously used ^{19}F -NMR labeling strategy compared with the present ^2H -NMR labeling method.

4.1. Assessment of the model

The error values from solutions determined in this study were of the order of the intrinsic experimental error which was estimated to ~ 1 kHz. Even by using data points from the non-native Ala substitutions Ile (PGLa9 and PGLa13) or Gly (PGLa7 and PGL11), the

RMSD ranges were similar and revealed that no striking disturbance of the orientation or of the structure were induced by these mutations. This supplementary data allowed a refinement of the analysis and a full molecular order tensor determination. However, some best solutions were found with a higher RMSD values than the intrinsic experimental error. These deviations could originate from the assumption of a rigid standard α -helix used to model the peptide and contrast with previous studies where the same ^2H -NMR methodology has been used to analyze the orientation of transmembrane α -helical peptides, namely the WALP and the KALP peptides [90, 127, 129]. In these investigated systems, when the lipid bilayer thickness mismatch is not significant, orientation solutions are found with an RMSD below 1 kHz and show that the peptides are almost upright in the membrane. It has been confirmed that these transmembrane peptides form ideal symmetric α -helices.

In the present study, the investigated peptide has an amphipathic character when folded into an α -helix, which leads to some deviation of the model. First, the averaged structure may differ from a straight α -helix. It is shown that for such an amphipathic helix the hydrogen bonds from the CO and NH group of the backbone are looser and longer when located on the interface with the water layer compared to the ones located on the hydrophobic face [130, 131]. These characteristics cause the peptide helix to be bent. Such effects were not taken into account in the current structure model. It is also clear that the variation of residues in the PGLa sequences is a source of small variations in the torsion angles of the backbone compared to the very regular Ala-Leu-Ala repeat in the WALP peptides. To illustrate the variations from structural variation, the angle β between the C_α - C_β and the helix axis was varied of few degrees around the standard value of 121.1° . These variations in β have been also investigated for the WALP peptide and have given different optima in different lipids system [127]. In the present case, much better minima could be found for other values of β , but these minima were still giving the same orientation for the peptide (Table IV.4).

Similar observations have been done using the less natural CF_3 -Phg label [75] in different α -helix model and reveal that uncertainties in the structure model are a major source of error. Another source of error is the rigid body assumption. The existence of different internal motions may induce a non-negligible error using this rigid model. As revealed at P/L=1:200, PGLa seemed to be more mobile at the N-terminus. However, these different motions were of minor importance for PGLa. The assumption of an uniaxially symmetric ordering tensor was also appropriate, as the rhombicity of the order tensor obtained from the full order tensor determination was quite low and no noticeable difference in the orientation were observed between both types of calculations.

IV.4. Best fit solutions (τ , ρ , S_{mol} , β) in a model of an uniaxial symmetric order tensor.

Peptide system	List of labeled residues used in the analysis	τ (°)	ρ (°)	S_{mol}	β (°)	RMSD (kHz)
P/L=1:200						
	A6 A8 A10 A14	98	115	0.66	121	1.3
	A6 A8 A10 A14	97	113	0.67	124	0.4
P/L=1:50						
	A6 A8 A10 A14	126	110	0.75	121	0.5
	A6 A8 A10 A14	128	109	0.75	119	0.2

With regard to these potential error sources and the RMSD value obtained in the present calculations, it was concluded that the model of a rigid ideal α -helix was suitable and gave a reliable interpretation, given that the labels used are still limited to the central helical part of PGLa, were relatively close to each other and did not disturb the structure as also shown by the biological tests [III.2.3, III.3.3].

4.2. Concentration-dependent re-alignment of PGLa

At low concentration, the peptide was found in the so-called surface state or S-state: the helix axis lie along the membrane surface and the Lys side chains point up to the water phase. A slight decrease in the motion from the N-terminus to the C-terminus was noticed. Such an effect has been already described for PGLa being in the S-state and incorporated in unsaturated lipids by measuring the anisotropy width of ^{15}N -labels in the backbone [57]. From the hereby accurate determination of the tilt angle of 99° , we could explain this gradual mobility change by the fact that the C-terminus was slightly deeper inserted into the lipid core. This difference in insertion is also consistent with the fact that there are more polar residues toward the N-terminus (see Table IV.1).

The full order tensor determination afforded more information on the averaging motion of the peptide. One can basically visualize the amphipathic helical peptide as being a cylindrical shape with two faces along the rotation axis relating to the amphipathicity. In such a symmetrical model, the position of the highest order z-axis lay almost along the hydrophobic/hydrophilic moment consistent with the fact that the overall amphipathicity is the main force driving the orientation. Thus, as the substitution of one Ile or one Gly by an Ala did not change the overall character of peptide, data from these points were consistent with an unperturbed peptide orientation. The x axis lay almost along the helix axis. By locating the peptide in the principal frame of the molecular order tensor, one could describe

the motion of the peptide: the pitching (oscillation of the tilt of the peptide) is more pronounced than the listing (oscillation around the helix axis). The listing oscillation appears to be hindered by the charged residues not being readily immersed inside the hydrophobic part of the membrane.

At the higher concentration of P/L=1:50, though the lysine side chains were still found pointing up to the water phase, the tilt was increased by $\sim 30^\circ$ to 126° . This also confirmed the previous ^{19}F -NMR results [75]. It is interesting to note that in this case the rhombicity η was found to be close to zero. One explanation for the vanishing rhombicity would be that an oligomerization process of the peptide occurred. From a theoretical point of view, such oligomerization could increase the symmetry of the peptide assembly and induce axially symmetrical motion along the normal axis [132]. In fact, it is likely that a dimerization occurs and reduces the motion of the assembly by preventing the peptide to pitch. This oligomerization would also explain that the peptide was found to tilt much more steeply inside the membrane.

Indeed, for several related AMPs, dimerization is known to occur. Wakamatsu et al. [122] have demonstrated that Mag2, a natural AMP from the same family as PGLa [I], is able to form anti-parallel dimers in the presence of DLPC vesicle. From the calculated structure they have deduced that such dimers would have a tilt of around 35° with respect to the membrane surface, an angle similar to the present results. Recently, another magainin analogue, MSI-78, has been found by NMR to associate into an anti-parallel dimer in micelles [125]. MSI-103, an AMP which is designed from a 3-fold repeat of a 7-mer sequence from PGLa, is also able to form parallel dimers in lipid vesicles as revealed by REDOR NMR distance measurement [133, 134]. In the proposed dimers of MSI-103, the peptide-peptide interface is located on the alanine-rich domain, opposite to the lysine-rich side.

In the hypothesis of PGLa dimer formation, the results from this study allow us to speculate about the interface. First, one has to recall that from the single splittings observed and the unique solutions calculated there was only a single orientational population for the PGLa peptide. Consequently, if dimers are formed, they are likely to be anti-parallel. If as for MSI-103, the interface is located on the Ala-rich quadrant constituted of A6, A10 and A14 (see Figure I.5), because of the small tilt angle, the dimer may not have the thickness to span the membrane and some Lys side chains would be immersed in the hydrophobic bilayer core. Though thinning of PC membranes has been reported in the presence of AMPs, the reduction in thickness is only of the order of a few Å and this may not be sufficient to support this picture. If PGLa forms anti-parallel dimers like Mag2, the contact interface would be located

on either the G7-G11 or the I9-I13 side. It is interesting to notice that neither the Ile nor the Gly replacement by Ala-d₃ seemed to induce any orientational change. Thus such a dimer interface might be quite loose. However, Gly and Ala are among the residues most frequently found on membrane peptide dimer interfaces and have a relatively similar hydrophobicity [126, 135, 136]. Therefore, the substitution of one Gly in the dimer interface by an Ala residue may not dramatically induce a change of contact site and crossing angle. On the opposite side of the helix, the substitution of an Ile by an Ala may not directly disturb the dimerization but would change the whole hydrophobicity of the peptide and its interaction, hence its orientation, with the alkyl core of the lipid layer. This was already postulated for the substitution of Ile13 from the biological test results. From the orientation results Ile13 is found more deeply inserted than Ile9 in the lipid layer. Here it was also noticed that the Ile13 data point deviated more than the others from the best fit curve than the others (Figures IV.2.B and IV.3.B) probably due to the different hydrophobic feature relevant at this position.

Finally, it could thus be postulated that the re-alignment of PGLa occurred at high peptide concentration through anti-parallel dimer formation, with the interface probably located in the G11-G7-A-14-A10 quadrant (see Figure I.5).

4.3. Comparison with previous ¹⁹F- and ¹⁵N-NMR results

First of all, these ²H-NMR results confirmed the re-alignment of PGLa with a 30° increase in the tilt angle, which had been previously shown using the potentially more conformationally and orientationally disturbing label CF₃-Phg. Those studies had demonstrated the reliability and efficiency of the highly NMR-sensitive ¹⁹F nucleus. However, in a closer comparison of the calculated orientation angles (Table IV.5), one still notices slight deviations between the two strategies.

The CF₃ methyl group has, through the phenyl ring directly attached to C_α, a fixed orientation relative to the peptide backbone. Thus, its orientation relative to the external magnetic field and consequently to the peptide backbone can be deduced from its ¹⁹F homo-nuclear dipolar interaction in a similar way as for the quadrupolar splittings in Ala-d₃ labeled peptide [II.1]. The NMR interaction for both these labels has a (3cos²θ-1) dependence, where θ is the angle between the C_α-C_β bond of the labeled residue and the magnetic field. Therefore, the interactions are scaled with a constant factor. This constant is theoretically the ratio between the maximal interaction frequencies, reduced by their respective experimental molecular order parameter. The maximal values for the dipolar coupling of the CF₃-Phg

residue and for the quadrupolar coupling of the Ala-d₃ residue are $\Delta_{CF_3}(\max) = 15.8$ kHz [119] and $\Delta v_q(\max) = 84$ kHz [II.2], respectively. Given the best orientation found using only native Ala substitution data, the dipolar coupling of CF₃-Phg labeled PGLa could be back-predicted. Table IV.6 gathers the deduced results compared with the experimental values.

Table IV.5. Comparison between PGLa orientation calculations based on Ala-d₃ and CF₃-Phg labeling strategies

P/L system and NMR-label	List of labeled residues used in the analysis				τ (°)	ρ (°)	S_{mol}	RMSD (kHz)
P/L = 1:200								
Ala-d ₃ (unsigned splittings)	A6	A8	A10	A14	98	115	0.66	1.3
		I9	A10	I13 A14	94	117	0.66	1.3
CF ₃ -Phg (signed splittings) ^a		I9	A10	I13 A14	89	116	0.63	0.3 (1.6) ^b
P/L = 1:50								
Ala-d ₃ (unsigned splittings)	A6	A8	A10	A14	126	110	0.75	0.5
		I9	A10	I13 A14	128	107	0.75	0.2
CF ₃ -Phg (signed splittings) ^a		I9	A10	I13 A14	123	95	0.63	0.2 (1.0) ^b

^a Results from [75].

^b RMSD multiply by a factor $\Delta v_q(\max) / D(\max) = 84 / 15.8$ kHz for the sake of comparison.

Table IV.6 Deviations of the calculated ¹⁹F-NMR splitting from the experimental splitting of CF₃-Phg labels.

Labeled position	Ala-d ₃ experimental splitting	Ala-d ₃ calculated splitting ^a	CF ₃ -Phg calculated splitting ^b	CF ₃ -Phg experimental splitting ^c	CF ₃ -Phg splittings ratio ^d
P/L=1:200					
9	5.2	4.9	0.9	0 ^e	(0)
10	15.0	-14.7	-2.6	0 ^e	(0)
13	26.4	20.6	3.7	+5.6	1.5
14	26.6	-25.5	-4.6	-5.4	1.2
P/L=1:50					
9	30.0	-28	-4.4	-4.7	1.1
10	30.3	-30.8	-4.9	-3.1	0.6
13	20.1	-17.3	-2.7	-3.3	1.2
14	21.5	-18.4	-2.9	-5.3	1.8

^a from native Ala substitution best fit ²H-NMR analysis

^b Ala-d₃ calculated splitting multiplied by a factor $D(\max) \cdot S_{mol}(CF_3-Phg) / \Delta v_q(\max) \cdot S_{mol}(Ala-d_3)$

^c data from [75]

^d being the ratio between the CF₃-Phg experimental splitting and the CF₃-Phg calculated splitting

^e splitting too small to be resolved

At low peptide concentration, two ^{19}F values could not be resolved and it appeared that A10 was quite divergent. It is, however, possible that I9 gives 1 kHz and that A10 gives a positive value as seen from the experimental spectra [119].

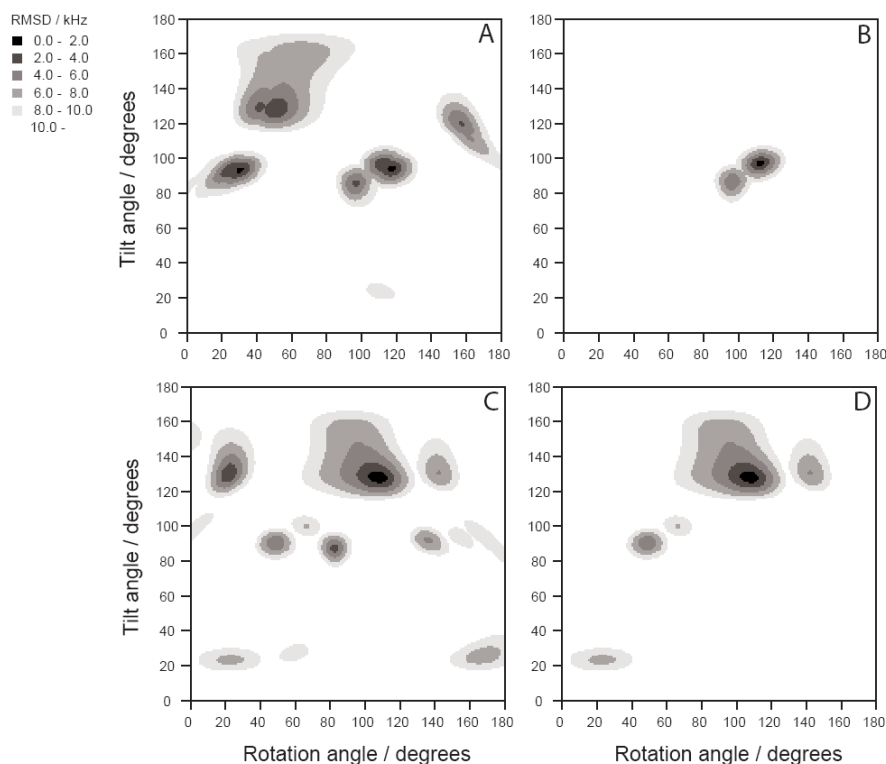


Figure IV.6. RMSD plot of PGLa in DMPC at $P/L=1:200$ (panel A and B) and $P/L=1:50$ (panel C and D). Analyses were done with absolute data values from PGLa9, PGLa10, PGLa13, PGLa14 (panel A and C), and with the absolute data values from PGLa10, PGLa14 and values from PGLa9, PGLa13, including the signs from ^{19}F data (panel B and D).

At higher peptide concentration, the Ala to $\text{CF}_3\text{-Phg}$ substitution data point deviate substantially from the theoretical values, whereas the Ile to $\text{CF}_3\text{-Phg}$ substitution data are in good correlation. Indeed $\text{CF}_3\text{-Phg}$ is expected to be quite hydrophobic, probably as hydrophobic as Ile. On the other hand, Ala is only half as hydrophobic as Ile [126]. In membrane peptides, bulk hydrophobic residues are also more likely to be exposed to the hydrophobic bilayer core than to participate in the dimer interface [126, 135]. These are quite important parameters to consider not only for the packing of the PGLa dimer but also for the lipid-peptide interface. It is thus not surprising to find these slight orientational deviations when replacing Ala by $\text{CF}_3\text{-Phg}$. But it is worth noting, that this ^{19}F -NMR analysis still gives reliable orientation results as the labeling positions have been consciously chosen. Furthermore, the signs of the ^{19}F splittings correlate with the signs calculated for the ^2H -NMR values. It is interesting to note that using the signs from the ^{19}F splittings of the Ile to $\text{CF}_3\text{-Phg}$

substitutions, the corresponding ^2H -NMR couplings allow to discriminate between all multiple solutions below 2 kHz RMSD as depicted in figure IV.6.

5. Conclusions

First of all, the reliability of the CF_3 -Phg NMR method was confirmed here and its accuracy assessed. From a practical point of view, this ^{19}F -NMR methodology has a plethora of advantages thanks to its high sensitivity and absence of natural background. Several experimental conditions like pH, temperature or peptide concentration can easily and rapidly be screened. In a previous study, PGLa in DMPC membranes in a concentration range from 1:8 and up to 1:3000 have been easily detected and have shown a two-state concentration-dependent re-orientation [120].

Secondly, it was shown that despite of the unknown sign of the ^2H quadrupolar splitting, it was possible to get very accurate and reliable orientation analysis from 4 native Ala substitutions in the middle of the peptide helix. It was also found that a single Ile or Gly could be replaced by Ala without inducing any structural or orientational changes of the peptide under the present experimental conditions. This made it possible to get more motional information, and two different methods to determine peptide orientation were compared. Both gave the same peptide alignment in the membrane. It was concluded that PGLa underwent a concentration dependent re-alignment from a surface state to a tilted state, probably by anti-parallel dimer formation with peptide-peptide contacts on the Gly-Ala rich face of the helix.

V. Conditions affecting the re-alignment of the antimicrobial peptide PGLa in membranes as monitored by solid-state ^2H -NMR spectroscopy

The results presented in this chapter have been published as [4] in Biochimica et Biophysica Acta by P. Tremouilhac, E. Strandberg, P. Wadhwani, and A.S. Ulrich in 2006.

The previous chapter demonstrated that the re-alignment of PGLa peptide depends on its concentration in the membrane. This re-alignment is an important step in the Shai-Huang-Matsuzaki model describing the antimicrobial action. It was also shown that using a simple model for the molecular order, a reliable analysis can quickly be done, though part of the dynamical information is lost. Overall, it showed the feasibility of getting highly accurate orientational data from a set of only four non-perturbingly ^2H -labeled peptides which hold for any alignment state in the membrane. The study presented in this chapter makes use of these results to screen several other conditions affecting the above mentioned re-alignment.

1. Stating the problem

In chapter I, the model of the membrane permeabilization process for cationic amphipathic peptides was introduced. The concentration dependent pore formation implicates a cooperative process between several peptides and is thought to be responsible for both anti-bacterial and hemolytic activities. The origin of this cooperativity has been explained by a theory based on surface adsorption of scaled particles [137], but it is also consistent with a direct peptide-peptide interaction like dimer formation, as postulated in the previous chapter, or with medium-range interactions through membrane deformation. There is experimental evidence supporting both cases. Some AMPs like to form dimers in a membrane environment [122, 124, 125], and synthetic dimers are shown to be more active to induce membrane leakage [138-140]. AMPs are also shown to induce local thinning of the membrane and modify its elasticity [69]. This cooperation leads to loss of integrity of the lipid bilayer. The bacterial cytoplasmic membrane permeabilization process by cationic AMPs is believed to

involve the formation of a “toroidal wormhole” pore (see Figure I.7). This transmembrane pore should be formed by a few fully inserted peptides, interleaved with anionic lipids to compensate the high positive charge from the peptides within the pore. Theoretical studies assessed the energetics and stability of pores constituted by such cationic peptides being in a transmembrane state [141, 142]. Other *in silico* studies have dealt with the formation of such pores with the aim of getting more information on peptide orientation in membranes [141, 143, 144]. Experimentally, there is direct evidence for a defined pore structure as corroborated by the liposomal leakage of particles having a specific size [88]. Water filled pores have also been directly detected using in-plane neutron scattering measurements [72, 145, 146]. These experiments revealed a radius for the water column in the range of 15 to 25 Å, as the pore size could vary according to the sample composition. It was estimated that only 4-7 peptide monomers are located in each pore [69, 88], which is too few to shape a pore if the lipids do not participate in the structure. However, the peptides are not directly visible in these neutron scattering experiments and there is no detailed analysis of the lipid-peptide arrangement which would confirm the model. Indeed, only very few studies can give exact information on the state of the peptide in these pores. Even if oriented CD (OCD) experiments have shown a re-alignment of the peptides, they can, a posteriori, not give the exact orientation of the peptide. More recently, Toke et al. have suggested from several REDOR distance NMR measurements that the peptide MSI-103 (also known as K3), a peptide derived from PGLa, is compatible with such toroidal pores having the peptide in the transmembrane state [134], but those results might be biased because of the specific experimental conditions where lipids are not in a liquid crystalline phase. Actually, from NMR experiments, no AMP has so far been directly shown to be in a transmembrane state in a liquid crystalline phase lipid system (see [2] for a review of NMR on peptides) and overall, detailed information is indeed still needed for an accurate structure determination of such pore for understanding the mechanism. In particular, for PGLa little is known about its mode of membrane permeabilization. Re-alignment of the peptide to a tilted orientation was shown [IV], but no transmembrane insertion, as implied by the standard toroidal pore model, has yet been found, and more generally no evidence of such toroidal pores has yet been reported for PGLa. Its membrane activity being selective, it clearly depends on membrane environmental conditions.

Thus, the aim of this chapter is to find conditions for which PGLa pores would be detected by solid-state NMR. The orientational behavior of PGLa is investigated using the previously described ²H-NMR spectroscopic method [II, IV]. A set of four peptides each singly labeled with the non-perturbing Ala-d₃ at one native alanine position was used to

determine the orientation of the PGLa molecule in model membranes. In chapter IV, it had been shown that four such labels allow carrying out an accurate orientational analysis, hence in some cases, peptide analogues with Ile or Gly replaced by Ala- d_3 were also used. To screen the re-alignment conditions, the parameters varied were (i) the presence of negatively charged lipids, (ii) the peptide/lipid ratio, and (iii) the level of hydration of the sample. In detail, the membrane models were constituted of DMPC or DMPC/DMPG (3:1). Peptide concentration ranged from a peptide to lipid ratio (P/L) of 1:200, to 1:20. The hydration of the system was controlled by the type of sample preparation. The glass-plates (GP) method preparation afforded a limited hydration of the lipid/peptide bilayers with 96% relative humidity. The multilamellar vesicle (MLV) method used an excess of water with 50% (w/w) of total sample hydration. Effects on the lipid membrane were also studied by ^{31}P -NMR spectroscopy as toroidal wormholes involve a significant contribution of lipid head-groups.

Through this wide range of experimental conditions, a rough phase diagram of the peptide orientation is drawn. In the view of the new results, comparisons are done with the data obtained with ^{19}F -NMR and the influence of sample preparation is discussed. All obtained orientational data are addressed with an eye on the toroidal wormhole model of pore formation.

2. Materials and methods

2.1. Sample preparation

PGLa (wt), PGLa6, PGLa7, PGLa8, PGLa9, PGLa10, PGLa11, PGLa13, PGLa14 of the pure peptide stocks synthesized as previously described [III], were employed after LC-MS control. Sample preparation followed the general method described in part [II.2.2.2]. In some case, MLVs were prepared to obtain a water content of either 40% or 75% (w/w) of the total sample. Additional MLV mixtures were prepared with PGLa and filled into a 5 mm MAS rotor.

2.2. NMR spectroscopy

General methods for NMR data acquisition were described previously [II.2.2.3]. The spinning rate for MAS ^{31}P -NMR experiment was 1 or 4 kHz and spectra were referenced to

H₃PO₄ (85%) set to 0 ppm. For experiments with 1 kHz spinning frequency, spinning sidebands were fitted with Lorentzian peaks using the DM-Fit program [147], and a Herzfeld-Berger analysis [148] using the software HBA 1.5 [149] afforded the principal elements of the ³¹P CSA tensor. All measurements were carried out at 308K.

2.3. Calculation

The PGLa peptide was modeled as a regular α -helix as described in [II.2.1] and the calculations were done assuming a uniaxially symmetric order tensor of the peptide using the three parameters τ , ρ and S_{mol} . The accuracy were assessed by RMSD determination from the experimentally observed data [II.2.1].

3. Results

In this study, both MLV and GP samples were employed. In the previous chapter MLVs had been employed as they afford a better filling of the coil at low P/L ratio. Their use is limited by the dynamics of the embedded peptide, which has to rotate fast around the membrane normal to make it possible to directly measure the splitting [II.1.3][90]. Since GP samples provide better resolution and easier splitting evaluation even when the peptides do not rotate around the bilayer normal [II.1.3], they were here also preferentially used especially for high P/L. Thus PGLa was investigated in GP samples when inserted in DMPC membranes at a P/L ratio of 1:100, 1:50, and 1:20, and in DMPC/DMPG (3:1) membranes at a ratio of 1:50 and 1:20. The spectra obtained are shown in Figure V.1. The well resolved splittings indicated a well defined orientation of the peptide. Even at P/L=1:20 no disordered aggregation state was observed.

For comparison, spectra obtained from MLVs samples are shown in Figure V.2.A. The splittings are readable up to a P/L of 1:50 in DMPC. From the broadening of the Pake pattern, it was concluded that the diffusional rotation of PGLa around the membrane normal stops at a P/L between 1:50 and 1:20.

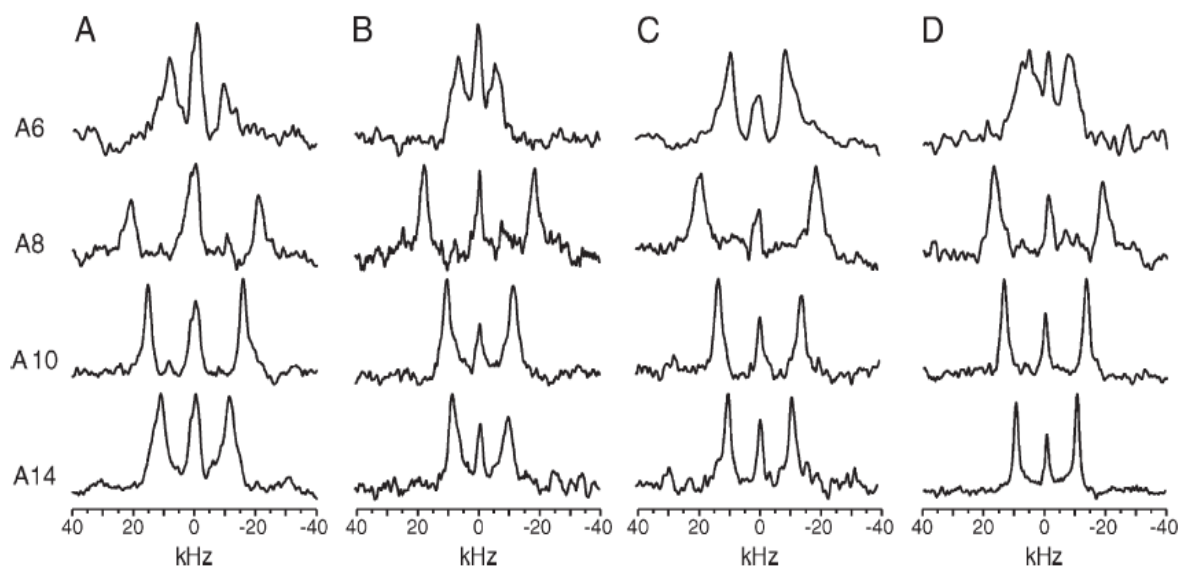


Figure V.1. ^2H -NMR spectra of PGLa with non-perturbing Ala- d_3 labels in different positions in GP samples. (A) PGLa at P/L=1:100 in DMPC. (B) PGLa at P/L=1:20 in DMPC. (C) PGLa at P/L=1:50 in DMPC/DMPG (3:1). (D) PGLa at P/L=1:20 in DMPC/DMPG (3:1). (Adapted [4]).

Table V.1. ^2H -NMR splittings of PGLa in kHz, measured in DMPC or DMPC/DMPG samples.

	MLV samples ^a					GP samples				
	1:200 ^b		1:100 ^b	1:50 ^b		1:100 ^b	1:50 ^b		1:20 ^b	
	PC ^c	PC/PG ^c	PC ^c	PC ^c	PC/PG ^c	PC ^c	PC ^c	PC/PG ^c	PC ^c	PC/PG ^c
PGLa6	15.6 ^d	14.4	8.3	1.0 ^e	12.0	17.5	18.2 ^d	17.5	12.4	12.2
PGLa8	17.2 ^d	18.4	22.6	24.8	36.0	42.0	42.0 ^d	39.2	37.4	35.7
PGLa10	15.0 ^d	15.0	15.6	22.2	20.0	30.9	30.8 ^d	27.5	21.6	26.7
PGLa14	26.6 ^d	25.6	20.8	18.6	16.6	22.5	21.5 ^d	20.0	18.6	18.6

^a Splittings were measured from the 90° peaks of the powder pattern and multiplied by a factor of 2 to correspond to the 0° signal.

^b Peptide-to-lipid molar ratio in the samples.

^c DMPC or DMPC/DMPG (3:1) lipid bilayers.

^d Data from [3].

^e Splitting too small to resolve, estimated value.

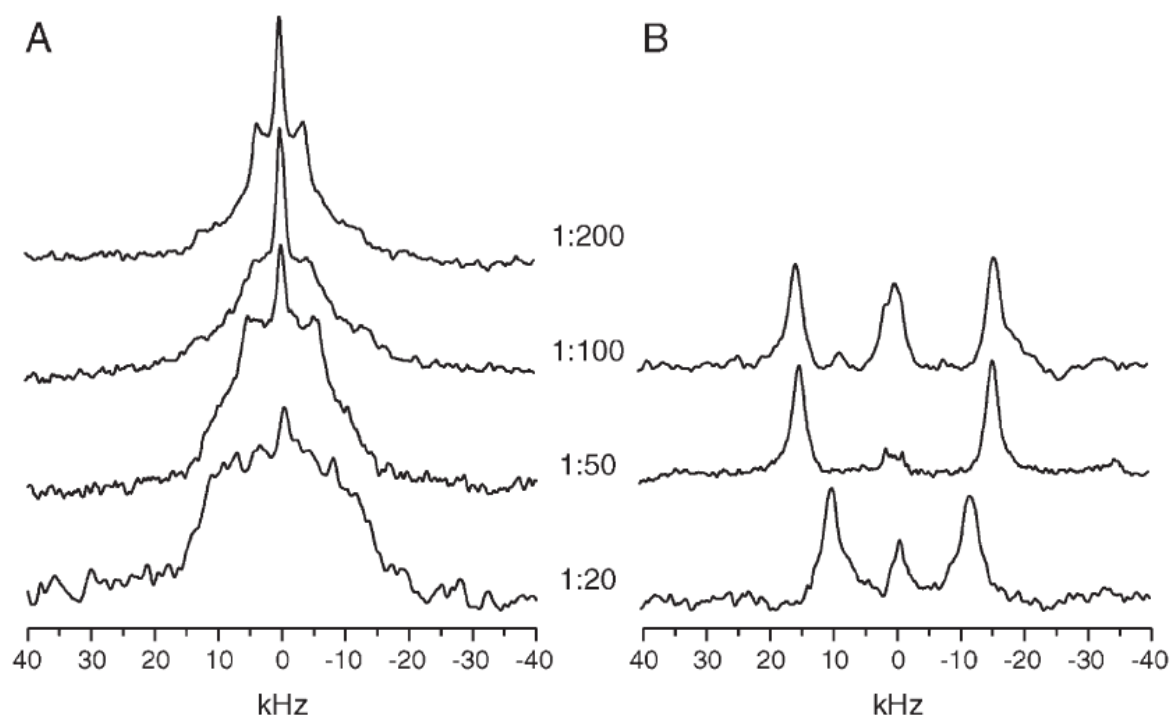
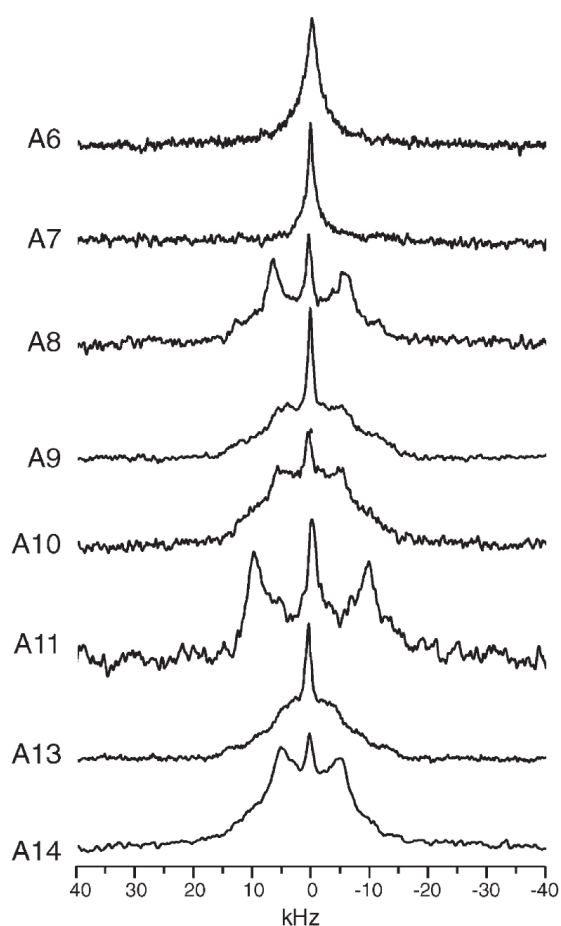


Figure V.2. Comparison of ^2H -NMR spectra from PGLa10 in DMPC at 2H-NMR spectra of PGLa10 in DMPC at different peptide-to-lipid ratios. (A) MLV samples in which the lipid forms multilamellar vesicles. (B) Macroscopically oriented GP samples: a uniform membrane alignment is induced by glass plates. (Adapted from [4]).



As mentioned, MLV and GP samples can be prepared while controlling the content of water at different degrees of full or partial hydration [150, 151]. In this study, GP samples were prepared by hydrating at 96% relative humidity. To examine the effect of higher hydration, series of MLVs samples were also made in DMPC at P/L of 1:200, 1:100 and 1:50, and in DMPC/DMPG (3:1) at P/L of 1:200 and 1:50 to allow a systematic comparison. The ^2H -NMR spectra from MLV samples at P/L=1:50 in DMPC are shown in Figure V.3.

Figure V.3. ^2H -NMR spectra of PGLa with Ala3 labels in different positions in MLV samples. at P/L=1:100 in DMPC.

3.1. ^{31}P -NMR study of the lipid bilayers

The alignment of the membrane surface was assessed by ^{31}P -NMR in all samples. For the MLV samples in static experiments, spectra showed powder shapes typical of a liquid crystalline lamellar phase. In the GP samples containing DMPC only, a single peak at low field was indicative of perfectly oriented membranes with their mean surface normal aligned along B_0 . Only a small contribution of unoriented lipid domains was observed. By integrating the intensities of each contribution, all GP samples were estimated to be at least 80% oriented. In the case of DMPC/DMPG (3:1) samples, two peaks were resolved in the presence of PGLa (P/L = 1:50 and P/L = 1:20). The intensity ratio of these peaks was 3:1, hence the larger peak was identified as DMPC. To confirm this, in identical samples containing PGLa (wt) at P/L=1:20, the amount of DMPG was increased such that the ratio of DMPC/DMPG was 1:1. The ratio between the peaks then became 1:1 (data not shown). The peaks were consequently assigned to DMPC and DMPG, respectively.

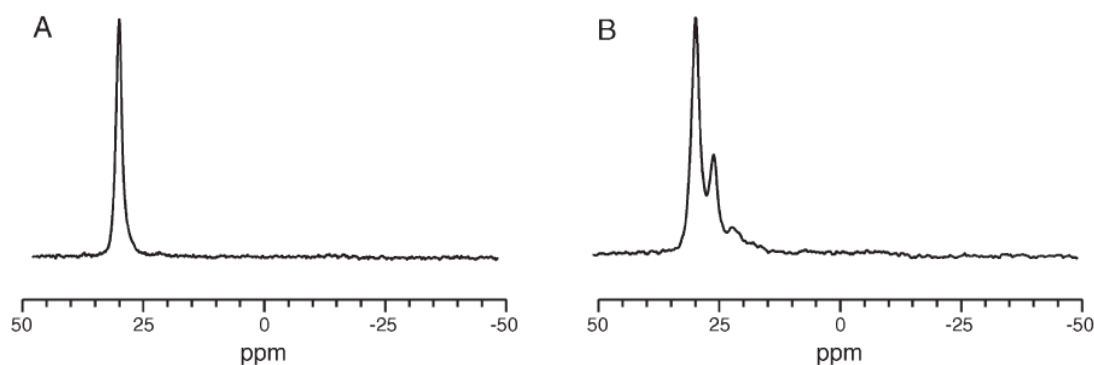


Figure V.4. ^{31}P -NMR spectra of GP samples. (A) PGLa in DMPC at P/L=1:50. (B) PGLa in DMPC/DMPG (3:1) at P/L=1:50. (Adapted from [4]).

In DMPC/DMPG at P/L=1:20, further experiments using MAS-NMR techniques showed no apparent change in the isotropic chemical shift values of both lipids upon addition of PGLa. The fitting of side-bands according to the two lipid populations revealed the principal CSA parameters for DMPC and DMPG in the presence or absence of peptide, which are presented in Table V.2. The reduction of the anisotropy in pure DMPC upon addition of PGLa has been previously reported [75]. Here, in a system of DMPC/DMPG lipids, the anisotropy of the anionic lipid was slightly reduced whereas the anisotropy of the zwitterionic lipid was increased in the presence of PGLa. It was thus deduced that PGLa induced lipid segregation.

Such effects have also been observed for Mag2 [13] and for the scorpion toxin pandinin 2 [152].

Table V.2. Principal ^{31}P -CSA parameters of DMPC/DMPG (31:1) lipids in MLV samples without or with PGLa at P/L=1:20.

	σ_{iso} (ppm)	σ_1 (ppm)	σ_2 (ppm)	σ_3 (ppm)	δ_σ (ppm)	η	% Peak integration
PC/PG (15:5)							
DMPG	0.53	19.8	-8.9	-9.2	19.2	0.02	30
DMPC	-0.58	21.4	-11.5	-11.5	21.9	0.00	70
PGLa/PC/PG (1:15:5)							
DMPG	0.53	18.9	-7.9	-9.4	18.4	0.08	29
DMPC	-0.58	25.6	-13.3	-14.1	26.21	0.03	71

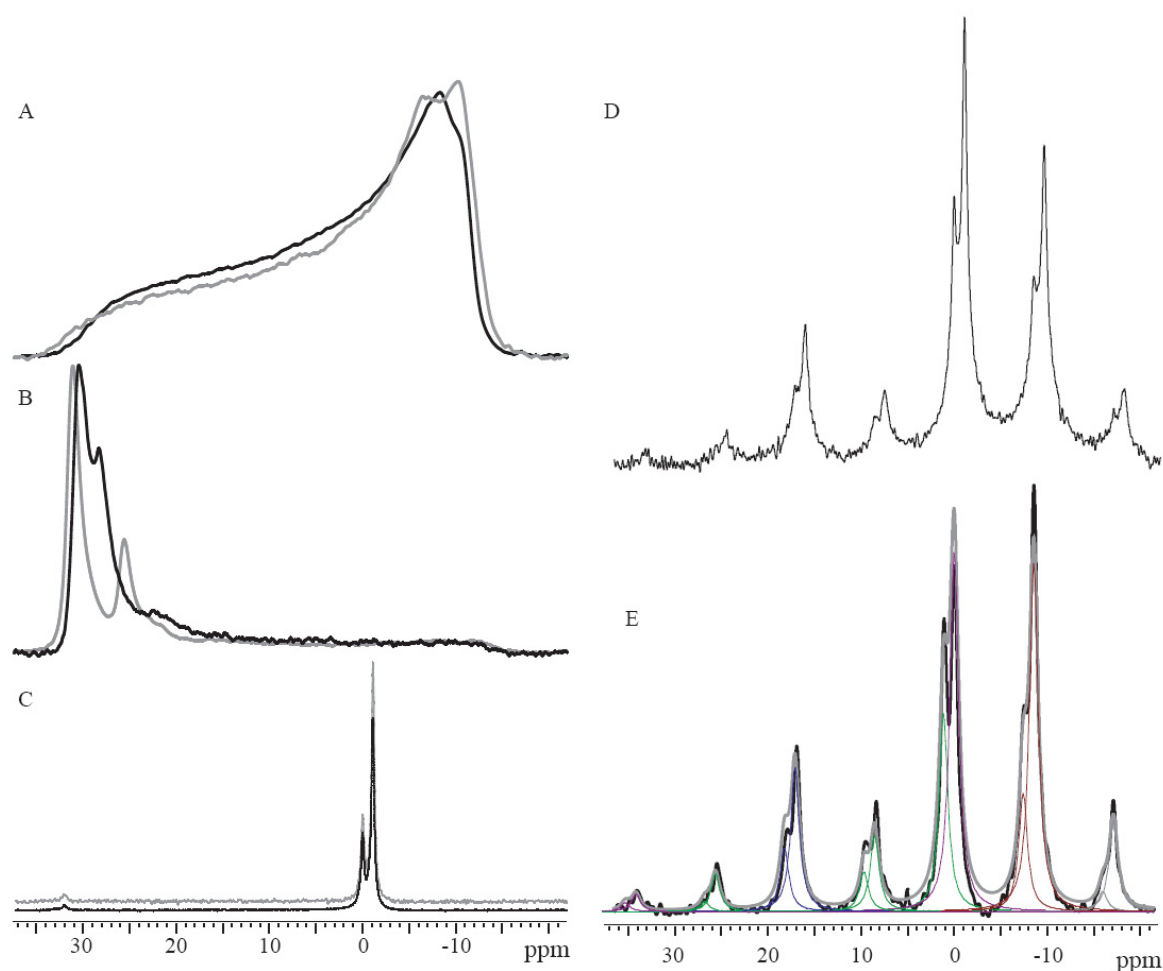


Figure V.5. ^{31}P -NMR spectra of DMPC/DMPG (3:1) samples. Left-handed panel: pure lipid system (grey-colored curves) and in the presence of PGLa at P/L=1:20 (black curves). (A) MLVs in a static unoriented MLV sample. (B) GP-sample with the normal aligned along B_0 . (C) MLVs rotated at the magic angle (at 4 kHz spinning speed). Right-handed panel: MLVs of DMPC/DMPG (3:1) rotated at the magic (at 1 kHz spinning speed) without peptide (D) or in the presence of PGLa at P/L=1:20 (E). The experimental curves are depicted with a thick black line. The fitted curves are depicted in grey. Each individual peak was first fitted with a lorentzian curve as depicted with thin grey lines.

3.2. ^2H -NMR results

In Table V.1 are gathered all ^2H -NMR splitting for the different sets of experiments on the four labeled peptides where a native Ala was replaced by Ala- d_3 . The data from the previous study were added for better comparison. From these splittings, the peptide alignment in terms of τ , ρ , and S_{mol} was calculated for each system. Table V.3 shows the results with their respective RMSD.

Table V.3. Best-fit values from the orientational analysis of PGLa in DMPC or DMPC/DMPG samples, using the ^2H -NMR data from Table XX.

	MLV samples					GP samples				
	1:200 ^a		1:100 ^a		1:50 ^a	1:100 ^a		1:50 ^a		1:20 ^a
	PC ^b	PC/PG ^b	PC ^b	PC ^b	PC/PG ^b	PC ^b	PC ^b	PC/PG ^b	PC ^b	PC/PG ^b
τ ($^\circ$)	98 ^c	98	105	111	126	124	126 ^c	126	125	121
ρ ($^\circ$)	115 ^c	115	112	116	103	111	110 ^c	109	104	113
S_{mol}	0.66 ^c	0.62	0.57	0.63	0.53	0.78	0.75 ^c	0.69	0.57	0.70
RMSD (kHz)	1.32 ^c	1.02	0.38	0.30	0.85	0.71	0.45 ^c	0.54	0.34	0.19

^a Peptide to lipid molar ratio in the samples.

^b DMPC or DMPC/DMPG (3:1) lipid bilayers.

^c Data from [3].

3.3 Orientation of PGLa in DMPC lipid samples

In DMPC samples, it was shown in chapter III that at P/L=1:200, PGLa lies on the membrane surface with a tilt angle of $\tau=98^\circ$, and at P/L=1:50 it tilts into the membrane with $\tau=126^\circ$. These two orientations are referred to as the surface state (S-state) and the tilted state (T-state), respectively. In both states, PGLa has the lysines pointing to the water phase with a ρ angle between 110° - 115° . In this chapter the aim is to obtain a threshold concentration that triggers such an S- to T-state re-alignment, as well as to check if a fully inserted transmembrane peptide is obtained with increased peptide concentration.

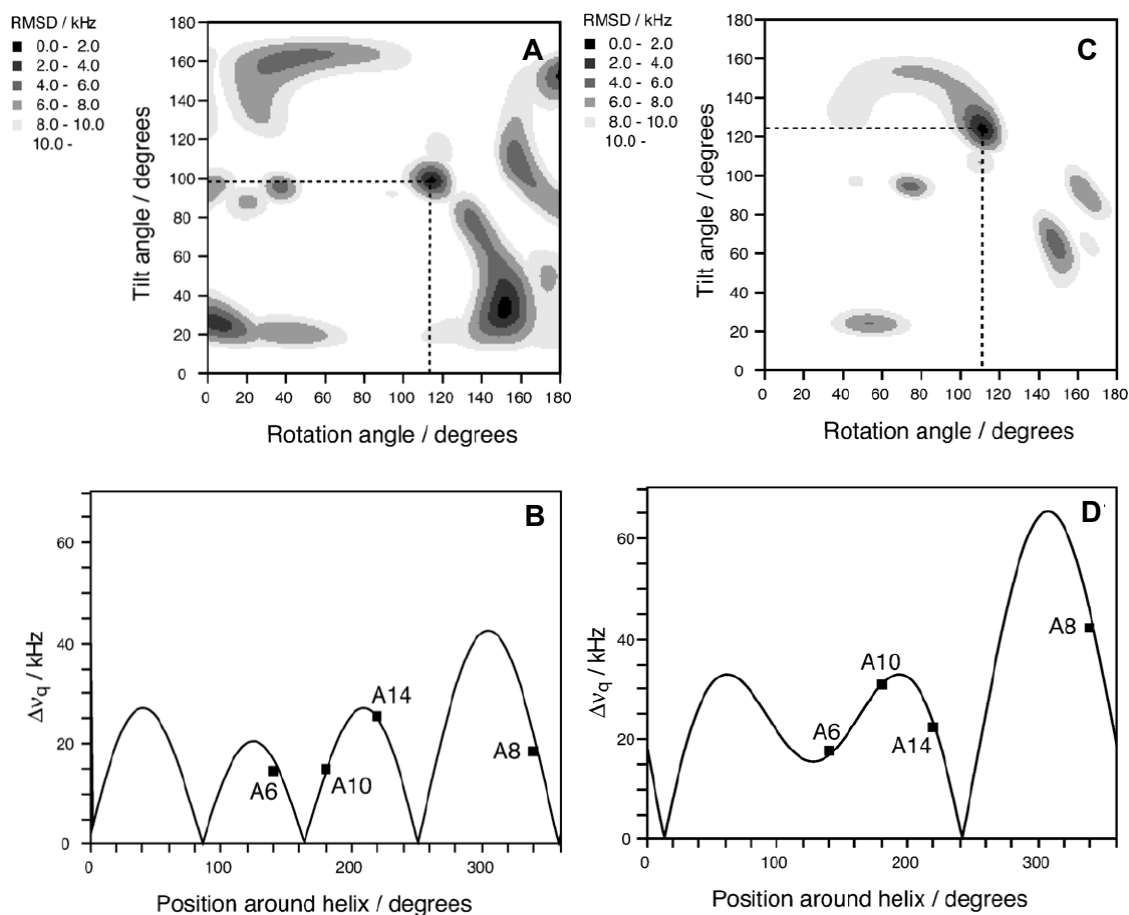


Figure V.6. Left-hand panels: Orientational analysis for PGLa in DMPC 1:100-GP. (A) RMSD plot. The dotted lines indicate the best fit value, $\tau=98^\circ$ and $\rho=115^\circ$. This corresponds to the S-state. (B) Quadrupolar wave plot of the best-fit values fitted to the experimental ^2H -NMR data (filled squares). (C) RMSD plot, the dotted lines indicate the best fit value, $\tau=124^\circ$ and $\rho=111^\circ$. This corresponds to the T-state. (D) The quadrupolar wave plot of the corresponding best solution fitted to the experimental ^2H -NMR data (filled squares). Right-hand panels: Orientational analysis for PGLa in DMPC/DMPG 1:200-MLV. (Adapted from [4]).

The S-state is illustrated in Figure V.6.A and V.6.B with data from P/L=1:200 in MLV samples. At an intermediate P/L ratio of 1:100 in GP samples, the calculations revealed an orientation that corresponds to the T-state with $\tau=124^\circ$ and $\rho=111^\circ$. Figure V.6.C shows the RMSD plot on the τ - ρ map for the best calculated S_{mol} and Figure V.6.D, the corresponding quadrupolar wave curve. It was deduced that the threshold concentration where the orientation switches from the S- to the T-state is above P/L=1:100 and below P/L=1:200 in GP samples.

Remarkably, at full hydration, with P/L=1:100 and P/L=1:50 MLV samples the best fit of $(\tau, \rho, S_{\text{mol}})$ exhibits a similar azimuthal rotation angle but a tilt angle about half-way between the S- and the T-state tilts of $\tau=105^\circ$ and $\tau=110^\circ$, respectively. A set of eight labeled peptides was then used in experiments for calculation to allow a complete comparison with the previous data of GP samples at P/L=1:50 [IV]. All additional labeled peptides (except for PGLa13) concurred with this new intermediate state, as depicted in figure V.7. Repeating the

experiment with a new PGLa13 sample confirmed the deviation for this labeled position. At higher concentration of P/L=1:20 for which the peptide motion was limited on the surface on the membrane (as depicted in figure V.2) no further increase of the tilt was found and PGLa was shown to be in the T-state with $\tau=125^\circ$ and $\rho=104^\circ$.

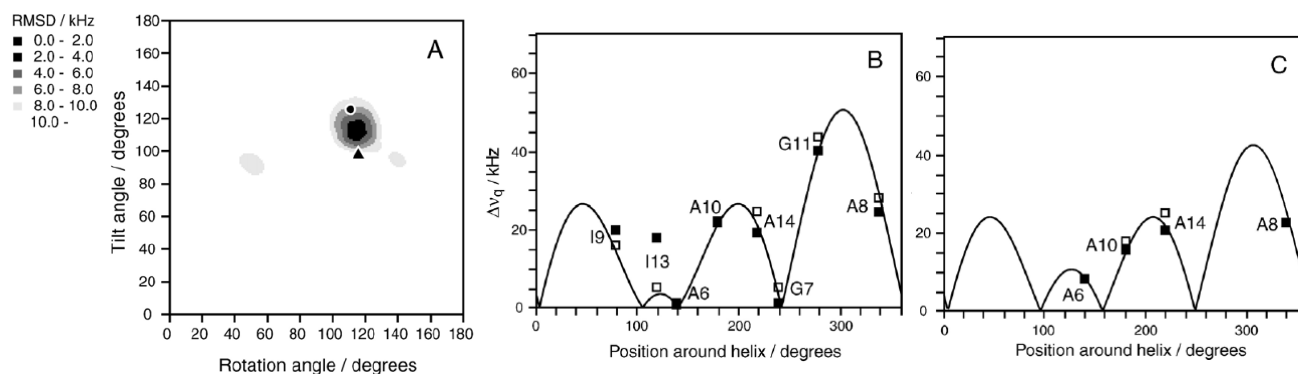


Figure V.7. (A) RMSD plot for PGLa in DMPC 1:50 MLVs. The darkest area indicating the best fit with $\tau=111^\circ$ and $\rho=116^\circ$ lies half-way between the S-state (triangle) and the T-state (circle). (B) The corresponding quadrupolar wave plot is constructed from the experimental ^2H NMR data (filled squares) of the four non-perturbing Ala- d_3 labels, and further data from other substitutions are also included. The curve shows the calculated splittings as a function of the amino acid position around the helical wheel for $\tau=111^\circ$ and $\rho=116^\circ$. The open squares indicate the hypothetical quadrupolar splittings that would arise from fast exchange between 55% S-state (PGLa in DMPC 1:200-MLV) and 45% T-state (PGLa in DMPC 1:50-GP). (At positions 6 and 10, the filled and open squares overlap completely.) (C) Quadrupolar wave plot for PGLa in DMPC 1:100 MLV. The curve shows the calculated splittings as a function of the amino acid position around the helical wheel for $\tau=105^\circ$ and $\rho=112^\circ$. Filled squares correspond to the ^2H -NMR data of the four non-perturbing Ala- d_3 labels, while open squares represents the values calculated for fast exchange between 80% S-state and 20% T-state. (Positions 6 and 8 give the filled and open squares overlapping each other completely). (Adapted from [4]).

3.4. Orientation of PGLa in DMPC/DMPG lipid samples

The influence of DMPG was investigated by adding DMPG lipids to the samples, as bacterial membranes contain anionic lipids and their negative charge is expected to trigger the antimicrobial activity [I]. Thus, samples were prepared using a 3:1 DMPC/DMPG lipid mixture and P/L of 1:200, 1:50 in MLVs and of 1:50, 1:20 in GP sample. The set of the four non-perturbingly labeled PGLa peptides was used.

All these DMPC/DMPG samples showed PGLa being either in the S-state or in the T-state (Table V.3). Only at low concentration (P/L=1:200), PGLa was found in the S-state

(Figure V.6.C and V.6.D). At a P/L=1:50 in MLV sample, in contrast with the MLVs system for DMPC, PGLa was found in the pure T-state.

3.5. Molecular order parameter

For all but one system, the values of S_{mol} were higher in GP samples than in MLVs, as one could expect from the constraints induced by the glass plates and the lower hydration. The order of GP systems ranged from the highest of all values, $S_{\text{mol}}=0.78$ in DMPC at P/L=1:100, to $S_{\text{mol}}=0.69$. For MLVs, S_{mol} was between 0.66 and 0.53 for the least ordered system of all with DMPC/DMPG at P/L=1:50. The exception of the DMPC/DMPG system at P/L=1:20 showed an intriguingly low value of $S_{\text{mol}}=0.57$, below the value for most of the MLV systems. In general, DMPC samples gave higher values of S_{mol} than DMPC/DMPG samples, likewise GP samples gave higher values than MLVs, and high peptide concentration gave higher values than low peptide concentration.

3.6. Influence of hydration

Several MLV samples with either 40% or 75% (w/w) water content were prepared to assess the role of hydration. First, control samples without any peptides were recorded. These samples revealed an important contribution of residual deuteron intensity from its natural abundance in the lipids and water. When ^2H -labeled peptide was added, it was not possible to exactly quantify its signal from the different populations. However, reliable qualitative observations were possible as seen from Figure V.8. It was noticed that PGLa contributed to significantly to the isotropic peak in the DMPC MLV sample at 75% water content. At lower hydration or in the presence of anionic lipid, this contribution disappeared. It was concluded that the cationic PGLa could bind to uncharged DMPC membranes only to a certain extent, and that excess water allowed PGLa to unbind from the lipids. In charged DMPC/DMPG systems, on the other hand, the peptides were electrostatically attracted to the membrane, hence the water content was not relevant for binding.

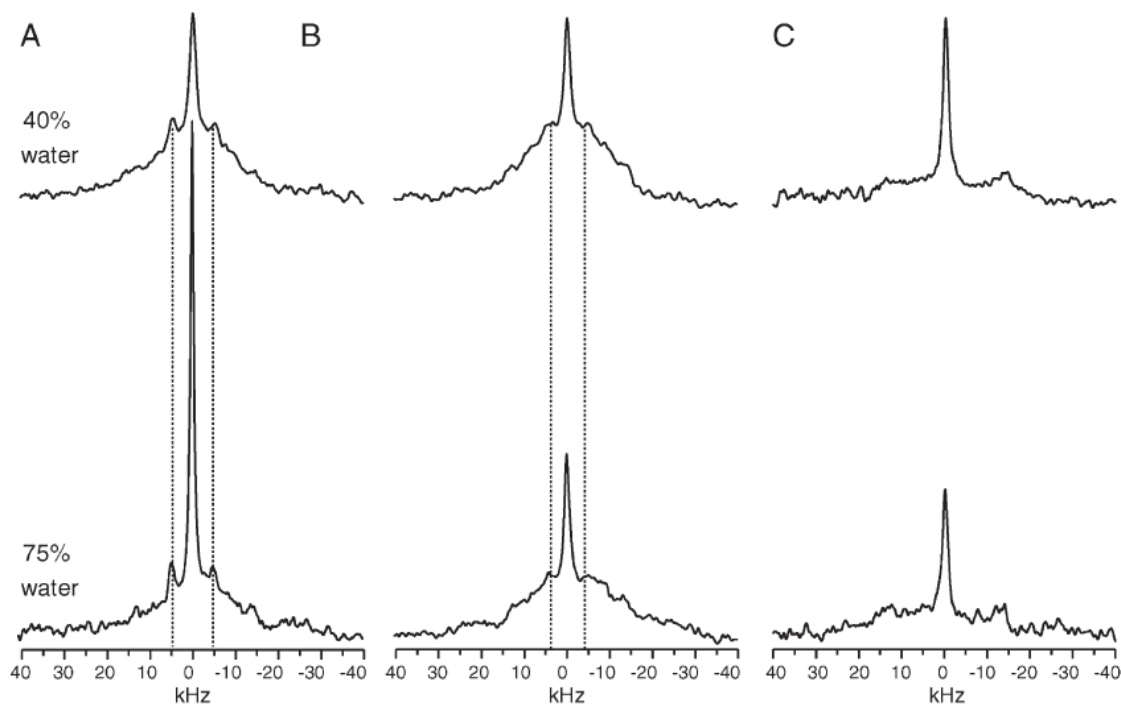


Figure V.8. ^2H -NMR spectra for PGLa8 in MLV samples with different contents of water. (A) PGLa at P/L=1:200 in DMPC, (B) PGLa at P/L=1:200 in DMPC/DMPG (3:1). (C) Pure lipid control, DMPC/DMPG (3:1). (Adapted from [4]).

4. Discussion

In this study, four non-perturbingly Ala- d_3 labeled PGLa peptides were systematically analyzed to obtain orientational constraints. Based on the experimental evidence of Chapter IV, the peptide was modeled as a rigid regular α -helix with uniaxially symmetric ordering tensor. This allowed calculating the orientational state and the overall order of the PGLa peptide in different lipid-water environments, and thus a rough phase diagram was obtained as depicted in Figure V.9. The reliability of the method could be assessed by the RMSD between the back-calculated splittings and the experimental values. Errors within the range of the experimental uncertainty were found in all cases. In some case, additional substitutions at non-native Ala positions could improve the orientation determination. Besides these practical aspects, the new data presented in this chapter allowed the mechanism of action of PGLa to be studied in more detail and addressed it within the known model of action regarding the phase behavior of the lipid and the re-alignment tendency of the peptide.

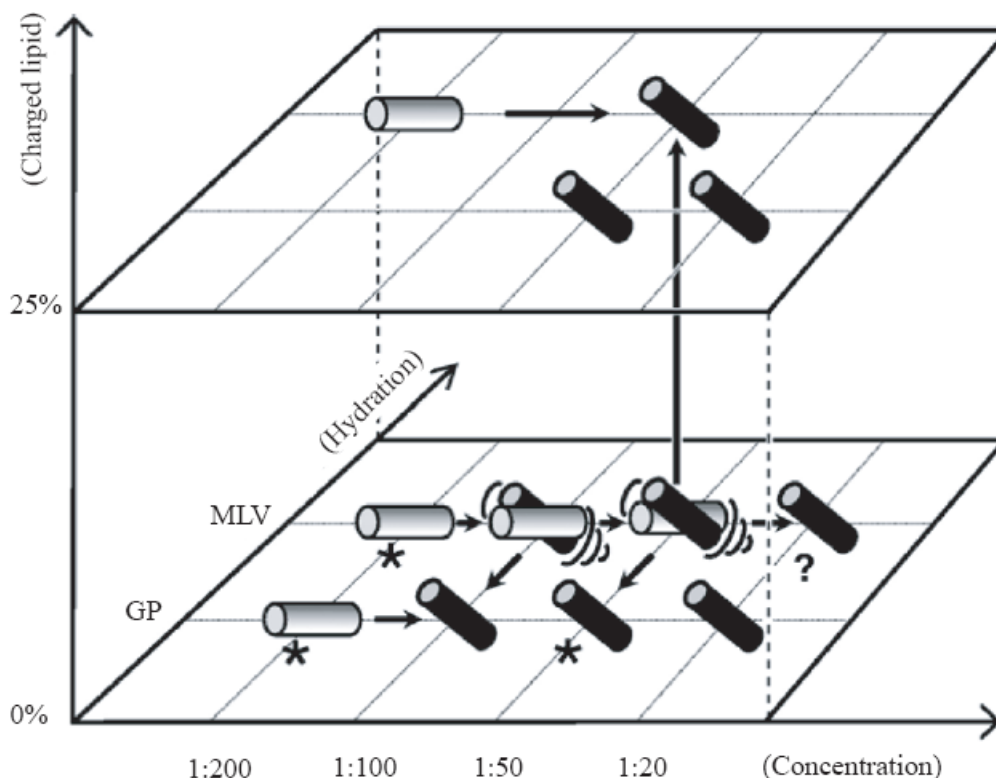


Figure V.9. Phase diagram of the alignment of PGLa in DMPC membranes, as a function of (i) peptide concentration (molar peptide-to-lipid ratio), (ii) sample hydration (using either oriented samples (GP) equilibrated at 96% humidity, or fully hydrated multilamellar vesicles (MLV) with 50% total water content), and (iii) the presence of negatively charged DMPG. The alignment of the cylinders schematically depicts the monomeric S-state (white, $\tau=98^\circ$) and the (presumably dimeric) tilted T-state (black, $\tau=125^\circ$) of the α -helix. The asterisks indicate the previous results in DMPC from ^{19}F -NMR (1:200 and 1:50 in GP, [119, 120]) and ^2H -NMR (1:200 in MLV, and 1:50 in GP[3]). The overlapping cylinders at DMPC MLVs at 1:50 and 1:100 represent intermediate PGLa alignments that are consistent with a fast exchange between the S- and T-states. The thick arrows indicate the forward direction in this S \rightarrow T equilibrium, as affected by changing any of the three variables. Note that the PGLa alignment in DMPC at 1:20 could not be addressed experimentally in MLVs (as indicated by the question mark) since PGLa ceases to rotate fast about the bilayer normal, but the immobilized peptide is presumably well oriented in the T-state as known from the corresponding data in GPs. (Adapted from [4]).

4.1. Phase behavior of the lipid membrane

According to the Shai-Huang-Matsuzaki model, anionic lipids are expected to play a decisive role in the proposed pore formation and structure. As a part of the toroidal wormhole, the lipid head groups should tilt in the inner plane of the bilayer. The pore allows also the lipids to rapidly translocate to the other bilayer leaflet [73]. Such insertion in the membrane plane and such fast translocation should give rise to, respectively, a signal at the high field

edge or an isotropic signal. For example, an isotropic phase formation has been observed for mastoparan, an AMP from bee venom, inserted in DMPG membranes [16], and MSI-78, a magainin analogue, is reported to induce a hexagonal phase arrangement [153]. In this study, however, no such signals were observed and the ^{31}P -NMR spectra demonstrated that the bilayers for all samples are in a lamellar phase. Nevertheless, specific PGLa-lipid interactions were still observed.

DMPG is known to mix quite well with DMPC as one can see from ^{31}P -NMR spectra of pure or mixed lipid systems giving rise to a single signal. However, in the presence of PGLa, two distinct lipid signals could be observed, a DMPC peak and a DMPG peak. Thus, the presence of the cationic peptide induced a lipid separation. It has been shown that charged species, like DNA segments, amphiphiles or electrolytes, which are bound to membrane surfaces, can induce lipid segregation and domain formation [154, 155]. PGLa also reduces the anisotropy of ^{31}P nuclei in pure DMPC samples with increased concentration [75]. This has been observed for other similar peptide-lipid systems by NMR [156, 157] and has been correlated with a global thinning of the membrane as also shown by X-ray reflexivity for Mag2 [110, 158]. However, here in the case of DMPC/DMPG samples, the anisotropy width of DMPC was found to increase while the anisotropy width of DMPG is decreased upon addition of PGLa. These variations were not very large but still noticeable. Such opposite effects on the lipid headgroups are likewise observed for the human antimicrobial peptide LL-37 in PC/PG lipid membranes [24]. They can lead to a global thickening of the membrane as observed for Mag2 in DMPC/DMPG (3:1) membranes by X-ray reflectivity [158]. Thinning of one leaflet of a bilayer may be compensated on the other side by thickening as it is described by Leontiadou et al. in the simulation of a lipid-Mag2 analogue system [16]. Preliminary results on deuterated lipids (data not shown) supported this interpretation.

Another noticeable effect was seen on the asymmetry parameter of DMPG which seemed to increase. Such an increase in the asymmetry parameter has been previously observed for lipid-peptide interactions as shown for cytochrome-c in PC/PE/CL lipid membranes [159]. This could be induced by a slight reorientation of the lipid headgroups to the inner part of the bilayer.

To sum up, no clear evidence for a toroidal wormhole was found from ^{31}P -NMR data, but the results did not exclude such a model. Indeed, they showed that PGLa interacted specifically with anionic lipids, segregating the zwitterionic ones.

4.2. Peptide re-alignment under different conditions

Regarding the state of AMPs in a specific membrane permeabilization process, it is shown by OCD for the template peptide Mag1 that the ensemble of bound peptides above a threshold concentration progressively re-aligns in DMPC/DMPG from a surface state below $P/L=1:60$ to a transmembrane state at $P/L=1:10$ [160]. Using OCD, this re-alignment has been also reported for alamethicin [111, 161] and melittin [162]. However, OCD does not yield an accurate tilt angle and does not provide any information about the azimuthal rotation angle.

In this study, non-perturbing Ala- d_3 NMR labels were used to identify a two-state behavior of PGLa over a wide range of experimental conditions. The two states could be determined very accurately, revealing at the same time the azimuthal orientation of the peptide corresponding to the hydrophilic lysine side chains pointing to the water. The observed re-alignment may be explained by a clustering of two peptides, possibly by dimer formation.

An apparent progressive re-alignment was also observed, but only for MLVs samples at $P/L=1:100$ and $P/L=1:50$ giving a tilt angle for the peptide inbetween the S- and T-state. This could be interpreted as the co-existence of two populations corresponding to the T- and S-state being in fast exchange on the NMR time-scale (exchange frequency higher than the observed splittings of 50 kHz), hence giving only one averaged splitting. Figure V.8 shows the best-fit curve obtained with calculated splitting for a fast exchange process. At $P/L=1:100$, the splittings conveyed 80% contribution from peptide in a S-state and 20% in the T-state. With the concentration increased to $P/L=1:50$, splittings calculated with 55% S-state and 45% T-state fitted well to experimental data as shown in table V.4. Only PGLa13 did not fit well. This peptide also showed decreased biological activity in both hemolytic and antimicrobial tests [III.3.3]. As already mentioned in section IV.4.2, this could originate from a decreased hydrophobicity at a region which should deeply interact with the lipid core (see the helical wheel projection in Figure I.5), for this reason lowering its membrane affinity.

This concentration-dependent orientational transition can be correlated with OCD observations on other systems. Indeed, above a threshold concentration defined by lipid composition and hydration, any additional peptide binding to the membrane surface will lead to the T-state alignment. The origin of this cooperativity between peptides could not be addressed here but its environmental dependence was clearly observed. In fact, the affinity with the membrane directly drove the concentration of bound peptide, as seen from Figure V.8. In more diluted system, anionic lipids are mandatory to attract PGLa [48]. Here, the use

of DMPC lipids and high hydration in MLVs samples shifted the equilibrium between free peptides and membrane bound peptides, so that the full transition between S- and T-state was spread over a wider P/L range. Previous experiments using ^{19}F -labeled PGLa in DMPC had shown that this transition range is narrower in GP samples [75].

Table V.4. Experimental and calculated ^2H -NMR splittings of PGLa in DMPC bilayers.

Peptide	P/L=1:200 MLV (S-state) ^{a, b}	P/L=1:50 oriented (T-state) ^b	P/L=1:50 MLV ^{a, c}	Average of 55% S-state, 45% T- state ^d	P/L=1:100 MLV ^{a, c}	Average of 80% S-state, 20% T-state ^e
PGLa6	15.6	-18.2	1.0 ^f	0.4	8.3	8.5
PGLa7	-9.6	-2.5	1.0 ^f	-6.4	N/A	N/A
PGLa8	17.2	42.0	24.8	28.4	22.6	22.4
PGLa9	-5.2	-30.0	20.0	-16.3	N/A	N/A
PGLa10	-15.0	-30.3	22.2	-21.9	15.6	-18.2
PGLa11	37.0	52.1	40.2	43.8	N/A	N/A
PGLa13	26.4	-20.1	18.0	5.5	N/A	N/A
PGLa14	-26.6	-21.5	19.6	-24.3	20.8	-25.5

^a Splittings were measured from the 90° peaks of the powder pattern and multiplied by a factor of 2 to correspond to the 0° signal.

^b Data from [3]. Signs are taken from the best-fit curves calculated from unsigned ^2H -NMR data and signed ^{19}F -NMR data.

^c Absolute values; the signs of splittings are not known from direct ^2H -NMR measurements.

^d The minimum was calculated by the least square method, excluding the PGLa13 data point.

^e The minimum was calculated by the least square method

^f Splitting too small to resolve, estimated value.

4.3. The T-state and the pore structure

The mechanism of action of AMPs can be different according to the lipid composition. In the case of melittin, the permeabilization of the membrane is shown to be specific for zwitterionic lipids and unspecific for anionic lipids [162, 163]. Here, charged lipids do not seem to change the mechanism of action for PGLa, as all orientational states found to resemble the S- or T-states described in Chapter IV. Furthermore, specific membrane permeabilization is usually attributed to an assembly of peptides which adopt a transmembrane orientation above a threshold surface concentration. These transmembrane peptides spanning the membrane thickness form a pore [I]. In the present study, at a P/L ratio at which PGLa is already known to induce PC/PG liposome leakage [41], no transmembrane state was observed. In fact, even at P/L=1:20 PGLa was found to be only in the T-state. The

125° tilt of the T-state does not allow the peptide to span the membrane. It might be that the proposed toroidal pores still occur, but that their life-time and rate of formation are too short to be observable by NMR. Alternatively, the structure of PGLa pores might differ from this model.

Interestingly, molecular dynamics studies show similar orientation results. It is known that a single α -helical molecule of Mag2 is stable when surface bound, but a recent MD simulation by Leontiadou et al. has shown that an analogue of Mag2, inserted into a DPPC membrane, has a stable α -helical structure, and that when a local concentration of P/L=1:64 to 1:32 is reached, the helical peptides form a funnel like cluster with the peptides having a tilt angle of $\tau=115^\circ$ (according to our definition) with a standard deviation of 20° [143]. This funnel allows first the full insertion of a peptide molecule and thus the formation of a pore through which water and lipid molecules can translocate. The data presented here on the orientation of PGLa corroborated the results of this MD simulation, even though the lipid system and the peptide are different and differences in time scale between simulations and experiments have to be considered.

5. Conclusions

In the present study, the use of four non-perturbingly Ala-d₃ labeled PGLa peptides successfully led to the accurate monitoring of the orientational behavior of PGLa over a wide range of conditions. PGLa was shown to re-align above a threshold concentration of the membrane bound peptide. The mechanism of permeabilization of this peptide appeared to be the same in presence or absence of anionic lipids, as the same re-alignment was observed in DMPC and in DMPC/DMPG membranes. The difference in biological activity could thus be explained by a shift of this threshold re-alignment concentration due to different membrane affinities in the initial binding event. This membrane affinity was driven by charge and hydration. Anionic lipids appeared not only necessary to bind higher amount of PGLa on the membrane, but to interact specifically with the peptide and to form a separate phase.

The peptide in the active state was found to be only partially tilted inside the membrane. This orientation of the peptide did not match with the usual toroidal wormhole model having the peptide in a transmembrane state. This tilted state was thus interpreted by cluster formation of the peptides, and potentially through dimer formation.

VI. Synergistic transmembrane alignment of the PGLa/Mag2 hetero-dimer

The NMR analysis presented in this chapter have been published as [5] in the Journal of Biological Chemistry by P. Tremouilhac, E. Strandberg, P. Wadhwani, and A.S. Ulrich in 2006.

The previous chapters described the orientation of PGLa in DMPC and DMPC/DMPG lipid membranes. Two states were found, a surface state (S-state) and a tilted state (T-state). Thus, the mechanism of action of PGLa may differ from the usual depiction of the Shai-Huang-Matsuzaki model which postulates the formation of pores with fully inserted transmembrane peptides (I-state). However, a transient transmembrane orientation of PGLa was not excluded and could possibly not be measured by NMR because of a short life-time of the pore and slow rate of formation. Going further in the analysis of PGLa in membranes, the present chapter now deals with the behavior of PGLa in the presence of the related peptide Magainin 2 (Mag2) produced by the same frog in the same gland [I]. The aim is to address how the action of PGLa differs when acting together with Mag2 and to explain the functional synergism known for PGLa and Mag2 by orientational changes in the membrane.

1. Stating the problem

On the one hand, the action of PGLa is interpreted through its re-alignment above a threshold membrane surface concentration from a surface state (S-state) to a tilted state (T-state) [III, IV] [3, 4, 75]. However, this tilted state with an angle of 125° (with respect to the membrane normal) does not allow a peptide to span the membrane, therefore, if pores are formed by PGLa, they must be transient. On the other hand, Mag2, another natural AMP co-secreted with PGLa [I], has been shown to form pores according to the toroidal wormhole model. Such pores have been directly detected by X-ray reflectivity under certain conditions, but the orientation of the peptide is not known [146]. Mag2 has been found lying flat on the surface (S-state) by ^{15}N -NMR [164-168] and has not yet been observed in a transmembrane

state (I-state) except for OCD [72, 160]. In these later studies, the transmembrane state of Mag2 is not described in detail and no accurate tilt angle has been measured. More interesting is the behavior of both these peptides when mixed together. Mixtures of PGLa and Mag2 have shown enhanced membrane activity with a maximum effect for an equimolar ratio, indicating the possible formation of hetero-dimers. Leakage of liposome is greatly enhanced [38, 42, 169, 170], confirming, as for single peptides, that this synergetic activity targets the cell membrane. This synergism is shown also for bacterial growth inhibition (vide infra and [170, 171]), and for an uncoupling of the respiratory process [169].

As a re-alignment of the peptide can be directly linked to its biological activity [IV, V], the orientation of PGLa in the presence of an equimolar amount of Mag2 was determined here by ^2H -NMR in liquid crystalline model membranes to shed light on the mechanism of this synergism. A set of eight Ala- d_3 labeled PGLa were used to get orientational constraints as described previously [IV, V][3, 4, 75]. The approach was based on the known conformation of the peptide, and the overall secondary structure content of the peptide mixture was controlled by CD. Given that the synergistic effect may be driven by direct peptide-peptide interactions like dimer formation, the biological activity of the peptide mixture was naturally checked using the methods described in [II] to control whether the labeling had induced any disturbance as discussed in [IV]. In parallel, OCD was also used to monitor and confirm any possible re-alignment. The results of these experiments are discussed and allowed a better understanding of the synergism mechanism.

2. Materials and methods

For this study, the peptides and lipids described in Chapter III were used.

2.1. Antimicrobial tests

PGLa or PGLa analogues were mixed with an equimolar amount of Mag2 or Mag2 analogues according to Table VI.1 to form peptide stock solutions. These mixtures as well as each single peptide alone were tested against two bacterial strains, *E. coli* and *A. hebeiensis* as described in Chapter III. To assess the differences in synergetic activity, the respective fractional inhibitory concentrations (FIC) [172] were also calculated. Given the equimolar ratio of peptides, the FIC parameter was defined as:

$$\text{FIC} = 1/2 [\text{MIC}(\text{PGLa}+\text{Mag2})/\text{MIC}(\text{PGLa}) + \text{MIC}(\text{PGLa}+\text{Mag2})/\text{MIC}(\text{Mag2})]$$

A value of 1 indicates a simple additive effect. A FIC value below 0.5 is a clear indication of synergism, whereas a value above 2 reveals antagonism.

Table VI.1. Table of the peptide mixtures. Two series of peptides mixtures were prepared with the peptide in column 1 mixed with an equimolar amount of each peptide in column 2.

Peptide 1	Peptide 2
Mag2 (wt)	PGLa (wt), PGLa7, PGLa9, PGLa11, PGLa13
PGLa (wt)	Mag2, Mag1, Mag2-amide, Mag2(E19Q)

2.2. CD/OCD measurements

CD spectroscopy on peptide/lipid large unilamellar vesicles (LUVs) was employed to confirm the secondary structure of the mixed peptides in the membrane environment. The same methodology and materials as previously described [III] were used, though instead of a single peptide, equimolar mixtures of PGLa analogues with Mag2 were studied with an overall P/L=1:50. The lipid system was DMPC/DMPG (3:1). Peptide secondary structures were predicted from the three algorithms (SELCON3, CONTIN, and CDSSTR).

Sample preparation for OCD measurement is described elsewhere [III]. As for the CD samples, the overall P/L was 1:50, and the lipid system DMPC/DMPG (3:1). The orientation and hydration of the bilayer system was achieved in a humidity chamber at 96% relative humidity. Measurements were carried out at 308 K.

2.3. NMR-sample preparation and spectroscopy

Oriented samples between glass plates (GP) were prepared as described previously [II.2.2]. Equimolar amount of Mag2 and labeled PGLa analogues were mixed with DMPC/DMPG (3:1) for an overall P/L=1:50. The orientation and hydration of the bilayer system was achieved in a humidity chamber at 96% relative humidity. ³¹P-NMR and ²H-NMR measurements were carried out at 308 K as described previously [II.2.2].

3. Results

3.1. Antimicrobial activity of the ^2H -labeled PGLa analogues

The antimicrobial activity of each labeled PGLa analogue was tested in the presence of Mag2 against two bacterial strains. Figure VI.1 depicts the antimicrobial activity for each PGLa analogue alone and for their mixture with Mag2. Calculation of the FIC values revealed clear synergistic activity for all systems, except for PGLa7/Mag2 against *E. coli*, which gave a FIC value on the border between synergism/additivity.

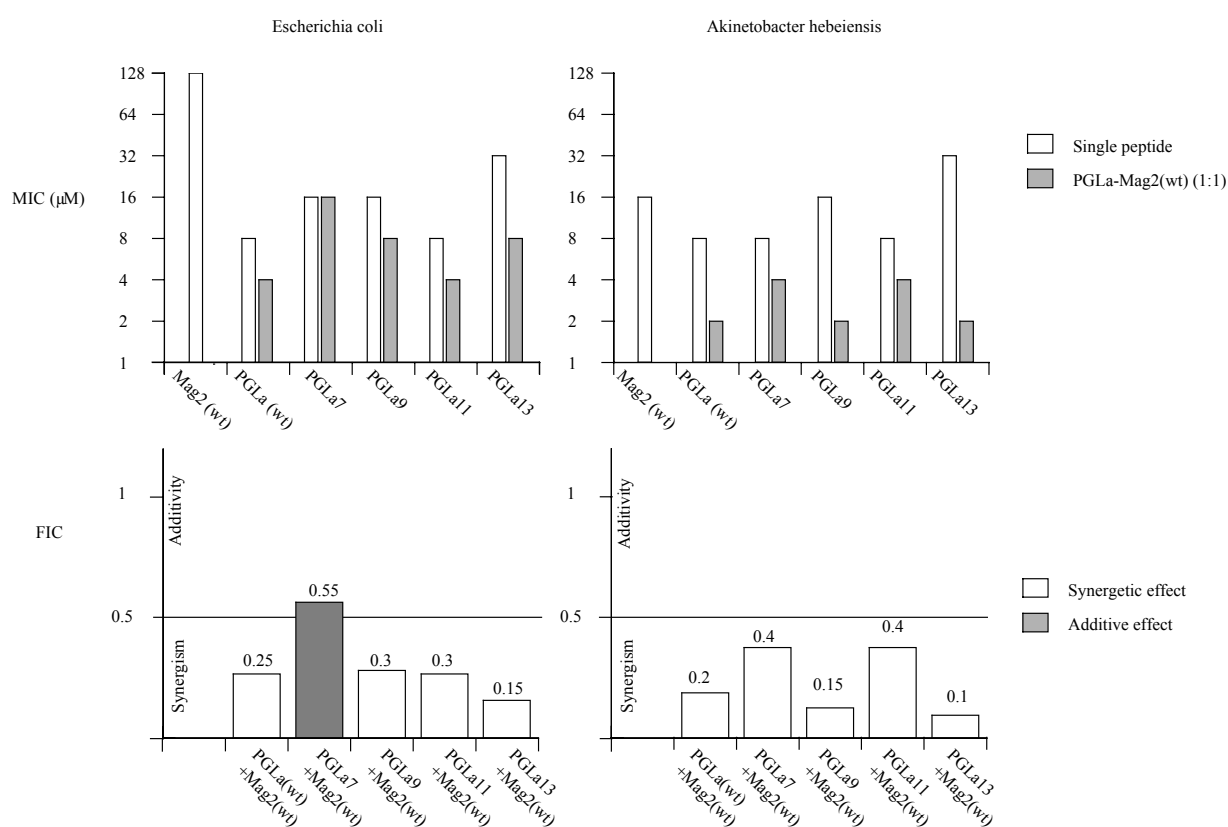


Figure VI.1. MIC and FIC values of PGLa (wt) and PGLa analogues mixed with an equimolar amount of Mag2.

3.2. Antimicrobial activity of Mag2 analogues

The antimicrobial activities of Mag2 analogues, namely Mag1, Mag2-amide and Mag2(E19Q) were tested alone and in the presence of PGLa. Figure VI.2 depicts the activities obtained for PGLa-Mag2 analogue mixtures compared to the Mag2 analogues alone. All Mag2 analogues showed similar activity when acting alone. Synergism was comparable for all systems except for Mag2(E19Q) which showed an additive effect against both strains.

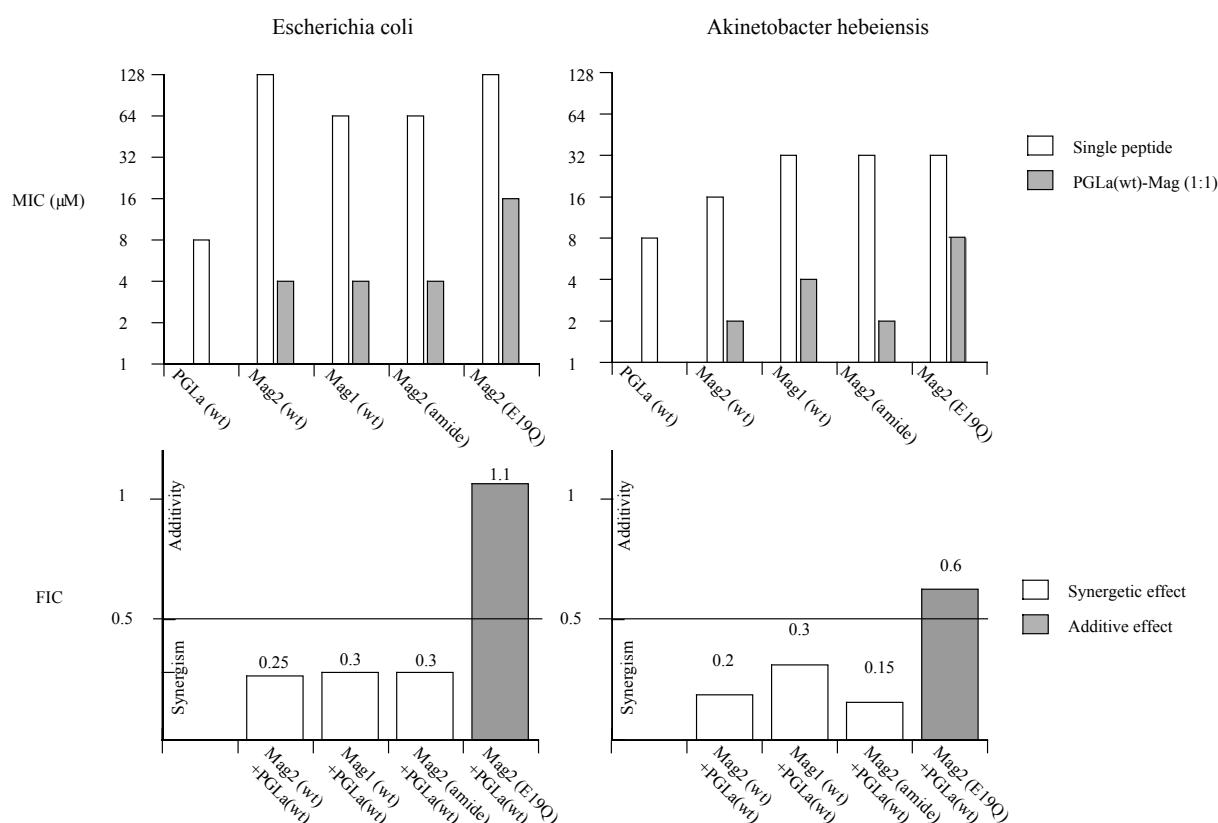


Figure VI.2. MIC and FIC values of PGLa (wt) mixed with an equimolar amount of Mag2 (wt) or Mag2 analogues.

3.3. Choice of lipid system

In the previous study [V], it was shown that a negatively charged lipid (DMPG) surface or lower hydration helps PGLa to bind the membrane and to re-orient to the T-state. It was also shown that DMPG may stabilize the formed pores. Hence PGLa was investigated by CD, OCD, and NMR at a concentration of P/L=1:100 in DMPC/DMPG (3:1) with an equimolar amount of Mag2, giving an overall P/L of 1:50. At both these ratios, PGLa alone is shown by NMR to be in the T-state [V]. If the presence of Mag2 would have no effect on PGLa, or simply an additive effect, then PGLa would be expected to stay in the T-state.

3.4. CD and OCD experiments

CD measurements were performed with each PGLa analogue in the presence of an equimolar amount of Mag2, in LUVs of DMPC/DMPG (3:1). The secondary structure

contents of the peptide mixture were calculated for each system, as illustrated in Figure VI.3 for each analogue in the absence or presence of Mag2. With the ratio of peptide/DMPG, there were more than two DMPG molecules for each positive charge of the peptides, hence all peptides were expected to be bound to the LUVs [48]. At this P/L, no micellization was expected as seen from the ^{31}P -NMR experiment of oriented samples (vide infra). The contribution of disordered structures was thus attributed to part of the peptides bound to the LUVs. Out of the three algorithms used, two of them (SELCON3 and CONTIN) gave very similar results with less than 1% deviation and with a good fit for SELCON3 and a relatively good fit for CONTIN. The structure contents of the peptide mixtures were then obtained by averaging the results of these two algorithms. It appeared that each mixture, except for PGLa11-Mag2, showed almost the same α -helical content with a few percent difference, and these contents were comparable with the ones of each individual labeled PGLa but with a reduced amount of α -helix. In the case of PGLa11-Mag2, a higher content of α -helical structure of around 5% percent, more than for PGLa alone, and a lower contribution from β -turn was found.

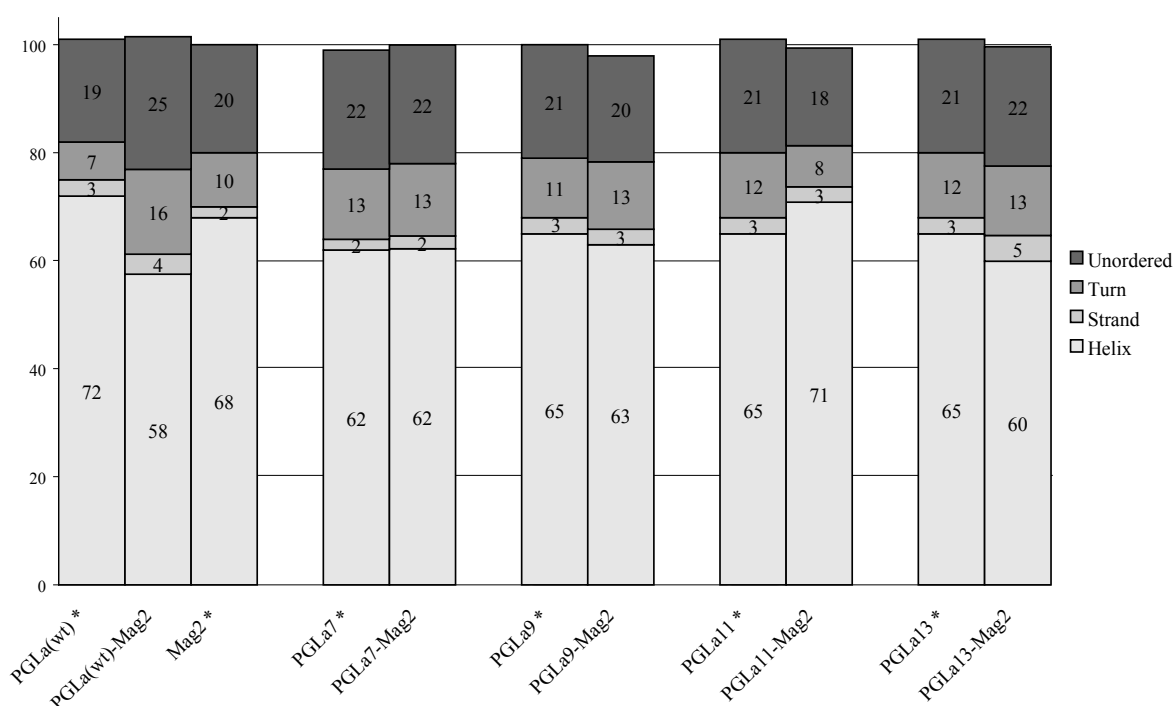


Figure VI.3. Secondary structure contents of peptides in the presence of DMPC/DMPG (3:1) LUVs at P/L=1:50 obtained from CD measurements at 308 K. The overall content of α -helix was found to be above 60% for all labels. (* data from [III]).

OCD can be used to monitor the orientation of α -helical peptides in oriented lipid membranes[III][105]. Unfortunately, OCD does not give an absolute tilt angle to describe the orientation of a peptide, because positions, heights, or widths of the spectral bands are usually model-dependent. Two spectra of the system with known orientation are normally needed to form a base for further spectral deconvolution [III]. Notably, OCD has been so far applied only to single peptide systems, where the peptide secondary structure was assumed to be independent of its concentration. In the present case, for the first time, OCD results for a dual peptide system are reported. As the peptides are known to act synergistically, the concentration of each peptide is likely to influence the structure of the other peptide through dimerization/aggregation, and thus a concentration series may be difficult to interpret. However, it is still possible to appreciate the presence and the shape of typical bands, especially by comparison with the LUV spectra giving the isotropic orientation distribution of the peptides [104]. Figure VI.4 depicts the OCD spectra compared to the CD spectra of LUVs samples. For the sake of contrast, the spectra from LUV samples were normalized to the same height as the ones of OCD to allow a qualitative estimation of the orientation. Any other arithmetics between non-equivalent systems would be hazardous, as spectra could not be normalized to one another.

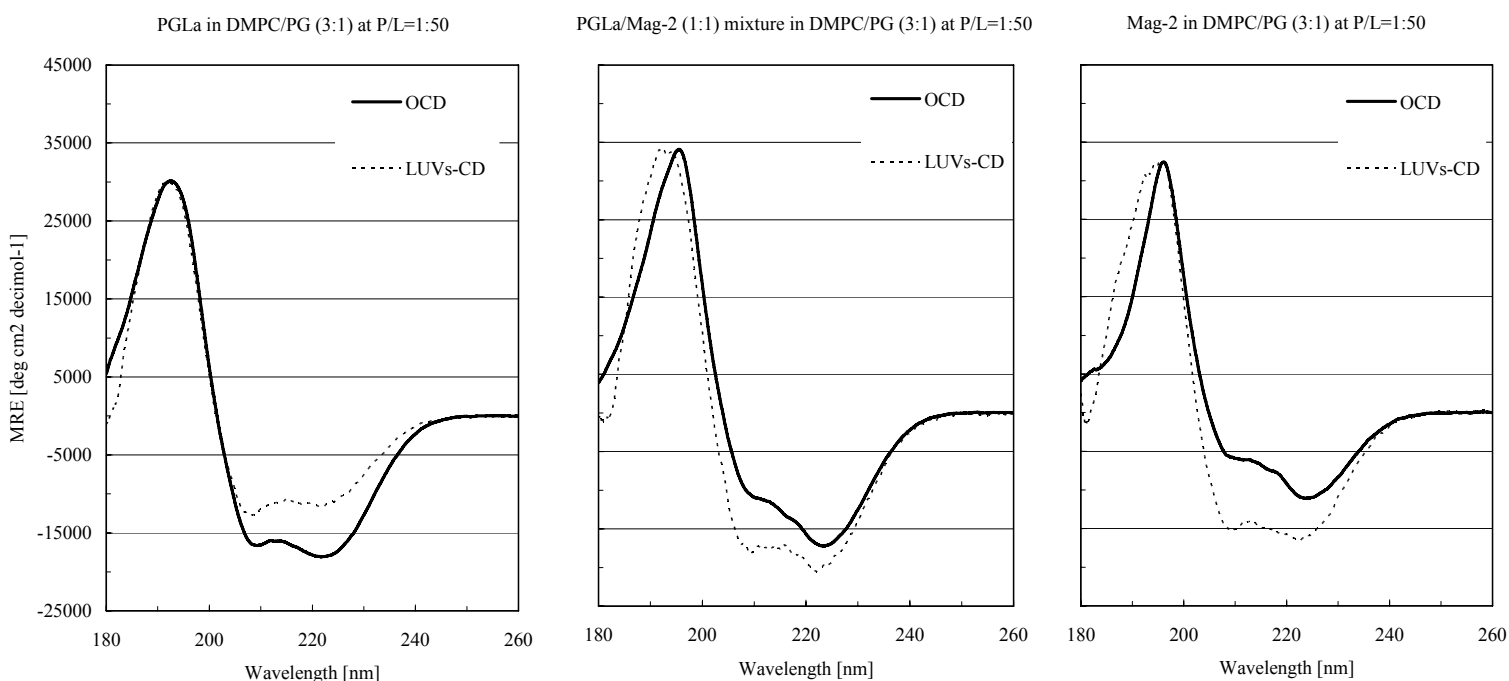


Figure VI.4. OCD and CD spectra of peptides incorporated in oriented DMPC/DMPG (3:1) membranes.

The previous NMR analysis [V] gave under these conditions (PGLa in DMPC/DMPG (3:1) at P/L=1:50) a tilt of 125° , in other words the peptide long axis is near the magic angle ($180^\circ - 125^\circ = 55^\circ \approx 54.7^\circ$), with respect to the membrane normal for both MLV samples (excess hydration) and GP samples (96% relative humidity). Thus in OCD samples, the angle between the peptide axis and the optical axis (the UV beam) should be the same and it would be expected to get consequently an OCD spectrum similar to the LUV spectrum. However, the bands from the OCD spectrum did not fully overlap with the LUV bands. The positive bands between 185 and 200 nm were very similar (neglecting a less than 0.5 nm shift, as small shifts are expected from different motion of the non helical part at different hydration). Overall, OCD confirmed that PGLa alone at a concentration of P/L=1:50 is on average not fully inserted but only tilted around 55° or 125° relative to the membrane normal.

The OCD spectrum of Mag2, in contrast, showed a clear difference compared to the isotropic CD spectra. The disappearance of the negative band around 208 nm together with an overall decrease in amplitude and a small red shift of the band around 190 nm are typical indication for an increased population of inserted peptides compared to PGLa [105, 160].

The OCD spectrum of the PGLa/Mag2 mixture where each peptide has P/L=1:100 (overall P/L=1:50) showed similar features of the peptides being in an inserted state. Though the overall decreased was less pronounced than for Mag2, the appearance of the helix band around 190 nm was more marked. Furthermore, the red shift of this positive band and the disappearance of the negative band around 208 nm relative to the one around 220 nm were much more pronounced. It could be concluded that, on average, the peptides were much more inserted than PGLa alone, though it was not possible to distinguish contributions from PGLa and Mag2. Due to the uncertainties in concentration determination, it could not be fully excluded that effects in the observed averaged orientation were simply additive, though insertion seemed to be deeper in the mixture.

3.5. ^{31}P -NMR spectroscopy

The quality of orientation of the samples was assessed by ^{31}P -NMR. Using the program DMFit [147], spectra could be fitted to three lipid populations, namely two oriented ones with a 3:1 integration ratio attributed to DMPC and DMPG, respectively, and an unoriented population, as depicted in figure VI.5. For all samples the part of unoriented lipid was around 20%. There were no indications of non-lamellar or isotropic lipid populations.

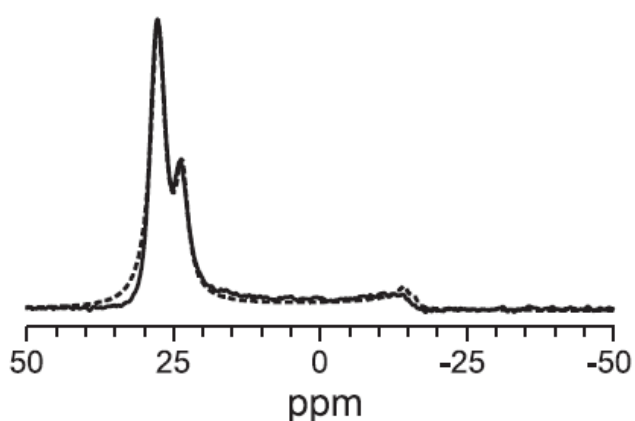
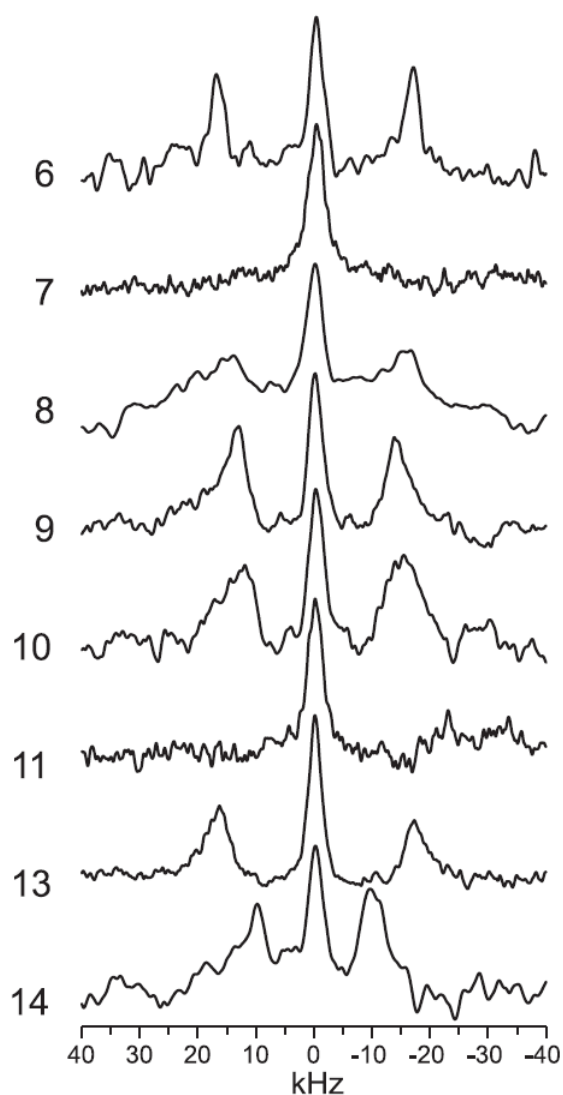


Figure VI.5. ^{31}P -NMR spectra of PGLa/Mag2/DMPC/DMPG in a 1:1:75:25 ratio. The solid line corresponds to the experimental spectrum from PGLa7. The dashed curved is a simulation which corresponds to two oriented lipid population from DMPC/DMPG with a ratio 3:1, and an unoriented part accounting for less than 20%. Experimental spectra from other samples gave similar results. (Adapted from [5]).

3.6. ^2H -NMR spectroscopy

The spectra obtained for the eight labeled PGLa analogues in the presence of Mag2 are



shown in Figure VI.6. The splittings from these spectra are gathered in Table VI.2 together with the values previously obtained in absence of Mag2 at the same overall P/L=1:50 [V] for the sake of comparison. It clearly appeared that PGLa experienced a strong influence of Mag2 and that it underwent orientational or dynamic changes as all the splittings differed between PGLa and PGLa/Mag2 samples. From these data, the alignment of PGLa was calculated using the procedure reported before. The result of this analysis is given in Table VI.3.

Figure VI.6. ^2H -NMR spectra of Ala- d_3 labeled PGLa. The investigated system was PGLa/Mag2/DMPC/DMPG in a 1:1:75:25 ratio. The labeled position is indicated on the left side of each spectrum. (Adapted from [5]).

Table VI.2. ^2H -NMR quadrupolar splittings in kHz of the peptides at P/L=1:50

		PGLa6	PGLa7	PGLa8	PGLa9	PGLa10	PGLa11	PGLa13	PGLa14
Quadrupolar splitting (kHz)	PGLa	17.5 ^a	2.5 ^b	39.2 ^a	30.0 ^b	27.5 ^a	52.1 ^b	20.1 ^b	20.0 ^a
	PGLa/Mag2	33.6	3.0 ^c	30.5	25.5	29.2	1.0 ^c	32.7	18.6

^a Data from [4].^b Data from [3].^c Splitting not well resolved, estimated value.Table VI.3. Best fit structural parameters are calculated from the splittings of labeled PGLa. τ is the tilt angle, ρ is the azimuthal rotation angle, S_{mol} is the motional order parameter and the RMSD gives the error between calculations and experiment. PGLa is bound to DMPC/DMPG (3:1) membranes in presence or absence of Mag2 at P/L=1:50.

Peptide system	List of residues replaced by Ala-d ₃ from the labeled peptides used	τ (°)	ρ (°)	S_{mol}	RMSD (kHz)
PGLa	A6 A8 A10 A14	126	109	0.69	0.5
PGLa/Mag2	A6 A8 A10 A14	158	93	0.84	0.7
PGLa/Mag2	A6 G7 A8 I9 A10 G11 I13 A14	164	88	1	5.3
PGLa/Mag2	A6 G7 A8 I9 A10 I13 A14	156	98	0.83	1.1
PGLa/Mag2	A6 G7 A8 I9	157	99	0.84	0.6
PGLa/Mag2	A6 G7 A8 I9 A10	156	100	0.82	0.6

It had been above shown that four experimental splitting values from peptides where native Ala residue were replaced by Ala-d₃ are enough to determine reliable peptide orientation [IV]. However, in the present case, the direct interaction of PGLa with another peptide, Mag2, through putative dimer formation may induce structural modifications. Thus, four supplementary labeled PGLa analogues, where Ile and Gly residues were replaced by Ala-d₃, were included to allow refining of the calculations.

In the previous study, PGLa in DMPC/DMPG (3:1) at P/L=1:50 was found to be inserted at an angle of 126° and an azimuthal rotation angle of 109° with the lysine side chains pointing up to the bulk water phase. In the present case using only the data points from native Ala replacements, a tilt of 158° was found. The order parameter was notably higher for the mixture with a value of 0.84 and this indicated a restriction in the motion compared to pure PGLa.

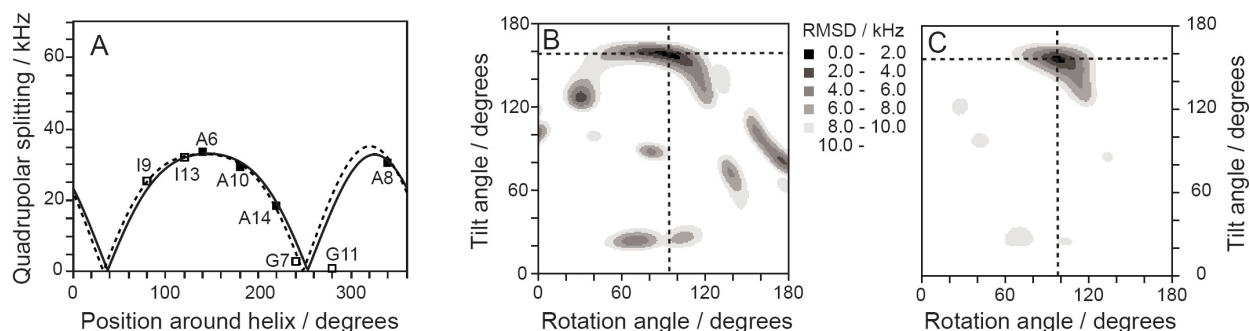


Figure VI.7. (A) Quadrupolar wave plots of PGLa based on the experimental ^2H -NMR splittings of Ala- d_3 substituted for native alanine (filled squares), or for isoleucine or glycine (open squares). Residue numbers are given next to the data points. The solid curve represents the best-fit using only the four non-perturbing labels in the native alanine positions. The dashed curve represents the best-fit when also the potentially perturbing labels at I9, I13 and G7 are taken into account. One further label at position G11 was not included in this fit, due to its considerable deviation from the curve. (B) Determination of τ and ρ (and S_{mol}) from an RMSD plot of PGLa/MAG/DMPC/DMPG (1:1:75:25), using only the ^2H -NMR data from the four non-perturbing positions A6, A8, A10 and A14 in PGLa. (C) RMSD plot calculated from seven labeled Ala- d_3 positions (not using G11), showing a unique minimum that confirms the best-fit solution from panel B.

If all 8 data points are used, an almost similar state is found but with a relatively high RMSD of 5.3 kHz. It appeared that the value of PGLa11 induce a high RMSD for the calculation. When the PGLa11 data point was not used, the 7 remaining data points gave a good fit with a similar orientation as obtained from only native Ala replacement as seen from Figure VI.7. Analysis of the N-terminal segment of the peptide (position 6-10) also gave the same fit as with the native Ala data points. For all calculations, the molecular order was higher than without Mag2. This indicated the possible formation of larger assemblies.

4. Discussion

The two antimicrobial peptides PGLa and Mag2 are naturally co-secreted from frog integument against bacterial invasion, and they are known to have synergistic activity against bacteria. In the present study, the aim was to interpret this synergism by orientational analysis of PGLa. Eight PGLa analogues labeled with Ala- d_3 were used to determine the orientation state of the PGLa in lipid bilayer system in the presence of Mag2. Biological tests were also performed to check any disturbance from labeling and to aid the possible interpretation of synergism by dimer formation.

4.1. Orientation of PGLa in the presence of Mag2

The solid-state NMR analysis used here requires the structure of the investigated peptide to be known. In the previous chapters, PGLa was assumed to be α -helical in the investigated system based on CD measurements [III.2] and solution NMR measurements in micelles [57]. Furthermore, no good fit could be obtained using any other structural models [75, 119]. Contrary to these systems, two distinct peptides, PGLa and Mag2 were in the present study simultaneously investigated, and it must be considered that they may interact with one another and modify their respective structures. As explained previously [II], from CD measurements only the overall content of secondary structures can be estimated. Thus, CD measurements do not reveal if Mag2 peptide is much less α -helical than PGLa or vice versa. It is however not likely that at this small concentration of P/L=1:100 for each peptide, their structures would dramatically change. Considering that all peptides were bound to vesicles, the increase in the contents of turn and disordered conformation was still compatible with the central part of the peptides being α -helical, and the terminal region left disordered or forming kinks, as both peptides and other analogues show such features in lipid environment [55, 57, 112, 125, 167]. It was then concluded that the α -helical model for PGLa was still acceptable and the NMR analysis could be pursued as previously described [II, IV, V].

In the preceding studies, PGLa was found in such DMPC/DMPG lipid system, to assume either the T- or the S-state. At low hydration the peptide is therefore expected to lie flat on the membrane surface at P/L=1:200 or below, and to be slightly tilted into the membrane with an angle of 125° at P/L ranging from 1:20 to 1:100. This T-state does not allow the peptide to span the membrane. In this study, using 4 to 7 labeled peptides which were suitable for the analysis as seen from the biological tests and the CD measurements, PGLa at P/L=1:100 and in the presence of an equimolar amount of Mag2 was shown to be inserted with an angle of around 158° . This nearly upright orientation is quite interesting as it gives the peptide an effective length across the membrane of $\sim 20 \times 1.5 \times \cos(158^\circ) \text{ \AA} = 29 \text{ \AA}$ assuming a 1.5 \AA length per residue for an α -helix. This length is enough to span a DMPC/DMPG membrane assuming a thickness close to that of pure DMPC being $\sim 26 \text{ \AA}$ [94]. This orientation is in remarkable agreement with a pore structure according to the toroidal or barrel-stave models.

To check these remarkable NMR results, OCD measurements were done, as the average orientation of helical peptides can be monitored with this method. Mag2 was shown to be on average well tilted inside the DMPC/DMPG membrane with an angle $>125^\circ$, though

no accurate value could be determined. It was consistent with other results from Ludtke et al. [72, 160]. The fact that this inserted state has not yet been seen by NMR may be simply due to a wrong choice of lipid. In the previous NMR studies, unsaturated lipids had been used (see [2] for a review on lipid-AMP systems studied by NMR). Ludtke et al. show with OCD that in such lipids Mag2 lies on the surface, whereas with saturated lipid it inserts into the membrane [72]. In the same DMPC/DMPG lipid mixture, PGLa however did not show such insertion, and the OCD data corroborated the previous NMR results though some differences between the CD and OCD spectra were noticed. These differences could originate from an insufficient removal of the lipid background which has a negative band around 210 nm. It could also be due to a different motion of the disordered part of the peptide, which may change its motion according to the hydration. And least but not last, it could probably reveal that insufficient resolution or dynamic of exchange in such lipid system prevented ^2H -NMR to pick up the contribution of a potential small residual amount of peptides in the S-state. More interesting is the OCD of the PGLa/Mag2 mixture. At a P/L of 1:100, Mag2 alone is found by OCD lying flat on the surface [72, 160]. As mentioned, PGLa, at P/L=1:100 should be in the T-state. Nevertheless, when mixed together, the spectra revealed typical features of both peptides being in an inserted I-state. These features seemed to be more marked than for Mag2 alone.

For the three systems PGLa, Mag2, and PGLa/Mag2 (1:1), it is shown that the diameter of the pores at identical P/L should be almost the same, as 2 nm sized calcein molecules are released from LUV but not larger particles like dextran [170]. Thus, the origin of synergism has been explained by a higher pore formation rate from PGLa and more stable pore structure from Mag2. The present analysis showed that the presence of Mag2 directly acted on the orientation of PGLa and stabilized it in a transmembrane state. It is the first time that such an accurate transmembrane state for a cationic AMP is reported.

4.2. Hetero-dimer formation and pore structure

The origin of the cooperativity between PGLa and Mag2 is another relevant point to examine. It is thought to originate from hetero-dimer formation. Homo-dimerization processes are already assumed to occur for PGLa explaining the re-alignment and membrane activity of the peptide. The S-state is identified with monomers and the T-state with dimers [IV.4]. Indeed, it is demonstrated by a cross linking study in a PGLa/Mag2/liposome system

that parallel hetero-dimers are preferentially formed [123, 170]. In the present study, the order parameter of PGLa, S_{mol} increased from ~ 0.7 to ~ 0.8 in the presence of Mag2. This decrease in motion would be expected for the formation of stable larger assemblies. It was also possible to examine the possible dimer interface by the indirect use of PGLa analogues and the biological test of Mag2 analogues.

Indeed, contrary to the previous analysis [IV, V], the splitting from PGLa11 did not fit well to the other data points. A glycine residue in the middle of a peptide is known to break the α -helix for soluble proteins [173, 174]. However, for transmembrane helices of proteins it has shown to favor helix-helix contacts and to be associated with dimer interfaces [175, 176]. In the present case, the glycine residue at position 11 (G11) seemed to be a kink residue as seen from CD measurements: the replacement of the glycine 11 by an alanine enhanced the overall helicity, and in parallel decreased the turn content of the PGLa associated with Mag2. These effects were not observed when considering PGLa11 alone. It might be possible to interpret this within several conformational populations as synergetic activity against bacteria was not lost. The NMR analysis of the peptide segment below this residue revealed the same transmembrane orientation. Even if not enough data points were available to analyse the C-terminal part of the peptide, the values from PGLa13 and PGLa14 supported the same orientation for this part. If dimer formation occurs in the vicinity of the 11th residue, the presence of a methyl group may change the azimuthal angle of PGLa. From the helical wheel projection of PGLa and the quadrupolar wave analysis in Figure VI.7, one can see that such a rotation of $\sim 20^\circ$ is enough to greatly modify the splitting. Thus the deviation of PGLa11 could be interpreted by the need to form a hetero-dimer with a contact at position 11. Consequently, PGLa11 gave a different azimuthal angle due to steric hindrance because of the incorporated methyl group. It is noticed that this mutation did not affect the splitting value of the putative PGLa homo-dimer in the T-state [IV.] On the other side of the PGLa helix, the replacement of Ile at position 9 and 13 by Ala-d₃ decreased the bactericidal activity of PGLa, probably due to decreased hydrophobicity. Nevertheless, the synergism was highly conserved. This supports that a probable contact does not occur on this side of PGLa but rather on the side of the G11 residue.

According to the toroidal wormhole model, positive charges are compensated by the anionic lipid headgroups which insert between the transmembrane peptides. From ³¹P-NMR, no non-lamellar phases were observed and the spectra were similar to those observed in the presence of the AMP MSI-78 for which wormhole formation is proposed [153]. It was excluded that the unoriented lipid contribution arose from specific involvement in the

wormhole structure as the peptides should preferentially interact with DMPG and the ratio of oriented DMPC/DMPG was 3:1. Indeed, it is not necessary that the DMPG headgroups insert deeply in the membrane core as side chains of lysine residues are able to snorkel out of the membrane [177]. In the case of insertion of dimers with several positively charged residues this may be different.

The MIC determinations of Mag2 analogues gave interesting information. The antimicrobial activity of some mutated analogues and the synergism with PGLa were conserved when Lys residue was moved near to the C-terminus (Mag1) or when the global charge was increased and the polarity decreased by amidation of the C-terminus (Mag2-amide). Mag2(E19Q), in which the global charge of Mag2 is increased by amidation of the glutamic acid at position 19 (E19), showed similar activity as Mag2. However, for Mag2(E19Q), the synergism with PGLa was lost against both bacterial strains tested. As parallel hetero-dimers are preferentially formed [123], it was therefore postulated that the E19 residue of Mag2 is involved in a salt bridge with probably a lysine residue at position 15 or 19 of PGLa. This salt bridge could certainly be important for the formation of the hetero-dimer responsible for synergism.

5. Conclusions

In this study, an accurate orientation of PGLa in a system of PGLa/Mag2/DMPC/DMPG in a 1:1:75:25 ratio could be determined by ^2H -NMR analysis. It was shown that in this environment and in contrast to the previous results, PGLa adopted a transmembrane orientation as depicted in Figure VI.8. This is certainly the first time that such a transmembrane orientation is accurately reported for a cationic AMP. This orientation was attributed to the formation of a parallel hetero-dimer which is stabilized by a salt bridge between the glutamic acid residue at position 19 of Mag2 and probably the lysine at position 15 or 19 of PGLa. For transmembrane peptides, packing of helices often occur between two Gly residues or between an Ala and a Gly residue [126]. Thus, the dimer contact could occur between G11 of PGLa and G13 or A15 of Mag2, as both these residues are located on the same quadrant and in the middle of the Mag2 helix. It is shown that the pores formed by Mag2 are more stable than those formed by PGLa, whereas the rate of formation is higher for PGLa pores than for Mag2 pores, and that the mixture combines the advantages of both peptides [123]. In conclusion, the higher antimicrobial activity of the mixture compared to

PGLa alone could be explained by the high stability of the formed pores constituted by transmembrane hetero-dimers.

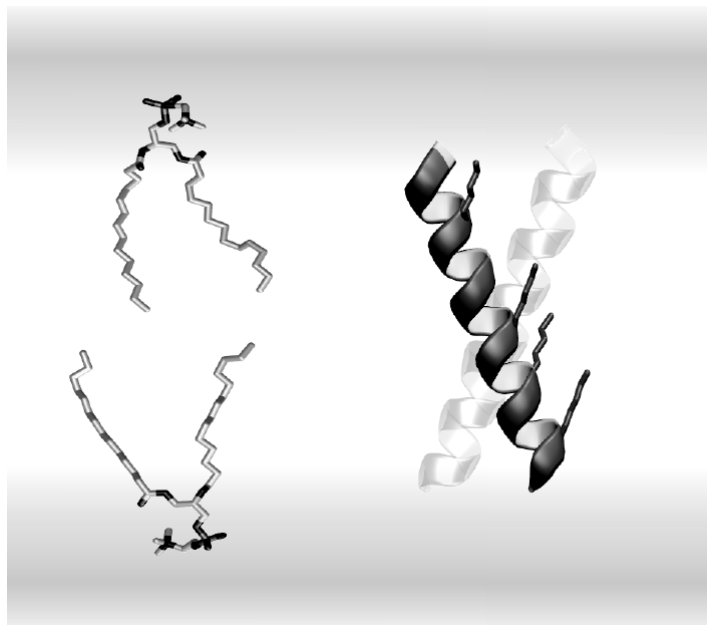


Figure VI.8. α -helical PGLa in the I-state with an angle $\tau=153^\circ$ and $\rho=98^\circ$ is depicted in the presence of Mag2 with its lysine side chains in black. The membrane surface orientation is indicated by the grey/white interfaces. On the left side, two DMPC molecules from an hydrated DMPC bilayer are shown for the sake of length comparison.

VII. Summary

The prevalence of AMPs in all living species reflects their relevance for the host defense system. Their efficiency and conservation in controlling bacterial growth through the ages have drawn much interest for new drug development, as traditional antibiotics increasingly suffer from bacterial resistance. The microbicidal action of AMPs is attributed to a destabilization of the bacterial membrane integrity. This study has focused on the behavior of the frog peptide PGLa in a membrane environment. Such magainin-derived peptides and especially Mag2 itself have often been seen as an archetype for the bacterial membrane permeabilization process. It is thought that such cationic AMPs will insert into the membrane and form pores, with a ring of transmembrane peptides interleaved with anionic lipid head groups to compensate the charges. This is the toroidal wormhole model integrated in a more general description, the Shai-Huang-Matsuzaki model. Enhancing the rate of formation or the stability of these pores could directly improve the antimicrobial activity.

On the one hand, a detailed structure of such a pore has not yet been reported, and on the other hand, little was known about the mechanism of action of PGLa. Even if Mag2 and PGLa are both α -helical amphipathic peptides when bound to membranes, they have some structural differences which influence their respective lipid interactions. Therefore, the behavior of PGLa in membranes was investigated using solid-state NMR spectroscopy. Solid-state NMR can give information on the orientation of bonds and thus reveal relevant structural properties of the peptide. Such orientational constraints combined with a three-dimensional model for the peptide led to the determination of its orientation in different membrane environments, and consecutively several biophysical interpretations were possible.

Practically, for this NMR analysis it is crucial to have suitable NMR labels at defined sites to select the NMR information. Solid phase peptide synthesis allows to specifically incorporate NMR sensitive nuclei into peptides. Several PGLa analogues carrying at a single site an Ala- d_3 label were thus successfully synthesized using an Fmoc strategy and purified by HPLC. To get enough orientational constraints, peptide analogues having Ile or Gly residues replaced by Ala- d_3 were also synthesized. The potential structural or biological modifications were then assessed by CD measurements in the presence of liposomes. This showed a similar secondary structure content for the PGLa analogues compared to the wild type. Furthermore, antimicrobial assays against Gram-negative bacteria did also not reveal any noticeable differences. These analyses already showed that the peptide could readily accommodate these ^2H -NMR labels. Secondly, one had to define a reliable model for the peptide structure and its

motion when incorporated in lipid membranes. The peptide was modeled as an α -helix between residues 6 and 14. This was corroborated by CD measurements and another previous solution NMR study. The corresponding peptide backbone with the C_{α} - C_{β} bonds was assumed to act as a rigid body undergoing overall wobbling. The molecular order originating from this wobble was fitted to a uniaxial and a biaxial model of motion. The labeled peptides were incorporated in oriented lipid membranes. The experiments were done at a temperature of 308 K. This temperature is biologically relevant as it keeps the membranes in a liquid crystalline phase. The orientation of the lipid membranes was monitored by ^{31}P -NMR. Simple quadrupolar echo ^2H -NMR experiments afforded orientational constraints of the peptide backbone which were then analyzed. From the results several conclusions could be drawn.

First of all, concerning the methodology, the rigid straight α -helical structure model was validated. Even if the signs of the quadrupolar splittings were not known, four data points alone were enough to calculate an accurate orientation of the peptide. In the present case, Ile and Gly could be replaced by Ala without inducing noticeable changes in biological activity or conformation of PGLa. This underlined the efficiency of the simple ^2H -labeling NMR approach compared to more sophisticated NMR strategies using ^{15}N or ^{13}C backbone labels. However, the method showed also some limits. Indeed, due to the non-negligible intrinsic experimental error, a slight bending of the peptide towards its helical axis as well as local structure fluctuations could not be excluded. Besides using more data points for a refinement of the analysis, it is also possible in this case to use molecular dynamic simulations in combination with the NMR orientational constraints to improve the structure analysis [178].

Another important conclusion is that the ^2H -NMR analysis confirmed the previous results obtained using the highly NMR sensitive CF_3 -Phg label. However, at high peptide concentration, where peptide-peptide interaction may be biologically relevant, some deviations compared to the present ^2H analysis were observed. This bulky label is therefore less appropriate for replacing Ala residues. Different ^{19}F labeling strategies using F_3 -Ala or other conformationally rigid trifluoromethyl-substituted alpha-amino residues could overcome these drawbacks [179, 180].

With regard to the biological findings of this study, the two S- and T-states behave, as depicted in Figure VII.1, which has been previously shown using the CF_3 -Phg labeling strategy. The peptides re-align from a surface state orientation to a tilted state when the membrane peptide concentration in the membrane is increased. This is a critical feature in the permeabilization process common to several membrane active peptides. However, in the T-state PGLa is only slightly inserted into the membrane and does not cross the whole bilayer

thickness as expected from the toroidal wormhole model. Nevertheless, it might be able to induce membrane defects or transient pores. Due to their short life-times, such pores or defects may not be seen with the present NMR experiments. In additional analyses, one should investigate if different populations of peptides were not overlooked because of the intrinsic experimental error or dynamic processes.

The origin of this re-alignment is still to be assessed. It is highly probable that dimer formation occurs. PGLa has an Ala-Gly rich domain which is often found in transmembrane dimer interfaces. Furthermore, the loss of biaxiality of the motion in the T-state could also be a consequence of peptide assembly. For a more detailed structure, distance constraints of such homo-dimers would be necessary. REDOR measurements between ^{19}F and ^2H labels could give this information.

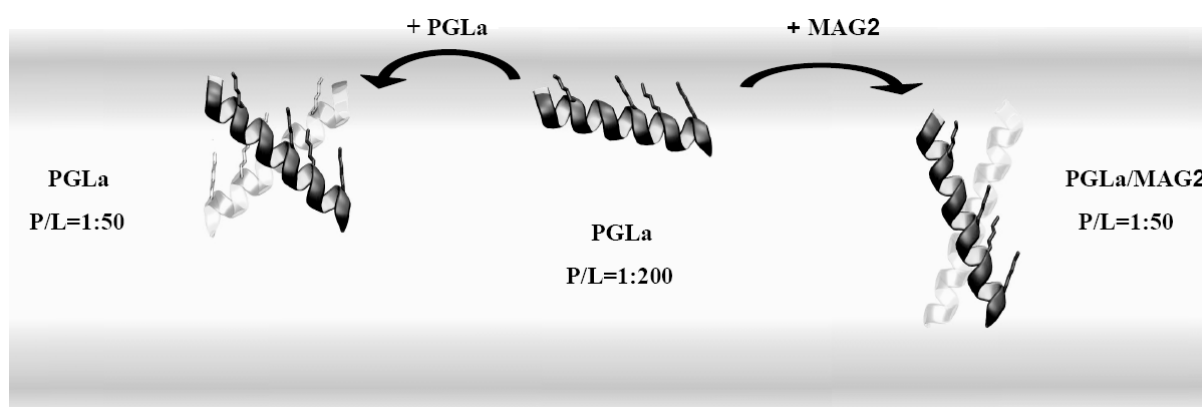


Figure VII.1. At low concentration, the peptides bind parallel to the membrane surface. When the membrane concentration of PGLa increases, the peptides adopt a T-state that are probably homo-dimer. However, in the presence of Mag2, hetero-dimers are formed which insert in the membrane and could form a stable toroidal wormhole.

Another point to discuss is the contribution of the lipids in the putative pore formation process. The present work showed that the presence of anionic lipids lowers the concentration range of this re-alignment, corroborating that bacterial cytoplasmic membranes, which usually contain a high amount of anionic lipids, are more susceptible to cationic AMPs and that the T-state reveals the active state of the peptide. In addition, it was shown that anionic lipid head groups are segregated in the presence of the peptide, even though the membranes in all cases stayed well oriented in a lamellar phase. This may indicate a difference from the toroidal wormhole model, which postulates that the lipid head groups are inserted in the pore. Again, in further developments, one should investigate whether different populations of lipids and exchanges were not overlooked because of higher dynamic processes. Moreover, studies of

the lipid acyl chains should be carried out, as interesting information like the thickness of the membrane, orientation of the lipid chains and location of the peptide could be obtained.

And last but not least, the influence of Mag2 on the orientation of PGLa has to be emphasized. These peptides are known to act synergistically in membrane permeabilization processes. Using ^2H -NMR, it was shown that PGLa almost fully inserts into DMPC/DMPG membranes in the presence of Mag2. Figure VII.1 depicts the difference of PGLa insertion in presence and absence of Mag2. This was certainly the first time that such a state for a cationic AMP was accurately described. This inserted I-state matched well with the toroidal wormhole model. Using antimicrobial assays on analogues of Mag2, it was shown that one acidic residue in Mag2 may be critical for the cooperation with PGLa. It was then postulated that a salt bridge between PGLa and this residue may favor transmembrane hetero-dimer formation. These transmembrane dimers could induce stable pores, which enhances the peptide membrane activity, and explains the synergism. Additional studies will be needed to analyse the orientation of Mag2 and to draw an accurate dimer model.

In conclusion, detailed information was obtained on the structure and mechanism of action of the PGLa peptide in lipid membranes, including its synergism with Mag2. This better understanding should help to develop new membrane active antibiotics. To keep one step ahead the evolution of bacteria, one may indeed continue developing new AMPs. This may provide better lasting antibiotic therapies because the membranes of pathogens are still a strategic target. Even if none of the few developed therapeutic AMPs has yet succeeded in passing phase III of clinical trials [181], there are still on-going attempts and no loss of interest in AMPs, especially since Mag2 or its derivatives are shown to have interesting anti-tumoral properties [169, 182-186] and to give transgenic plants better resistance against pathogens [187-190]. The AMPs may also be used to complement conventional antibiotics. The synergism of Mag2 with the conventional β -lactam antibiotics [191] is a good illustration.

References

1. Yount, N.Y., A.S. Bayer, Y.Q. Xiong, and M.R. Yeaman. 2006. *Advances in antimicrobial peptide immunobiology*. Biopolymers 84:435-458.
2. Strandberg, E. and A.S. Ulrich. 2004. *NMR methods for studying membrane-active antimicrobial peptides*. Concept Magn. Reson. A 23A:89-120.
3. Strandberg, E., P. Wadhvani, P. Tremouilhac, U.H. Durr, and A.S. Ulrich. 2006. *Solid-state NMR analysis of the PGLa peptide orientation in DMPC bilayers: structural fidelity of ^2H -labels versus high sensitivity of ^{19}F -NMR*. Biophys. J. 90:1676-1686.
4. Tremouilhac, P., E. Strandberg, P. Wadhvani, and A.S. Ulrich. 2006. *Conditions affecting the re-alignment of the antimicrobial peptide PGLa in membranes as monitored by solid state ^2H -NMR*. Biochim. Biophys. Acta 1758:1330-1342.
5. Tremouilhac, P., E. Strandberg, P. Wadhvani, and A.S. Ulrich. 2006. *Synergistic transmembrane alignment of the antimicrobial heterodimer PGLa/magainin*. J. Biol. Chem. 281:32089-32094.
6. Fahy, E., S. Subramaniam, H.A. Brown, C.K. Glass, A.H. Merrill, Jr., R.C. Murphy, C.R.H. Raetz, D.W. Russell, Y. Seyama, W. Shaw, T. Shimizu, F. Spener, G. van Meer, M.S. VanNieuwenhze, S.H. White, J.L. Witztum, and E.A. Dennis. 2005. *A comprehensive classification system for lipids*. J. Lipid Res. 46:839-862.
7. Singer, S.J. and G.L. Nicolson. 1972. *The fluid mosaic model of the structure of cell membranes*. Science 175:720-731.
8. Lee, A.G. 2003. *Lipid-protein interactions in biological membranes: a structural perspective*. Biochim. Biophys. Acta 1612:1-40.
9. Hunte, C. 2005. *Specific protein-lipid interactions in membrane proteins*. Biochem. Soc. Trans. 33:938-942.
10. Anderson, R.G.W. and K. Jacobson. 2002. *A role for lipid shells in targeting proteins to caveolae, rafts, and other lipid domains*. Science 296:1821-1825.
11. Almeida, P.F.F., A. Pokorny, and A. Hinderliter. 2005. *Thermodynamics of membrane domains*. Biochim. Biophys. Acta 1720:1-13.
12. Teuber, M. and J. Bader. 1976. *Action of polymyxin B on bacterial membranes. Binding capacities for polymyxin B of inner and outer membranes isolated from Salmonella typhimurium G30*. Arch. Microbiol. 109:51-58.
13. Yeaman, M.R. and N.Y. Yount. 2003. *Mechanisms of antimicrobial peptide action and resistance*. Pharmacol. Rev. 55:27-55.
14. Koronkiewicz, S. and S. Kalinowski. 2004. *Influence of cholesterol on electroporation of bilayer lipid membranes: chronopotentiometric studies*. Biochim. Biophys. Acta 1661:196-203.
15. de Almeida, R.F.M., A. Fedorov, and M. Prieto. 2003. *Sphingomyelin/phosphatidylcholine/cholesterol phase diagram: boundaries and composition of lipid rafts*. Biophys. J. 85:2406-2416.
16. Boman, H.G. 1998. *Gene-encoded peptide antibiotics and the concept of innate immunity: An update review*. Scand. J. Immunol. 48:15-45.
17. Erspamer, V., *Bioactive secretions of the amphibian integument*, in *Amphibian Biology. The Integument*. 1994: Surrey, Beatty and Sons, Chipping-Norton, N.S.W. p. 178-350.
18. Csordas, A. and H. Michl. 1970. *Isolation and structure of an hemolytic polypeptide from defensive secretion of european bombina species*. Monatsh. Chem. 101:182-189.

19. Zasloff, M. 1987. *Magainins, a class of antimicrobial peptides from Xenopus skin: isolation, characterization of two active forms, and partial cDNA sequence of a precursor*. Proc. Natl. Acad. Sci. U. S. A. 84:5449-5453.
20. Hultmark, D., H. Steiner, T. Rasmuson, and H.G. Boman. 1980. *Insect immunity. Purification and properties of three inducible bactericidal proteins from hemolymph of immunized pupae of Hyalophora cecropia*. Eur. J. Biochem. 106:7-16.
21. Richter, K., H. Aschauer, and G. Kreil. 1985. *Biosynthesis of peptides in the skin of Xenopus laevis: isolation of novel peptides predicted from the sequence of cloned cDNAs*. Peptides 6:17-21.
22. Andreu, D., H. Aschauer, G. Kreil, and R.B. Merrifield. 1985. *Solid-phase synthesis of PYLa and isolation of its natural counterpart, PGLa [PYLa-(4-24)] from skin secretion of Xenopus laevis*. Eur. J. Biochem. 149:531-535.
23. Soravia, E., G. Martini, and M. Zasloff. 1988. *Antimicrobial properties of peptides from Xenopus granular gland secretions*. FEBS Lett. 228:337-340.
24. Moore, K.S., C.L. Bevins, M.M. Bresseur, N. Tomassini, K. Turner, H. Eck, and M. Zasloff. 1991. *Antimicrobial peptides in the stomach of Xenopus laevis*. J. Biol. Chem. 266:19851-19857.
25. Reilly, D.S., N. Tomassini, C.L. Bevins, and M. Zasloff. 1994. *A Paneth cell analogue in Xenopus small intestine expresses antimicrobial peptide genes: conservation of an intestinal host-defense system*. J. Histochem. Cytochem. 42:697-704.
26. Richter, K., R. Egger, and G. Kreil. 1986. *Sequence of preprocaerulein cDNAs cloned from skin of Xenopus laevis. A small family of precursors containing one, three, or four copies of the final product*. J. Biol. Chem. 261:3676-3680.
27. Gibson, B.W., L. Poulter, D.H. Williams, and J.E. Maggio. 1986. *Novel peptide fragments originating from PGLa and the caerulein and xenopsin precursors from Xenopus laevis*. J. Biol. Chem. 261:5341-5349.
28. Sures, I. and M. Crippa. 1984. *Xenopsin: the neurotensin-like octapeptide from Xenopus skin at the carboxyl terminus of its precursor*. Proc. Natl. Acad. Sci. U. S. A. 81:380-384.
29. Giovannini, M.G., L. Poulter, B.W. Gibson, and D.H. Williams. 1987. *Biosynthesis and degradation of peptides derived from Xenopus laevis prohormones*. Biochem. J. 243:113-120.
30. Kuchler, K., G. Kreil, and I. Sures. 1989. *The genes for the frog skin peptides GLa, xenopsin, levitide and caerulein contain a homologous export exon encoding a signal sequence and part of an amphiphilic peptide*. Eur. J. Biochem. 179:281-285.
31. Moore, K.S., C.L. Bevins, N. Tomassini, K.M. Huttner, K. Sadler, J.E. Moreira, J. Reynolds, and M. Zasloff. 1992. *A novel peptide-producing cell in Xenopus: multinucleated gastric mucosal cell strikingly similar to the granular gland of the skin*. J. Histochem. Cytochem. 40:367-378.
32. Flucher, B.E., C. Lenglachner-Bachinger, K. Pohlhammer, H. Adam, and C. Mollay. 1986. *Skin peptides in Xenopus laevis: morphological requirements for precursor processing in developing and regenerating granular skin glands*. J. Cell Biol. 103:2299-2309.
33. Terry, A.S., L. Poulter, D.H. Williams, J.C. Nutkins, M.G. Giovannini, C.H. Moore, and B.W. Gibson. 1988. *The cDNA sequence coding for prepro-PGS (prepro-magainins) and aspects of the processing of this prepro-polypeptide*. J. Biol. Chem. 263:5745-5751.
34. Hunt, L.T. and W.C. Barker. 1988. *Relationship of promagainin to three other prohormones from the skin of Xenopus laevis: a different perspective*. FEBS Lett. 233:282-288.

35. Tennessen, J.A. 2005. *Molecular evolution of animal antimicrobial peptides: widespread moderate positive selection*. J. Evol. Biol. 18:1387-1394.
36. Resnick, N.M., W.L. Maloy, H.R. Guy, and M. Zasloff. 1991. *A novel endopeptidase from Xenopus that recognizes alpha-helical secondary structure*. Cell 66:541-554.
37. Matsuzaki, K., M. Harada, T. Handa, S. Funakoshi, N. Fujii, H. Yajima, and K. Miyajima. 1989. *Magainin 1-induced leakage of entrapped calcein out of negatively-charged lipid vesicles*. Biochim. Biophys. Acta 981:130-134.
38. Williams, R.W., R. Starman, K.M. Taylor, K. Gable, T. Beeler, M. Zasloff, and D. Covell. 1990. *Raman spectroscopy of synthetic antimicrobial frog peptides magainin 2a and PGLa*. Biochemistry 29:4490-4496.
39. Matsuzaki, K., M. Harada, S. Funakoshi, N. Fujii, and K. Miyajima. 1991. *Physicochemical determinants for the interactions of magainins 1 and 2 with acidic lipid bilayers*. Biochim. Biophys. Acta 1063:162-170.
40. Grant, E., Jr., T.J. Beeler, K.M. Taylor, K. Gable, and M.A. Roseman. 1992. *Mechanism of magainin 2a induced permeabilization of phospholipid vesicles*. Biochemistry 31:9912-9918.
41. Blazyk, J., R. Wiegand, J. Klein, J. Hammer, R.M. Epanand, R.F. Epanand, W.L. Maloy, and U.P. Kari. 2001. *A novel linear amphipathic β -sheet cationic antimicrobial peptide with enhanced selectivity for bacterial lipids*. J. Biol. Chem. 276:27899-27906.
42. Vaz Gomes, A., A. de Waal, J.A. Berden, and H.V. Westerhoff. 1993. *Electric potentiation, cooperativity, and synergism of magainin peptides in protein-free liposomes*. Biochemistry 32:5365-5372.
43. Bessalle, R., A. Kapitkovsky, A. Gorea, I. Shalit, and M. Fridkin. 1990. *All-D-magainin: chirality, antimicrobial activity and proteolytic resistance*. FEBS Lett. 274:151-155.
44. Wade, D., A. Boman, B. Wahlin, C.M. Drain, D. Andreu, H.G. Boman, and R.B. Merrifield. 1990. *All-D amino acid-containing channel-forming antibiotic peptides*. Proc. Natl. Acad. Sci. U. S. A. 87:4761-4765.
45. Mozsolits, H., H.J. Wirth, J. Werkmeister, and M.I. Aguilar. 2001. *Analysis of antimicrobial peptide interactions with hybrid bilayer membrane systems using surface plasmon resonance*. Biochim. Biophys. Acta 1512:64-76.
46. Jackson, M., H.H. Mantsch, and J.H. Spencer. 1992. *Conformation of magainin-2 and related peptides in aqueous solution and membrane environments probed by Fourier transform infrared spectroscopy*. Biochemistry 31:7289-7293.
47. Latal, A., G. Degovics, R.F. Epanand, R.M. Epanand, and K. Lohner. 1997. *Structural aspects of the interaction of peptidyl-glycylleucine-carboxamide, a highly potent antimicrobial peptide from frog skin, with lipids*. Eur. J. Biochem. 248:938-946.
48. Afonin, S., R.W. Glaser, M. Berditchevskaia, P. Wadhvani, K.H. Guhrs, U. Mollmann, A. Perner, and A.S. Ulrich. 2003. *4-Fluorophenylglycine as a label for ^{19}F NMR structure analysis of membrane-associated peptides*. ChemBiochem 4:1151-1163.
49. Wieprecht, T., O. Apostolov, M. Beyermann, and J. Seelig. 2000. *Membrane binding and pore formation of the antibacterial peptide PGLa: thermodynamic and mechanistic aspects*. Biochemistry 39:442-452.
50. Bessalle, R., H. Haas, A. Gorla, I. Shalit, and M. Fridkin. 1992. *Augmentation of the antibacterial activity of magainin by positive-charge chain extension*. Antimicrob. Agents Chemother. 36:313-317.
51. Matsuzaki, K., A. Nakamura, O. Murase, K. Sugishita, N. Fujii, and K. Miyajima. 1997. *Modulation of magainin 2-lipid bilayer interactions by peptide charge*. Biochemistry 36:2104-2111.

52. Dathe, M., H. Nikolenko, J. Meyer, M. Beyermann, and M. Bienert. 2001. *Optimization of the antimicrobial activity of magainin peptides by modification of charge*. FEBS Lett. 501:146-150.
53. Unger, T., Z. Oren, and Y. Shai. 2001. *The effect of cyclization of magainin 2 and melittin analogues on structure, function, and model membrane interactions: implication to their mode of action*. Biochemistry 40:6388-6397.
54. Wieprecht, T., O. Apostolov, and J. Seelig. 2000. *Binding of the antibacterial peptide magainin 2 amide to small and large unilamellar vesicles*. Biophys. Chem. 85:187-198.
55. Marion, D., M. Zasloff, and A. Bax. 1988. *A two-dimensional NMR study of the antimicrobial peptide magainin 2*. FEBS Lett. 227:21-26.
56. Gesell, J., M. Zasloff, and S.J. Opella. 1997. *Two-dimensional ¹H NMR experiments show that the 23-residue magainin antibiotic peptide is an alpha-helix in dodecylphosphocholine micelles, sodium dodecylsulfate micelles, and trifluoroethanol/water solution*. J. Biomol. NMR 9:127-135.
57. Bechinger, B., M. Zasloff, and S.J. Opella. 1998. *Structure and dynamics of the antibiotic peptide PGLa in membranes by solution and solid-state nuclear magnetic resonance spectroscopy*. Biophys. J. 74:981-987.
58. Iwahori, A., Y. Hirota, R. Sampe, S. Miyano, and N. Numao. 1997. *Synthesis of reversed magainin 2 analogs enhanced antibacterial activity*. Biol. Pharm. Bull. 20:267-270.
59. Iwahori, A., Y. Hirota, R. Sampe, S. Miyano, N. Takahashi, M. Sasatsu, I. Kondo, and N. Numao. 1997. *On the antibacterial activity of normal and reversed magainin 2 analogs against Helicobacter pylori*. Biol. Pharm. Bull. 20:805-808.
60. Wieprecht, T., M. Dathe, M. Beyermann, E. Krause, W.L. Maloy, D.L. MacDonald, and M. Bienert. 1997. *Peptide hydrophobicity controls the activity and selectivity of magainin 2 amide in interaction with membranes*. Biochemistry 36:6124-6132.
61. Dathe, M., T. Wieprecht, H. Nikolenko, L. Handel, W.L. Maloy, D.L. MacDonald, M. Beyermann, and M. Bienert. 1997. *Hydrophobicity, hydrophobic moment and angle subtended by charged residues modulate antibacterial and haemolytic activity of amphipathic helical peptides*. FEBS Lett. 403:208-212.
62. Wieprecht, T., M. Dathe, R.M. Epand, M. Beyermann, E. Krause, W.L. Maloy, D.L. MacDonald, and M. Bienert. 1997. *Influence of the angle subtended by the positively charged helix face on the membrane activity of amphipathic, antibacterial peptides*. Biochemistry 36:12869-12880.
63. Meincken, M., D.L. Holroyd, and M. Rautenbach. 2005. *Atomic force microscopy study of the effect of antimicrobial peptides on the cell envelope of Escherichia coli*. Antimicrob. Agents Chemother. 49:4085-4092.
64. da Silva, A. and O. Teschke. 2003. *Effects of the antimicrobial peptide PGLa on live Escherichia coli*. Biochim. Biophys. Acta 1643:95-103.
65. da Silva, A. and O. Teschke. 2005. *Dynamics of the antimicrobial peptide PGLa action on Escherichia coli monitored by atomic force microscopy*. World J. Microb. Biot. 21:1103-1110.
66. Matsuzaki, K., K. Sugishita, M. Harada, N. Fujii, and K. Miyajima. 1997. *Interactions of an antimicrobial peptide, magainin 2, with outer and inner membranes of Gram-negative bacteria*. Biochim. Biophys. Acta 1327:119-130.
67. Urrutia, R., R.A. Cruciani, J.L. Barker, and B. Kachar. 1989. *Spontaneous polymerization of the antibiotic peptide magainin 2*. FEBS Lett. 247:17-21.
68. Raimondo, D., G. Andreotti, N. Saint, P. Amodeo, G. Renzone, M. Sanseverino, I. Zocchi, G. Molle, A. Motta, and A. Scaloni. 2005. *A folding-dependent mechanism of*

- antimicrobial peptide resistance to degradation unveiled by solution structure of distinctin*. Proc. Natl. Acad. Sci. U. S. A. 102:6309-6314.
69. Huang, H.W. 2006. *Molecular mechanism of antimicrobial peptides: The origin of cooperativity*. Biochim. Biophys. Acta 1758:1292–1302.
 70. Duclohier, H. 1994. *Anion pores from magainins and related defensive peptides*. Toxicology 87:175-188.
 71. Matsuzaki, K., O. Murase, and K. Miyajima. 1995. *Kinetics of pore formation by an antimicrobial peptide, magainin 2, in phospholipid bilayers*. Biochemistry 34:12553-12559.
 72. Ludtke, S.J., K. He, W.T. Heller, T.A. Harroun, L. Yang, and H.W. Huang. 1996. *Membrane pores induced by magainin*. Biochemistry 35:13723-13728.
 73. Matsuzaki, K., O. Murase, N. Fujii, and K. Miyajima. 1996. *An antimicrobial peptide, magainin 2, induced rapid flip-flop of phospholipids coupled with pore formation and peptide translocation*. Biochemistry 35:11361-11368.
 74. Westerhoff, H.V., D. Juretic, R.W. Hendler, and M. Zasloff. 1989. *Magainins and the disruption of membrane-linked free-energy transduction*. Proc. Natl. Acad. Sci. U. S. A. 86:6597-6601.
 75. Glaser, R.W., C. Sachse, U.H. Durr, P. Wadhvani, S. Afonin, E. Strandberg, and A.S. Ulrich. 2005. *Concentration-dependent realignment of the antimicrobial peptide PGLa in lipid membranes observed by solid-state ¹⁹F-NMR*. Biophys. J. 88:3392-3397.
 76. Park, C.B., H.S. Kim, and S.C. Kim. 1998. *Mechanism of action of the antimicrobial peptide buforin II: buforin II kills microorganisms by penetrating the cell membrane and inhibiting cellular functions*. Biochem. Biophys. Res. Commun. 244:253-257.
 77. Laszlo Otvos Jr. 2005. *Antibacterial peptides and proteins with multiple cellular targets*. J. Pept. Sci. 11:697-706.
 78. Brown, K.L. and R.E. Hancock. 2006. *Cationic host defense (antimicrobial) peptides*. Curr. Opin. Immunol. 18:24-30.
 79. Ding, L., L. Yang, T.M. Weiss, A.J. Waring, R.I. Lehrer, and H.W. Huang. 2003. *Interaction of antimicrobial peptides with lipopolysaccharides*. Biochemistry 42:12251-12259.
 80. Thomas, C.J., N. Surolia, and A. Surolia. 2001. *Kinetic and thermodynamic analysis of the interactions of 23-residue peptides with endotoxin*. J. Biol. Chem. 276:35701-35706.
 81. Giacometti, A., O. Cirioni, R. Ghiselli, F. Orlando, W. Kamysz, M. Rocchi, G. D'Amato, F. Mocchegiani, C. Silvestri, J. Lukasiak, V. Saba, and G. Scalise. 2005. *Effects of pexiganan alone and combined with betalactams in experimental endotoxic shock*. Peptides 26:207-216.
 82. Giacometti, A., R. Ghiselli, O. Cirioni, F. Mocchegiani, G. D'Amato, F. Orlando, V. Sisti, W. Kamysz, C. Silvestri, P. Naldoski, J. Lukasiak, V. Saba, and G. Scalise. 2004. *Therapeutic efficacy of the magainin analogue MSI-78 in different intra-abdominal sepsis rat models*. J. Antimicrob. Chemother. 54:654-660.
 83. Peschel, A. and H.-G. Sahl. 2006. *The co-evolution of host cationic antimicrobial peptides and microbial resistance*. Nat. Rev. Micro. 4:529-536.
 84. Nizet, V. 2006. *Antimicrobial peptide resistance mechanisms of human bacterial pathogens*. Curr. Issues Mol. Biol. 8:11-26.
 85. Banemann, A., H. Deppisch, and R. Gross. 1998. *The lipopolysaccharide of Bordetella bronchiseptica acts as a protective shield against antimicrobial peptides*. Infect. Immun. 66:5607-5612.
 86. Bishop, J.L. and B.B. Finlay. 2006. *Friend or foe? Antimicrobial peptides trigger pathogen virulence*. Trends Mol. Med. 12:3-6.

87. Ge, Y., D.L. MacDonald, K.J. Holroyd, C. Thornsberry, H. Wexler, and M. Zasloff. 1999. *In vitro antibacterial properties of pexiganan, an analog of magainin*. *Antimicrob. Agents Chemother.* 43:782-788.
88. Matsuzaki, K. 1998. *Magainins as paradigm for the mode of action of pore forming polypeptides*. *Biochim. Biophys. Acta* 1376:391-400.
89. Humphrey, W., A. Dalke, and K. Schulten. 1996. *VMD: visual molecular dynamics*. *J. Mol. Graph.* 14:33-38, 27-38.
90. Strandberg, E., S. Ozdirekcan, D.T. Rijkers, P.C. van der Wel, R.E. Koeppe II, R.M. Liskamp, and J.A. Killian. 2004. *Tilt angles of transmembrane model peptides in oriented and non-oriented lipid bilayers as determined by ²H solid-state NMR*. *Biophys. J.* 86:3709-3721.
91. Losonczi, J.A. and J.H. Prestegard. 1998. *Nuclear magnetic resonance characterization of the myristoylated, N-terminal fragment of ADP-ribosylation factor 1 in a magnetically oriented membrane array*. *Biochemistry* 37:706-716.
92. Losonczi, J.A., M. Andrec, M.W.F. Fischer, and J.H. Prestegard. 1999. *Order matrix analysis of residual dipolar couplings using singular value decomposition*. *J. Magn. Reson.* 138:334-342.
93. Valafar, H. and J.H. Prestegard. 2004. *REDCAT: a residual dipolar coupling analysis tool*. *J. Magn. Reson.* 167:228-241.
94. Nagle, J.F. and S. Tristram-Nagle. 2000. *Structure of lipid bilayers*. *Biochim. Biophys. Acta* 1469:159-195.
95. Smirnov, A.I. and O.G. Poluektov. 2003. *Substrate-supported lipid nanotube arrays*. *125:8434-8435*.
96. Rance, M. and R.A. Byrd. 1983. *Obtaining high-fidelity spin-1/2 powder spectra in anisotropic media-phase-cycled Hahn echo spectroscopy*. *J. Magn. Reson.* 52:221-240.
97. Bennett, A.E., C.M. Rienstra, M. Auger, K.V. Lakshmi, and R.G. Griffin. 1995. *Heteronuclear decoupling in rotating solids*. *J. Chem. Phys.* 103:6951-6958.
98. Davis, J.H., K.R. Jeffrey, M. Bloom, M.I. Valic, and T.P. Higgs. 1976. *Quadrupolar echo deuteron magnetic resonance spectroscopy in ordered hydrocarbon chains*. *Chem. Phys. Lett.* 42:390-394.
99. Merrifield, R.B. 1963. *Solid phase peptide synthesis. I. The synthesis of a tetrapeptide*. *J. Am. Chem. Soc.*:2149.
100. Fields, G.B. and R.L. Noble. 1990. *Solid-phase peptide synthesis utilizing 9-fluorenylmethoxycarbonyl amino acids*. *Int. J. Pept. Protein Res.* 35:161-214.
101. Carpino, L.A. and G.Y. Han. 1972. *9-Fluorenylmethoxycarbonyl amino-protecting group*. *J. Org. Chem.* 37:3404-3409.
102. Moffitt, W. and J.T. Yang. 1956. *The optical rotatory dispersion of simple polypeptides. I*. *Proc. Natl. Acad. Sci. U. S. A.* 42:596-603.
103. Moffitt, W. 1956. *The optical rotatory dispersion of simple polypeptides. II*. *Proc. Natl. Acad. Sci. U. S. A.* 42:736-746.
104. Olah, G.A. and H.W. Huang. 1988. *Circular dichroism of oriented α -helix. I. Proof of the exciton theory*. *J. Chem. Phys.* 89:2531-2538.
105. Wu, Y., H.W. Huang, and G.A. Olah. 1990. *Method of oriented circular dichroism*. *Biophys. J.* 57:797-806.
106. Reichert, J., D. Grasnack, S. Afonin, J. Buerck, P. Wadhvani, and A.S. Ulrich. 2006. *A critical evaluation of the conformational requirements of fusogenic peptides in membranes*. *Eur. Biophys. J.*
107. Provencher, S.W. and J. Glockner. 1981. *Estimation of globular protein secondary structure from circular dichroism*. *Biochemistry* 20:33-37.

108. Johnson, W.C. 1999. *Analyzing protein circular dichroism spectra for accurate secondary structures*. Proteins 35:307-312.
109. Sreerama, N. and R.W. Woody. 1993. *A self-consistent method for the analysis of protein secondary structure from circular dichroism*. Anal. Biochem. 209:32-44.
110. Ludtke, S., K. He, and H. Huang. 1995. *Membrane thinning caused by magainin 2*. Biochemistry 34:16764-16769.
111. Chen, F.Y., M.T. Lee, and H.W. Huang. 2002. *Sigmoidal concentration dependence of antimicrobial peptide activities: a case study on alamethicin*. Biophys. J. 82:908-914.
112. Hicks, R.P., E. Mones, H. Kim, B.W. Koser, D.A. Nichols, and A.K. Bhattacharjee. 2003. *Comparison of the conformation and electrostatic surface properties of magainin peptides bound to sodium dodecyl sulfate and dodecylphosphocholine micelles*. Biopolymers 68:459-470.
113. Helmerhorst, E.J., I.M. Reijnders, W. van 't Hof, E.C. Veerman, and A.V. Nieuw Amerongen. 1999. *A critical comparison of the hemolytic and fungicidal activities of cationic antimicrobial peptides*. FEBS Lett. 449:105-110.
114. Rollins-Smith, L.A., C. Carey, J. Longcore, J.K. Doersam, A. Boutte, J.E. Bruzgal, and J.M. Conlon. 2002. *Activity of antimicrobial skin peptides from ranid frogs against Batrachochytrium dendrobatidis, the chytrid fungus associated with global amphibian declines*. Dev Comp Immunol 26:471-479.
115. Rautenbach, M., G.D. Gerstner, N.M. Vlok, J. Kulenkampff, and H.V. Westerhoff. 2006. *Analyses of dose-response curves to compare the antimicrobial activity of model cationic alpha-helical peptides highlights the necessity for a minimum of two activity parameters*. Anal. Biochem. 350:81-90.
116. Strandberg, E., D. Tiltak, M. Ieronimo, N. Kanithasen, P. Wadhvani, and A.S. Ulrich. 2007. *Influence of C-terminal amidation on the antimicrobial and hemolytic activities of cationic α -helical peptides*. Pure Appl. Chem. in press.
117. Marcotte, I., K.L. Wegener, Y.-H. Lam, B.C.S. Chia, M.R.R. de Planque, J.H. Bowie, M. Auger, and F. Separovic. 2003. *Interaction of antimicrobial peptides from Australian amphibians with lipid membranes*. Chem. Phys. Lipids 122:107-120.
118. Li, C., Y. Mo, J. Hu, E. Chekmenev, C. Tian, F.P. Gao, R. Fu, P. Gor'kov, W. Brey, and T.A. Cross. 2006. *Analysis of RF heating and sample stability in aligned static solid-state NMR spectroscopy*. J. Magn. Reson. 180:51-57.
119. Glaser, R.W., C. Sachse, U.H. Durr, P. Wadhvani, and A.S. Ulrich. 2004. *Orientation of the antimicrobial peptide PGLa in lipid membranes determined from ^{19}F -NMR dipolar couplings of 4-CF₃-phenylglycine labels*. J. Magn. Reson. 168:153-163.
120. Glaser, R.W. and A.S. Ulrich. 2003. *Susceptibility corrections in solid-state NMR experiments with oriented membrane samples. Part I: applications*. J. Magn. Reson. 164:104-114.
121. Huang, H.W. 2000. *Action of antimicrobial peptides: two-state model*. Biochemistry 39:8348-8352.
122. Wakamatsu, K., A. Takeda, T. Tachi, and K. Matsuzaki. 2002. *Dimer structure of magainin 2 bound to phospholipid vesicles*. Biopolymers 64:314-327.
123. Hara, T., Y. Mitani, K. Tanaka, N. Uematsu, A. Takakura, T. Tachi, H. Kodama, M. Kondo, H. Mori, A. Otaka, F. Nobutaka, and K. Matsuzaki. 2001. *Heterodimer formation between the antimicrobial peptides magainin 2 and PGLa in lipid bilayers: a cross-linking study*. Biochemistry 40:12395-12399.
124. Matsuzaki, K., O. Murase, H. Tokuda, S. Funakoshi, N. Fujii, and K. Miyajima. 1994. *Orientalional and aggregational states of magainin 2 in phospholipid bilayers*. Biochemistry 33:3342-3349.
125. Porcelli, F., B.A. Buck-Koehntop, S. Thennarasu, A. Ramamoorthy, and G. Veglia. 2006. *Structures of the dimeric and monomeric variants of magainin antimicrobial*

- peptides (MSI-78 and MSI-594) in micelles and bilayers, determined by NMR spectroscopy.* Biochemistry 45:5793-5799.
126. Liu, W., M. Eilers, A.B. Patel, and S.O. Smith. 2004. *Helix packing moments reveal diversity and conservation in membrane protein structure.* J. Mol. Biol. 337:713-729.
 127. van der Wel, P.C., E. Strandberg, J.A. Killian, and R.E. Koeppe II. 2002. *Geometry and intrinsic tilt of a tryptophan-anchored transmembrane alpha-helix determined by ²H NMR.* Biophys. J. 83:1479-1488.
 128. Prestegard, J.H., H.M. al-Hashimi, and J.R. Tolman. 2000. *NMR structures of biomolecules using field oriented media and residual dipolar couplings.* Q. Rev. Biophys. 33:371-424.
 129. Ozdirekcan, S., D.T.S. Rijkers, R.M.J. Liskamp, and J.A. Killian. 2005. *Influence of flanking residues on tilt and rotation angles of transmembrane peptides in lipid bilayers. A solid-state ²H NMR study.* Biochemistry 44:1004-1012.
 130. Kuntz, I.D., P.A. Kosen, and E.C. Craig. 1991. *Amide chemical-shifts in many helices in peptides and proteins are periodic.* J. Am. Chem. Soc. 113:1406-1408.
 131. Zhou, N.E., B.Y. Zhu, B.D. Sykes, and R.S. Hodges. 1992. *Relationship between amide proton chemical shifts and hydrogen bonding in amphipathic α -helical peptides.* J. Am. Chem. Soc. 114:4320-4326.
 132. Merlet, D., J.W. Emsley, P. Lesot, and J. Courtieu. 1999. *The relationship between molecular symmetry and second-rank orientational order parameters for molecules in chiral liquid crystalline solvents.* J. Chem. Phys. 111:6890-6896.
 133. Toke, O., R.D. O'Connor, T.K. Weldeghiorghis, W.L. Maloy, R.W. Glaser, A.S. Ulrich, and J. Schaefer. 2004. *Structure of (KIAGKIA)₃ aggregates in phospholipid bilayers by solid-state NMR.* Biophys. J. 87:675-687.
 134. Toke, O., W.L. Maloy, S.J. Kim, J. Blazyk, and J. Schaefer. 2004. *Secondary structure and lipid contact of a peptide antibiotic in phospholipid bilayers by REDOR.* Biophys. J. 87:662-674.
 135. Eilers, M., A.B. Patel, W. Liu, and S.O. Smith. 2002. *Comparison of helix interactions in membrane and soluble α -bundle proteins.* Biophys. J. 82:2720-2736.
 136. Senes, A., D.E. Engel, and W.F. DeGrado. 2004. *Folding of helical membrane proteins: the role of polar, GxxxG-like and proline motifs.* Curr. Opin. Struct. Biol. 14:465-479.
 137. Zuckermann, M.J. and T. Heimburg. 2001. *Insertion and pore formation driven by adsorption of proteins onto lipid bilayer membrane-water interfaces.* Biophys. J. 81:2458-2472.
 138. Dempsey, C.E., S. Ueno, and M.B. Avison. 2003. *Enhanced membrane permeabilization and antibacterial activity of a disulfide-dimerized magainin analogue.* Biochemistry 42:402-409.
 139. Mukai, Y., Y. Matsushita, T. Niidome, T. Hatekeyama, and H. Aoyag. 2002. *Parallel and antiparallel dimers of magainin 2: their interaction with phospholipid membrane and antibacterial activity.* J. Pept. Sci. 8:570-577.
 140. Hara, T., H. Kodama, M. Kondo, K. Wakamatsu, A. Takeda, T. Tachi, and K. Matsuzaki. 2001. *Effects of peptide dimerization on pore formation: Antiparallel disulfide-dimerized magainin 2 analogue.* Biopolymers 58:437-446.
 141. Kandasamy, S.K. and R.G. Larson. 2004. *Binding and insertion of α -helical antimicrobial peptides in POPC bilayers studied by molecular dynamics simulations.* Chem. Phys. Lipids 132:113-132.
 142. Zemel, A., D.R. Fattal, and A. Ben-Shaul. 2003. *Energetics and self-assembly of amphipathic peptide pores in lipid membranes.* 84:2242-2255.
 143. Leontiadou, H., A.E. Mark, and S.J. Marrink. 2006. *Antimicrobial peptides in action.* J. Am. Chem. Soc. 128:12156-12161.

144. Murzyn, K. and M. Pasenkiewicz-Gierula. 2003. *Construction of a toroidal model for the magainin pore*. J. Mol. Model. 9:217-224.
145. Yang, L., T.M. Weiss, T.A. Harroun, W.T. Heller, and H.W. Huang. 1999. *Supramolecular structures of peptide assemblies in membranes by neutron off-plane scattering: method of analysis*. Biophys. J. 77:2648-2656.
146. Yang, L., T.M. Weiss, R.I. Lehrer, and H.W. Huang. 2000. *Crystallization of antimicrobial pores in membranes: magainin and protegrin*. Biophys. J. 79:2002-2009.
147. Massiot, D., F. Fayon, M. Capron, I. King, S. Le Calvé, B. Alonso, J.-O. Durand, B. Bujoli, Z. Gan, and G. Hoatson. 2002. *Modelling one- and two-dimensional solid-state NMR spectra*. Magn. Reson. Chem. 40:70-76.
148. Herzfeld, J. and A.E. Berger. 1980. *Sideband intensities in NMR spectra of samples spinning at the magic angle*. J. Chem. Phys. 73:6021-6030.
149. Eichele, K. and R.E. Wasylshen, *HBA 1.5*. 2006: Dalhousie University & Universität Tübingen.
150. Ulrich, A.S. and A. Watts. 1994. *Lipid headgroup hydration studied by ²H-NMR: a link between spectroscopy and thermodynamics*. Biophys. Chem. 49:39-50.
151. Moraes, M.C. and B. Bechinger. 2004. *Peptide-related alterations of membrane-associated water: deuterium solid-state NMR investigations of phosphatidylcholine membranes at different hydration levels*. Magn. Reson. Chem. 42:155-161.
152. Nomura, K., G. Corzo, T. Nakajima, and T. Iwashita. 2004. *Orientation and pore-forming mechanism of a scorpion pore-forming peptide bound to magnetically oriented lipid bilayers*. Biophys. J. 87:2497-2507.
153. Hallock, K.J., D.K. Lee, and A. Ramamoorthy. 2003. *MSI-78, an analogue of the magainin antimicrobial peptides, disrupts lipid bilayer structure via positive curvature strain*. Biophys. J. 84:3052-3060.
154. Mitrakos, P. and P.M. Macdonald. 1996. *DNA-induced lateral segregation of cationic amphiphiles in lipid bilayer Membranes as detected via ²H-NMR*. Biochemistry 35:16714-16722.
155. Mitrakos, P. and P.M. Macdonald. 1997. *Domains in cationic lipid plus polyelectrolyte bilayer membranes: detection and characterization via ²H nuclear magnetic resonance*. Biochemistry 36:13646-13656.
156. Balla, M.S., J.H. Bowie, and F. Separovic. 2004. *Solid-state NMR study of antimicrobial peptides from Australian frogs in phospholipid membranes*. Eur. Biophys. J. 33:109-116.
157. Banerjee, U., R. Zidovetzki, R.R. Birge, and S.I. Chan. 1985. *Interaction of alamethicin with lecithin bilayers: a ³¹P and ²H NMR study*. Biochemistry 24:7621-7627.
158. Li, C. and T. Salditt. 2006. *Structure of magainin and alamethicin in model membranes studied by x-ray reflectivity*. Biophys. J. 91:3285-3300.
159. Pinheiro, T.J.T. and A. Watts. 1994. *Resolution of individual lipids in mixed phospholipid membranes and specific lipid-cytochrome c interactions by magic-angle spinning solid-state phosphorus-31 NMR*. Biochemistry 33:2459-2467.
160. Ludtke, S.J., K. He, Y. Wu, and H.W. Huang. 1994. *Cooperative membrane insertion of magainin correlated with its cytolytic activity*. Biochim. Biophys. Acta 1190:181-184.
161. Huang, H.W. and Y. Wu. 1991. *Lipid-alamethicin interactions influence alamethicin orientation*. Biophys. J. 60:1079-1087.
162. Yang, L., T.A. Harroun, T.M. Weiss, L. Ding, and H.W. Huang. 2001. *Barrel-stave model or toroidal model? A case study on melittin pores*. Biophys. J. 81:1475-1485.

163. Ladokhin, A.S. and S.H. White. 2001. *'Detergent-like' permeabilization of anionic lipid vesicles by melittin*. *Biochim. Biophys. Acta* 1514:253-260.
164. Marassi, F.M., C. Ma, J.J. Gesell, and S.J. Opella. 2000. *Three-dimensional solid-state NMR spectroscopy is essential for resolution of resonances from in-plane residues in uniformly ¹⁵N-labeled helical membrane proteins in oriented lipid bilayers*. *J. Magn. Reson.* 144:156-161.
165. Ramamoorthy, A., F.M. Marassi, M. Zasloff, and S.J. Opella. 1995. *Three-dimensional solid-state NMR spectroscopy of a peptide oriented in membrane bilayers*. *J. Biomol. NMR* 6:329-334.
166. Bechinger, B., M. Zasloff, and S.J. Opella. 1993. *Structure and orientation of the antibiotic peptide magainin in membranes by solid-state nuclear magnetic resonance spectroscopy*. *Protein Sci.* 2:2077-2084.
167. Marassi, F.M. and S.J. Opella. 1998. *NMR structural studies of membrane proteins*. *Curr. Opin. Struct. Biol.* 8:640-648.
168. Marassi, F.M. and S.J. Opella. 2000. *A solid-state NMR index of helical membrane protein structure and topology*. *J. Magn. Reson.* 144:150-155.
169. Westerhoff, H.V., M. Zasloff, J.L. Rosner, R.W. Hendler, A. De Waal, A. Vaz Gomes, P.M. Jongsma, A. Riethorst, and D. Juretic. 1995. *Functional synergism of the magainins PGLa and magainin-2 in Escherichia coli, tumor cells and liposomes*. *Eur. J. Biochem.* 228:257-264.
170. Matsuzaki, K., Y. Mitani, K.Y. Akada, O. Murase, S. Yoneyama, M. Zasloff, and K. Miyajima. 1998. *Mechanism of synergism between antimicrobial peptides magainin 2 and PGLa*. *Biochemistry* 37:15144-15153.
171. Rollins-Smith, L.A., J.K. Doersam, J.E. Longcore, S.K. Taylor, J.C. Shamblin, C. Carey, and M. Zasloff. 2002. *Antimicrobial peptide defenses against pathogens associated with global amphibian declines*. *Dev. Comp. Immunol.* 26:63-72.
172. Elion, G.B., S. Singer, and G.H. Hitchings. 1954. *Antagonists of nucleic acid derivatives. VIII. Synergism in combinations of biochemically related antimetabolites*. *J. Biol. Chem.* 208:477-488.
173. O'Neil, K.T. and W.F. DeGrado. 1990. *A thermodynamic scale for the helix-forming tendencies of the commonly occurring amino acids*. *Science* 250:646-651.
174. Mattice, W.L. 1986. *Helix breakers in block copolypeptides*. *Biopolymers* 25:1449-1459.
175. Javadpour, M.M., M. Eilers, M. Groesbeek, and S.O. Smith. 1999. *Helix packing in polytopic membrane proteins: role of glycine in transmembrane helix association*. *Biophys. J.* 77:1609-1618.
176. Russ, W.P. and D.M. Engelman. 2000. *The GxxxG motif: a framework for transmembrane helix-helix association*. *J. Mol. Biol.* 296:911-919.
177. Strandberg, E. and J.A. Killian. 2003. *Snorkeling of lysine side chains in transmembrane helices: how easy can it get?* *FEBS Lett.* 544:69-73.
178. Sternberg, U., R. Witter, and A.S. Ulrich. 2007. *All-atom molecular dynamics simulations using orientational constraints from anisotropic NMR samples*. *J. Biomol. NMR.*
179. Mikhailiuk, P.K., S. Afonin, A.N. Chernega, E.B. Rusanov, M.O. Platonov, G.G. Dubinina, M. Berditsch, A.S. Ulrich, and I.V. Komarov. 2006. *Conformationally rigid trifluoromethyl-substituted alpha-amino acid designed for peptide structure analysis by solid-state ¹⁹F NMR spectroscopy*. *Angew. Chem., Int. Ed. Engl.* 45:5659-5661.
180. Ulrich, A.S., P. Wadhvani, U.H. Dürr, S. Afonin, R.W. Glaser, E. Strandberg, P. Tremouilhac, C. Sachse, M. Berditchevskaia, and S. Grage, *Solid-state ¹⁹F-nuclear magnetic resonance analysis of membrane-active peptides*, in *NMR Spectroscopy of*

- Biological Solids*, A. Ramamoorthy, Editor. 2006, CRC Taylor and Francis group: New York. p. 215-236.
181. Gordon, Y.J. and E.G. Romanowski. 2005. *A review of antimicrobial peptides and their therapeutic potential as anti-infective drugs*. *Curr. Eye Res.* 30:505–515.
 182. Ohsaki, Y., A.F. Gazdar, H.C. Chen, and B.E. Johnson. 1992. *Antitumor activity of magainin analogues against human lung cancer cell lines*. *Cancer Res.* 52:3534-3538.
 183. Baker, M.A., W.L. Maloy, M. Zasloff, and L.S. Jacob. 1993. *Anticancer efficacy of magainin2 and analogue peptides*. *Cancer Res.* 53:3052-3057.
 184. Soballe, P.W., W.L. Maloy, M.L. Myrnga, L.S. Jacob, and M. Herlyn. 1995. *Experimental local therapy of human melanoma with lytic magainin peptides*. *Int. J. Cancer* 60:280-284.
 185. Lehmann, J., M. Retz, S.S. Sidhu, H. Suttmann, M. Sell, F. Paulsen, J. Harder, G. Unteregger, and M. Stockle. 2006. *Antitumor activity of the antimicrobial peptide magainin II against bladder cancer cell lines*. *Eur. Urol.* 50:141-147.
 186. Cruz-Chamorro, L., M.A. Puertollano, E. Puertollano, G.A. de Cienfuegos, and M.A. de Pablo. 2006. *In vitro biological activities of magainin alone or in combination with nisin*. *Peptides* 27:1201-1209.
 187. Xing, H., C.B. Lawrence, O. Chambers, H.M. Davies, N.P. Everett, and Q.Q. Li. 2006. *Increased pathogen resistance and yield in transgenic plants expressing combinations of the modified antimicrobial peptides based on indolicidin and magainin*. *Planta* 223:1024-1032.
 188. Vidal, J.R., J.R. Kikkert, M.A. Malnoy, P.G. Wallace, J. Barnard, and B.I. Reisch. 2006. *Evaluation of transgenic 'Chardonnay' (Vitis vinifera) containing magainin genes for resistance to crown gall and powdery mildew*. *Transgenic. Res.* 15:69-82.
 189. Chakrabarti, A., T.R. Ganapathi, P.K. Mukherjee, and V.A. Bapat. 2003. *MSI-99, a magainin analogue, imparts enhanced disease resistance in transgenic tobacco and banana*. *Planta* 216:587-596.
 190. Li, Q., C.B. Lawrence, H.Y. Xing, R.A. Babbitt, W.T. Bass, I.B. Maiti, and N.P. Everett. 2001. *Enhanced disease resistance conferred by expression of an antimicrobial magainin analog in transgenic tobacco*. *Planta* 212:635-639.
 191. Darveau, R.P., M.D. Cunningham, C.L. Seachord, L. Cassiano-Clough, W.L. Cosand, J. Blake, and C.S. Watkins. 1991. *Beta-lactam antibiotics potentiate magainin 2 antimicrobial activity in vitro and in vivo*. *Antimicrob. Agents Chemother.* 35:1153-1159.

List of publications

Posters presented in conferences:

Tremouilhac, P., E. Strandberg, P. Wadhvani, and A.S. Ulrich. *Solid-state NMR characterization of the antimicrobial peptide PGLa in membranes*. At the 1st EENC/AMPERE joint meeting. 2004. Lille, France.

Tremouilhac, P., E. Strandberg, P. Wadhvani, and A.S. Ulrich. *Observation of a Structural Re-alignment of the antimicrobial Peptide PGLa in Lipid Membranes by Solid State NMR*. At the 2nd Yamada Symposium on Key Natural Organic Molecules in Biological Systems. 2005. Hyogo, Japan.

Tremouilhac, P., E. Strandberg, P. Wadhvani, and A.S. Ulrich. *Synergistic re-alignment of antimicrobial peptides in membranes: from the surfacebound state to transmembrane insertion*. At the XXIInd International Conference on Magnetic Resonance in Biological Systems. 2006. Göttingen, Germany.

Articles:

Strandberg, E., P. Wadhvani, P. Tremouilhac, U.H. Durr, and A.S. Ulrich. 2006. *Solid-state NMR analysis of the PGLa peptide orientation in DMPC bilayers: structural fidelity of ²H-labels versus high sensitivity of ¹⁹F-NMR*. Biophys. J. 90:1676-1686.

Tremouilhac, P., E. Strandberg, P. Wadhvani, and A.S. Ulrich. 2006. *Conditions affecting the re-alignment of the antimicrobial peptide PGLa in membranes as monitored by solid state ²H-NMR*. Biochim. Biophys. Acta 1758:1330-1342.

Tremouilhac, P., E. Strandberg, P. Wadhvani, and A.S. Ulrich. 2006. *Synergistic transmembrane alignment of the antimicrobial heterodimer PGLa/magainin*. J. Biol. Chem. 281:32089-32094.

Curriculum vitae

Pierre TREMOUILHAC

Ingénieur diplômé de
l'Ecole Nationale Supérieure de Chimie de Lille

Geburtsdatum
Geburtsort
Staatsangehörigkeit
Familienstand

03.08.1978
Verneuil-sur-Avre (F)
Französisch
Ledig

Promotion

12/2003 - 05/2007
Promotion unter der Anleitung von Prof. Dr. A.S. Ulrich am Institut für biologische Grenzflächen - BioNMR Group - Forschungszentrum Karlsruhe / Lehrstuhl Biochemie, Institut für Organische Chemie, TH Karlsruhe

Schul-/Hochschulbildung

09/1993 - 06/1996
Gymnasium G. Faure, mit Abschluss (allgemeine Hochschulreife), Annecy (F)

09/1996 - 06/1999
Classes Préparatoires aux Grandes Ecoles, Lycée Berthollet, Annecy (F)

09/1999 - 09/2003
Ecole Nationale Supérieure de Chimie (TH für Chemie) de Lille (F)

05/2003 - 09/2003
Masterarbeit am Lehrstuhl Biochemie, Institut für Organische Chemie, TH Karlsruhe unter der Betreuung von Prof. Dr. A.S. Ulrich
Thema: „Chemische Synthese von Deuterium-markierten PGLa Peptiden und Untersuchung ihrer Orientierungen in Lipidmembranen durch Festkörper NMR“

09/2003
Diplôme d'ingénieur de l'ENSCL (Dipl. Chemieingenieur)

Berufserfahrung

07/2001 - 08/2001
Techniker-Hilfskraft im Analyselabor der städtischen Kläranlage, Vivendi Environment, Rumilly (F)

07/2002 - 08/2002
Ingenieur-Hilfskraft in der Neubauabteilung, Baikowsky Chimie, Annecy (F)